Development of a Tubular Biological Tissue-Engineered Heart Valve with Growth Potential

A DISSERTATION
SUBMITTED TO THE FACULTY OF
UNIVERSITY OF MINNESOTA
BY

Jay Matthew Reimer

IN PARTIAL FULFILLMENT OF THE REQUIREMENTS
FOR THE DEGREE OF
DOCTOR OF PHILOSOPHY

Dr. Robert T. Tranquillo, Advisor

May 2016

Acknowledgements

This doctoral dissertation would not have been possible without the support and guidance from colleagues, friends, and family. I would like to thank everyone for their contributions to my technical and personal development during this time.

I would like to especially thank my advisor, Bob Tranquillo, for providing me with the opportunity to work in an exciting field and for shaping me as a researcher. Thank you for your counsel, patience, and the opportunity to learn from you during my time as a graduate student.

Thank you to the members of the Tranquillo lab who supported this dissertation. I am grateful for Dr. Zeeshan Syedain for his role in my development as a researcher; I could always count on you for sound advice and to find free conference food. Many thanks to my fellow coworkers in Tranquillo West, Jeremy Schaefer and Dr. Jill Schmidt, for assisting me countless times in the hood and for making the lab an enjoyable place to work. Thank you in particular for Jill for putting up with our antics and for your baking prowess. I would also like to thank Naomi Ferguson, Susan Saunders, and Sandy Johnson for assistance culturing cells, sectioning tissues, staining slides, and performing numerous assays. Thank you also to the undergraduate students that worked with me for your enthusiasm, dedication, and research contributions.

A special thank you to Bee Haynie for sewing all of the valves for this project and making it seem easy. Your ability and friendship made working late in lab both productive and enjoyable. Thank you to Matt Lahti, Jim Berry, Peggy Norris, Sally Brinkman, and the rest of the Experimental Surgical Services Staff for technical assistance with the *in vivo* studies. I am also grateful to the UMN Medical Devices Center for printing and cleaning countless 3D printed parts. This work would not have been possible without financial support from the UMN Clinical and Translational Science Institute and the National Institutes of Health.

I am so grateful to my family and friends for their support and for making the good (and bad) days better during my graduate career. I especially want to thank my parents for many food ‘care packages’, proofreading word documents, and being there every step of the way. I can’t thank you enough for your unwavering support, guidance, and encouragement prior to and during graduate school.

Abstract

This thesis investigates tissue-engineered cardiovascular devices for pediatric patients and their function and growth potential in preclinical testing. Specifically, engineered tissue tubes were fabricated by entrapping dermal fibroblasts in a fibrin gel and allowing them to replace it with circumferentially-aligned extracellular matrix. Following *in vitro* culture, the engineered tubes possessed physiological strength and were decellularized to increase their shelf-life and reduce their immunogenicity. An allogeneic tubular heart valve was fabricated by inserting one engineered tube inside of another and attaching them together using degradable sutures.

Extensive hemodynamic testing was performed in order to optimize and verify valve design. The growth potential and *in vivo* function of a single engineered tube (as a pulmonary artery replacement) and pulmonary heart valve were evaluated in a growing lamb model. We observed extensive host cell invasion and growth of the valve root/single tube, but to a lesser degree in the leaflets, which resulted in diminished valve function. A modified animal model is proposed and proof-of-concept studies were performed in order to address this shortcoming.

Table of Contents

List of Tables

List of Figures

Chapter 1. Introduction to Heart Valves and Tissue Engineering Approaches

1.1 Summary

Tissue engineered heart valves are being developed in order to provide an alternative prosthetic valve to patients suffering from valvular heart disease. They aim to address the limitations of currently existing bioprosthetic and mechanical heart valves, which have a limited functional life or require lifelong anticoagulation, respectively. Tissue engineered valves generally consist of three parts: a biodegradable polymeric scaffold for initial structural integrity and cell attachment sites, entrapped or seeded cells that remodel that biodegradable scaffold, and stimulation paradigms to direct cellular activity (especially production of a functional extracellular matrix). *In vitro* functional testing is useful to assess valve designs based on their hydrodynamic performance under physiologic pressure and flow conditions. However, *in vivo* testing is crucial since tissue engineered heart valves aim to provide a living valve capable of cell-mediated repair, remodeling, and growth. The aforementioned considerations comprise the focus of this chapter.

Keywords: heart valve engineering, tissue engineered heart valves, biopolymer scaffold, synthetic polymer scaffold, animal model, pulse duplicator

1.2 Background

Valvular heart disease, a widespread disease that has been estimated to afflict ~2.5% of the US population, limits the efficient flow of blood through the heart due to improper valve opening or closing [1]. Incomplete valve opening due to reduced leaflet mobility is referred to as valve stenosis. Valve regurgitation occurs when the leaflets fail to coapt, such as leaflet prolapse, during diastole; this allows blood to flow backward through the valve. Valve dysfunction (regurgitation and/or stenosis) can occur progressively or result from a specific event. Most commonly, patients undergo progressive valve deterioration as they age due to leaflet calcification, hypertension, and/or atherosclerosis. A subset of patients suffers from congenital cardiovascular defects, which affect valve performance at a much younger age.

Congenital cardiovascular defects are estimated to affect at least 40,000 infants each year in the US alone and ~25% of these patients (240 / 100,000 live births [LBs]) require an invasive treatment within their first year of life [1,2]. Defects affecting heart valves include bicuspid aortic valves (1,370 / 100,000 LBs), Tetralogy of Fallot (40 / 100,000 LBs), pulmonary stenosis (60 / 100,000 LBs), pulmonary atresia (7-8 / 100,000 LBs), truncus arteriosus (7 / 100,000 LBs), and tricuspid atresia/stenosis (6.7 / 100,000 LBs) [1,3,4]. Tetralogy of Fallot encompasses multiple defects including a ventricular septal defect, pulmonary stenosis, an overriding aortic valve to the right, and right ventricular hypertrophy [5]. Atresia is a more extreme version of stenosis in which the valve opening is abnormally closed or absent.

Dysfunctional valves can sometimes be repaired (nearly 19,000 in the U.S. in 2011 alone), but are more commonly replaced, ~83% of the time (nearly 92,000 in the U.S. in 2011), with prosthetic valves to restore heart function. The aortic valve most commonly requires intervention, followed by the mitral, pulmonary, and tricuspid valves. The total number of heart valve procedures – stratified by procedure type, age, and valve position – can be seen in Table 1-1. For younger patients, congenital defects (such as Tetralogy of Fallot) can sometimes be repaired, but pulmonary regurgitation may persist.

This is typically well tolerated initially, but late pulmonary valve replacement is increasingly used due to the effects of prolonged pulmonary insufficiency [6-9]. These patients present a unique challenge for replacement valves as the child undergoes anatomical growth during their maturation.

1.2.1 Existing Therapies

Two general heart valve replacement options exist currently: bioprosthetic and mechanical heart valves [10,11]. These replacement valves are differentiated by their materials and design. There are two standard replacement procedures for prosthetic valves: surgical and transcatheter. Each valve and procedure type has advantages and disadvantages, which affect their selection for use in diseased patients [12-18].

1.2.1.1 Replacement Procedures

Surgical valve replacement, first developed in the early 1960's, traditionally includes opening the patient's chest cavity, putting the patient on bypass, and replacing the afflicted valve. More recently, transcatheter valve replacement has been developed, which utilizes specially designed, expandable bioprosthetic valves. This technique is much less invasive than traditional surgical valve replacement. Access to the defective valve is most commonly made through the femoral artery, but transapical and transaortic approaches have also been described. Since transcatheter valve replacement is relatively new, it is not yet indicated for all patient subsets despite some promising outcomes. Longer term patient monitoring to collect additional data will be needed in order to better understand the safety and efficacy of transcatheter versus surgical valve replacement.

1.2.1.2 Existing Replacement Valves

Bioprosthetic heart valves are derived from biological tissues whereas mechanical valves utilize inert materials such as pyrolytic carbon or titanium. Mechanical heart valves are thus typically very durable, and can maintain function after 30 years, but require aggressive anticoagulation to remain patent and to prevent thromboembolism [19]. Current anticoagulation regimens require patient lifestyle changes – such as routine

blood tests and dietary restrictions (avoiding vitamin K) – to ensure that therapeutic levels are maintained [14,19,20]. Furthermore, anticoagulation is associated with numerous side effects, including bleeding or hemorrhaging [13,16,19].

Bioprosthetic heart valves are generally more hemocompatible, but tend to perform adequately for only 10-20 years [13,21]. Tissue sources for bioprosthetic heart valves include bovine tissue, porcine tissue, and a limited supply of human cadaveric valves [22]. Tissues obtained for bioprosthetic heart valves are typically rendered inert by chemical fixation (non-human tissues) or cryopreservation, which can negatively affect the tissue's microstructure and *in vivo* durability [23-25]. Specifically, these treatments can limit host cell invasion, which is necessary for matrix repair and regeneration [23]. This deficiency limits the functional life of bioprosthetic heart valves and makes it more likely that patients younger than 65 will likely to require a reoperation to replace a worn out prosthetic heart valve.

The tissues for bioprosthetic valves are often sewn onto a rigid frame or an expandable stent (transcatheter valves), but can also be implanted without either. The tissues for transcatheter valves are the same as those used for traditional bioprosthetic valves and are thus not expected to have a longer functional lifetime. Given that transcatheter valves are relatively new, they have been more extensively used in patients who are considered at higher risk for traditional surgical valve replacement. However, the use of transcatheter valves is expected to grow in the future, pending continued demonstration of their safety and efficacy.

Reoperations to replace defective prosthetic valves are associated with a number of risks, including mortality [13,17,26]. Addressing bioprosthetic valve failure is challenging, although valve-in-valve procedures have been reported in which a second valve is inserted within the defective bioprosthetic valve [27-29]. However, concerns remain regarding the valve positioning, coronary obstruction, and higher pressure gradients due to a narrowed valve orifice [29].

1.2.1.3 Replacement Heart Valve Selection

The particular prosthetic valve and replacement procedure used depends on factors such as current disease status, expected patient lifespan, co-morbidities, patient preferences, and associated costs [13,19]. In general, mechanical valves are selected when the patient is expected to outlive the functional life of bioprosthetic valves or unable to withstand the anticoagulation regimen required for mechanical heart valve replacement. Valve selection for pediatric patients is especially problematic since neither mechanical nor bioprosthetic valves are capable of growth. Thus, these patients often must undergo one or more reoperations to replace outsized prosthetic valves. Additionally, the chemically-treated and cryopreserved tissues used are prone to calcification in children, which can result in valve failure.

1.2.1.4 Emerging Replacement Valves

Decellularization has also been extensively explored as a way to reduce the immunogenicity of allogeneic (human) and xenogeneic (non-human) tissues without cryopreservation or chemical fixation [24,25,30-33]. There are several published clinical trials that evaluated the use of decellularized, non-cryopreserved human heart valves in the pulmonary or aortic position [24,34-36]. Although the initial results have been promising, their long term function remains unproven and they are limited in supply due to donor shortage [22,25,31,32,35,37,38]. Decellularized xenogeneic valves have also been investigated extensively in animal models [31,33,39]. Although some human data has been reported, the study noted a high incidence of conduit failure within two years of implantation [40]. Furthermore, explant histology showed minimal host cell invasion, apart from the presence of inflammatory giant-type cells on the lumenal surface. Providing various sizes of decellularized native valves can be challenging, particularly for allogeneic valves where there are a limited number of donors.

A more detailed description of decellularized xenogeneic or allogeneic valves will not be discussed in this chapter, despite considering them to be tissue engineered heart valves (TEHVs). Additional information on these approaches can be found elsewhere and

in the citations provided above. Instead, the remainder of this chapter will focus on TEHVs that are not derived from native valves.

1.3 Tissue Engineered Heart Valves

Tissue engineered heart valves are being developed to address the shortcomings of current and emerging replacement options. In order to be a viable replacement option, TEHVs must first demonstrate excellent valve function (i.e. minimal regurgitation and low systolic pressure drops) under physiological pressures and flowrates. Additional design criteria include high durability, hemocompatibility, immunocompatibility, and capacity for growth (for pediatric applications). To date, most TEHV designs have focused on imitating the function rather than the form of native heart valves. For example, most tissues used for TEHVs consist of a single layer as opposed to the tri-layer tissue found in native heart valve leaflets.

Various approaches have been described to generate an engineered tissue suitable for a heart valve application. TEHVs typically consist of a degradable scaffold and cells, which are often exposed to chemical and/or mechanical stimulation to produce a desired response, such as collagen secretion. Although differing in various aspects, these approaches all aim to generate a "living" tissue capable of repairing and remodeling itself *in vivo*. The hope for such TEHVs is a longer functional life and/or somatic growth (pediatric patients). Reported studies have utilized various cell types, scaffold materials, mechanical/chemical stimuli, and valve designs [41]. Components reported in development of engineered tissues for TEHVs are discussed below.

1.3.1 Cell Sources

The primary responsibility for cells in heart valve tissue engineering is to remodel the starting polymer scaffold and secrete extracellular matrix components such as collagen, elastin, and/or proteoglycans. The cells' specific roles within the engineered tissue guide their selection. A universal cell type has yet to be identified or adopted for heart valve tissue engineering applications, though most researchers use a cell type that is

easily sourced and can be easily expanded *in vitro*. Commonly used cell types include smooth muscle cells (SMCs), myofibroblasts, dermal fibroblasts, and mesenchymal stem cells (MSCs) [42,43].

The cells generally fall into one of three categories depending on how they are obtained: autologous (from the same patient), allogeneic (from the same species), or xenogeneic (from a different species). Another method avoids isolating cells altogether and instead relies on *in situ* cell invasion and extracellular matrix deposition [44,45]. In one specific approach, valve molds were implanted subdermally for several weeks, during which time host cells invaded and secreted extracellular matrix proteins [46]. Another group implanted an electrospun scaffold into the designated valve position and allowed host cells to repopulate this matrix [47]. This non-traditional method avoids prolonged *in vitro* culture but is dependent on appropriate cell recruitment and tissue formation, which may vary between individuals. Other challenges include recruiting circulating cells, guiding their cell fate and behavior, and controlling tissue formation [45].

Historically for cardiovascular tissue engineering, and heart valve tissue engineering in particular, it has been important to consider the thrombogenicity and immunogenicity of the engineered tissue. These risks can be attenuated by using autologous cell sources. However, obtaining and expanding autologous cells can be a lengthy and arduous task, especially considering that these cells could behave differently depending on the individual and they may express a diseased phenotype. This process can be further complicated if a valve replacement is needed quickly, as can be the case for pediatric patients suffering from congenital defects.

1.3.1.1 Decellularization

The advent of decellularization has had an impact on heart valve tissue engineering. This process enables researchers to effectively remove the cellular components from a tissue, while leaving the extracellular matrix intact [48]. Acellular, non-fixed TEHVs offer several advantages over their cellularized counterparts. First,

decellularization allows TEHVs to be stored for longer periods of time prior to use, which is important for commercialization. Additionally, decellularization, if performed properly, removes the antigenic cellular components and would enable researchers to use allogeneic and possibly xenogeneic cells to batch-produce heart valve tissues. An in-depth description of decellularization protocols is outside the scope of this report, but there are several literature reviews that can provide more detail [49]. In general, these protocols use a combination of zwitterionic, ionic, or non-ionic detergents in addition to extensive rinsing or perfusion.

1.3.1.2 Recellularization

TEHVs rely on cells to remodel the matrix and respond to physiological growth cues over time. One factor to consider is that decellularized TEHVs must rely on host cell invasion and proliferation for tissue regeneration and growth. This recellularization process takes time and thus the acellular engineered tissue must also be able to withstand the *in vivo* environment without cells until sufficient cell invasion occurs. The invaded cells also must not grossly remodel the tissue such that the valve geometry and/or its function are compromised. The recruitment of endothelial cells to cover the blood contacting surfaces is particularly important, as this will reduce the thrombogenicity of the TEHVs.

1.3.2 Scaffold Materials

Polymeric scaffolds are an integral part of engineered tissues and provide initial mechanical support, an initial geometry, and attachment sites/cues for cells. These scaffolds are typically temporary and degrade as the cells secrete their own extracellular matrix. It is important to consider the initial mechanical strength of the scaffold and its degradation rate so that physical support for the cellular component of the engineered tissue is maintained during maturation. Additionally, the scaffold should be non-immunogenic and non-thrombogenic. It must also promote cellular attachment and interaction, and its degradation by-products should not elicit an inflammatory response [42,50]. The two most common sources of scaffold materials for TEHVs are grouped into

two categories: synthetic polymers and biopolymers. Recently, a hybrid scaffold has also been described that is unique from the two traditional categories.

1.3.2.1 Synthetic Polymer Scaffolds

Synthetic polymers are frequently used for heart valve tissue engineering. Primary advantages of this scaffold type are that they are widely available and can be configured to nearly any microscopic morphology and macroscopic geometry. Additionally, synthetic polymers can have a large range of mechanical and chemical properties based on how they are synthesized. Fabrication methods include salt-leaching, rapid prototyping, electrospinning, and phase-separation [42].

Synthetic polymers do not inherently contain biological signaling components like those found in biological polymers, although researchers have the ability to incorporate bioactive components [50]. Cell engraftment can be achieved by directly seeding cells onto the synthetic scaffold or using a cell carrier, such as fibrin. Controlling the polymer degradation rate is also important since it provides mechanical support and attachment sites for cells. Accelerated or slow degradation can affect the *in vitro* remodeling and maturation of the tissue. Additionally, if polymer degradation isn't completed prior to implantation, its degradation byproducts must not cause deleterious effects on adjacent cells [51].

One of the first reports of a TEHV made from a synthetic scaffold used a polyglycolic acid (PGA) – polylactic acid (PLA) copolymer layered between non-woven PGA [52]. Later, the use of polyhydroxyoctanoate (PHO) was explored to remedy problems associated with high scaffold stiffness, but ultimately proved to be less than ideal because of its slow degradation profile [53,54]. PGA coated with poly-4-hydroxybutyrate (P4HB) has a more favorable degradation profile and has seen more extensive use [55,56]. In general, most synthetic scaffolds for heart valve tissue engineering have been derived from aliphatic polyesters, polyhydroxyalkanoates, or combinations of the two [42,57].

1.3.2.2 Biopolymer Scaffolds

Biopolymer scaffolds naturally incorporate biological signaling components, which are important to modulate cell attachment and activity [42,50]. These materials can be obtained autologously to minimize immunocompatibility concerns, but this can introduce variability among the scaffolds, including purity and degradation rate, and it could limit commercialization and clinical use. For these reasons, xenogeneic sources of biopolymers are more commonly used in cardiovascular tissue engineering approaches. Another challenge associated with biopolymers is that they lack the initial mechanical strength required to withstand physiologic conditions. This has prompted researchers to explore various culture conditions and bioreactors (which will be discussed in more detail later), to improve the mechanical properties of the TEHVs.

Several biopolymer sources, particularly collagen and fibrin, have been explored for use in heart valve tissue engineering [42,50,57]. Unlike with synthetic polymers, cells can be directly entrapped into these scaffolds because polymerization occurs in an aqueous solution at physiological pH and temperature. The cell and monomer solutions are mixed together prior to polymerization to facilitate cell distribution throughout the resulting hydrogel. This method of cell seeding is advantageous because it enables researchers to incorporate cells directly, and homogeneously, into their nascent engineered tissue.

Type I collagen is a natural choice as a biological scaffold because it is a major extracellular matrix protein found in cardiovascular tissues, including heart valves. Collagens are homologous across species and thus are biocompatible and weakly immunogenic [58,59]. However, cells cultured in type I collagen gels exhibited lower collagen synthesis and cell proliferation compared to fibrin gels [59-61].

Fibrin has been an attractive biopolymer for heart valve tissue engineering because cells are able to proliferate more and produce more collagen and total protein than in collagen gels [62-64]. One challenge for the use of fibrin is controlling its degradation rate, as it can be enzymatically degraded rapidly depending on the cell type and *in vitro* conditions [62]. This degradation must be matched with the deposition of

cell-produced collagen to provide sufficient mechanical properties to the maturing engineered tissue.

1.3.2.3 Hybrid Scaffolds

Hybrid scaffolds are an alternative source to synthetic and biopolymeric scaffolds. These scaffolds have been recently described and are a combination of nitinol and cells seeded with [65] or without [66] a biological material (collagen). Other reports have previously demonstrated the capability of fabricating nitinol-based heart valves [67,68].

The hybrid scaffolds are fabricated by coating the metal meshes with cell-seeded collagen gels, which produce matrix proteins over a period of multiple weeks. These scaffolds are inherently strong and are capable of withstanding physiological pressure gradients due to the incorporation of the metal mesh [67,69]. Although the biological scaffold material or the cells are not the primary load bearing component, they serve to improve the biocompatibility of the TEHV [70].

One of the major issues using this type of scaffold is cell-metal interface and ensuring that there is proper attachment and cellular responses to these materials. Hybrid scaffolds are also not optimal for pediatric patients since they are inert and lack the ability to grow with the patient. Apart from these concerns, the *in vivo* function of TEHVs with hybrid scaffolds has yet to be assessed [41].

1.3.3 Stimulation Paradigms

The conditions imposed upon the nascent tissue have a significant impact on cellular function and ultimately tissue development. Most engineered tissues undergo some sort of mechanical conditioning to generate a mechanically robust and mature tissue in order to withstand physiologic conditions. This maturation process, particularly for approaches that use biopolymer scaffolds to grow connective tissues, often focuses on biochemical and mechanical stimulation paradigms to enhance cellular collagen synthesis. Biochemical agents are most commonly added to the culture medium periodically and have demonstrated the ability to stimulate collagen synthesis *in vitro*.

These agents include fibroblast growth factor (FGF), transforming growth factor (TGF), plasmin, insulin, and ascorbic acid [71-73].

Cells are able to sense mechanical stimuli via mechanotransduction, which can be utilized in order to induce a desired cellular response [74,75]. Most commonly, researchers mechanically stretch the engineered tissue to stimulate cellular collagen production. These systems are often capable of applying complex strain and shear stress patterns in the constructs. Regardless of the design, bioreactors must meet certain requirements such as adequate gas exchange, nutrient delivery, and sterility. For heart valve tissue engineering, bioreactors that replicate physiological pulsatile pressures or utilize controlled cyclical stretch have been described [76-88]. The most suitable system depends on a number of factors such as the desired level of control on the regimen, bioreactor complexity, and valve design.

Bioreactors require a number of components in order to replicate physiologic pulsatile pressure waveforms. Common features amongst the different designs include: a pump to induce fluid motion, a mounting chamber for the TEHV, a culture medium reservoir, compliance chambers for energy dissipation, and a tunable element to control system pressure [43]. These systems condition the whole valve during the entire cardiac cycle (systole and diastole). Another iteration of these systems is to simulate only diastolic pressure conditions by exposing the leaflets to cyclic back pressure [81]. An example system and its components are described in more detail in Figure 1-1.

Although the aforementioned systems can replicate physiological pressure conditions, the strain magnitude depends on the tissue properties and is not controlled. There have been published reports demonstrating the advantages of using incremental strain regimens and/or transmural flow [76-78]. Syedain and colleagues designed a cyclic stretch bioreactor capable that had a defined strain magnitude by mounting a TEHV within a latex tube [77]. Since the latex tube was much stiffer than the engineered tissue, strain magnitudes could be prescribed throughout the culture period independent of the tissue properties.

1.4 Valve Design

Traditional TEHVs, those using synthetic or biopolymeric scaffolds, must be fabricated into the heart valve geometry. The inherent properties of synthetic and biopolymeric scaffolds allow researchers to fabricate TEHVs in ways not possible with traditional bioprosthetic valves or decellularized native tissues. Almost all TEHV designs incorporate distinct leaflets that open and close in response to pressure gradients. Valvular function also can be achieved by attaching an engineered tissue tube to a three-pronged frame or to create a tubular valve [89] that is the functional equivalent of a trileaflet valve [90-92]. Some valve designs for pediatric patients also incorporate a root, or flow conduit, since cardiovascular congenital defects can affect the outflow tract as well as the leaflets [88,93].

Biopolymeric and synthetic scaffolds are easily moldable since they often begin as an aqueous solution or typically incorporate a thermoplastic polyhydroxyalkanoate (such as P4HB), respectively [42,55,94,95]. This has enabled researchers to use casting molds (as shown in Figure 1-2) that integrate the valve root and leaflets together. This allowed researchers to create valves with leaflets directly attached to the root from the onset of valve fabrication [73,83].

While these molds were innovative and provided a proof of concept, there are several challenges associated with this approach. First, machining the molds is challenging given the unique geometries utilized. Additionally, the presence of sharp corners and high stress points in these molds can lead to tissue thinning and tearing. Another major challenge is ensuring that valve geometry and coaptation is maintained throughout the culture period. Although cell induced compaction can be exploited to generate anisotropic tissues [73,96], over-compaction can result in geometrical changes that compromise the valve. For example, over-compaction in the leaflet channels results in loss of coaptation.

A simpler approach is based on a tubular valve design [89]. Instead of using a complex mold to define the heart valve root and leaflet geometries, tissue tubes are

constrained such that they collapse inward under back pressure at three equi-spaced positions (commissures) around the circumference that anchor the tube (Figure 1-3). This creates the equivalent of three leaflets, which respond to dynamic pressure gradients across a tubular heart valve. These principles have been applied to heart valve tissue engineering as researchers have reported tubular TEHVs using tubular tissues based on synthetic and biopolymer scaffolds [88,90,92,93]. Most tubular TEHVs utilize a single tube that is attached to a frame, an expandable stent, or designed to be implanted within the native vasculature.

The use of inert frames, stents, chemically fixed tissues, or embedded synthetic materials preclude them from growing and are thus suboptimal for pediatric patients. One new approach avoids these components and might be more suitable for pediatric valve replacements [93]. It consists of two completely biological, decellularized engineered tubes (primarily cell-produced collagen) that are attached using a degradable suture line and does not incorporate any inert materials, frames, or stents. It relies on host cell invasion and matrix production to fuse the two engineered tubes along the degradable suture line and subsequently respond to physiologic growth cues *in vivo*. However, it remains to be seen whether this, or other, TEHVs are amenable to long term function and growth.

1.5 *In Vitro* Functional Testing

Functional testing systems in the laboratory are invaluable in validating and improving valve designs for TEHVs prior to expensive animal studies. These pulsatile flow testing systems are similar to some of the aforementioned bioreactor systems in terms of components required. They are not exclusive to TEHVs, but instead are useful for testing all types of valves (including mechanical and bioprosthetic valves). They typically include pressure and flow probes, a pump to induce fluid motion, compliance chambers, a valve housing chamber, and a fluid reservoir [85].

The primary goal of functional testing is to elucidate the TEHV's function under physiologic pressure and flow conditions [97]. Important hydrodynamics include systolic

pressure drop, regurgitation, and effective orifice area (EOA). Detailed descriptions of these metrics and other valve testing requirements can be found in ISO 5840. A high speed camera is typically placed end-on to visualize and record leaflet motion during the cardiac cycle. This allows researchers to visualize any fluttering, prolapse, or asymmetry in the valve leaflets. An additional camera can be used to visualize root motion if it is incorporated into the prosthetic heart valve and the test system allows for it.

Accelerated wear testing (AWT) is a type of functional testing designed to evaluate the fatigue properties of prosthetic heart valves under pulsatile flow and physiologic loading. Complete valve opening and physiologic diastolic pressure gradients are the only requirements for AWT. This allows researchers to utilize higher frequency pumps to evaluate a heart valve's durability after a large number of cycles. Traditional mechanical and bioprosthetic heart valves must withstand 600 million or 200 million cycles per ISO 5840, respectively. Often valves undergo full functional testing (physiologic flow and pressure conditions) periodically during AWT to assess their hydrodynamic performance.

The appropriate number of test cycles for TEHVs is unclear since engineered valves are designed on the premise that cells will repair and remodel the extracellular matrix following implantation [42]. These cells can be either transplanted with the valve or host cells that repopulate the acellular valve, or a combination of both. The complex *in vivo* environment cannot be completely mimicked with *in vitro* systems. The ideal number of cycles depends on the timeline necessary for cellular production of matrix proteins needed to sustain valve function following implantation. Discussions with the FDA on these points will be crucial to ensure that the protocols for appropriate *in vitro* functional tests and their duration are established as TEHVs become closer to commercialization.

1.6 *In Vivo* Testing

Large animal testing is a requirement for the preclinical assessment of prosthetic heart valves. These tests allow researchers to assess the performance of the surgical

procedure and valve's hydrodynamic performance in a beating heart over an extended period of time. These studies are highly regulated and require approval by a standard governing body known as the Institutional Animal Care and Use Committee, or IACUC. The following sections highlight the animal models and results with TEHVs to date.

1.6.1 Animal Models for TEHVs

Chronic *in vivo* TEHV studies are conducted primarily in sheep, which are the current "gold standard" for preclinical prosthetic heart valve replacement studies [98]. Studies with TEHVs are often performed in the pulmonary position of sheep due to the lower pressure gradients associated with this position compared to the aortic valve. Congenital defects also often affect this valve. Sheep are advantageous because they have similar normal cardiovascular physiological parameters (blood pressure, cardiac output, heart rate, and intracardiac pressure) and valve diameters that are similar to humans. The ovine model is also an aggressive calcification model, particularly in juvenile animals, compared to other large animal models.

Canine models were common historically since they have good temperaments and can be trained easily. However, they are not as common now due to the occurrence of leaflet fusion and high collateral coronary circulation [98]. Swine models are advantageous since they have very similar cardiac anatomy to humans in terms of their valves, coronary arteries, and conduction system. However, they have a high incidence of postoperative mortality and arrhythmias which limits their widespread use. There has also been a report of a non-human primate model being used, but this is currently not very common [99].

Heart valve replacement studies, particularly those with TEHVs, are conducted using healthy animals and primarily aim to assess valve function. Naturally occurring and reproducible valvular defects have been described in rats and mice, but are much less common in larger animal models [100]. Researchers have described large animal models with iatrogenic valve stenosis, regurgitation, and anatomical abnormalities [98,100]. However, these are not commonly used, particularly for TEHV studies.

The animal model's growth rate is also important to consider when conducting chronic animal studies, particularly if the desired valve orifice sizes and study aims necessitate using immature animals. Growing animal models are intriguing for TEHV studies since they aim to assess somatic growth of the TEHV, which is an unmet clinical need for pediatric valve replacement patients. Accelerated growth rates compared to human can result in "prosthesis-patient mismatch" and valve stenosis if the animal outgrows its prosthetic heart valve [18]. The aforementioned animal models all reach full maturity within 12-18 months of age, which is substantially faster than in humans [98,101-103]. This timescale can be challenging for TEHVs, especially pediatric valves, which rely on transplanted or invaded cells to dictate growth in response to physiological cues.

1.6.2 Preclinical Testing Results with TEHVs

Shinoka et al. [104] was one of the first to demonstrate the feasibility of TEHVs for valve replacement. A single sheep pulmonary valve leaflet was replaced with autologous or allogeneic tissue engineered leaflets, which were fabricated by seeding a combination of fibroblasts, smooth muscle cells, and endothelial cells seeded onto polyglactin/PGA mesh sheets. Lambs with one of these allogeneic leaflets experienced leaflet retraction and an acute inflammatory response despite receiving immunosuppression therapy, whereas those with an autologous leaflet did not. While the single leaflet approach has limited applications, this study demonstrated the feasibility of tissue engineering in heart valve replacements.

The same research group soon developed a complete trileaflet TEHV by seeding autologous (ovine) myofibroblasts and endothelial cells onto a PGA/P4HB scaffold [55]. Following pulsatile bioreactor culture, the TEHVs were implanted into the pulmonary position of sheep for up to 20 weeks and valve function was monitored via echocardiography. The tensile strength of the engineered leaflets were initially higher than those of the native leaflets, but was comparable after 20 weeks *in vivo.* Histology showed increased organization and layering similar to native leaflets after 20 weeks with

presence the presence of collagen, glycosaminoglycans, and elastin. Although the TEHV leaflets remained functional throughout the duration of the study, significant regurgitation was observed after 16 and 20 weeks. Authors attributed this loss of valve function to the enlarging flow conduit and/or shrinkage of the TEHV leaflets.

A minimally invasive TEHV was fabricated by seeding myofibroblasts or stem cells onto a PGA/P4HB scaffold using fibrin as a cell carrier [105]. Following bioreactor culture, the TEHVs were transapically implanted into the pulmonary position of sheep for either 4 or 8 weeks. Examination following explantation revealed thickened and non-coapting leaflets. A similar approach, but without bioreactor culture, demonstrated valve function up to 4 weeks in the pulmonary position of primates [106]. Substantial cellular remodeling and endothelial cell coverage was observed without tissue thickening. However, structural shortening of the TEHV leaflets was detected after explantation.

Autologous pulmonary and aortic TEHVs have been explored in canine and goat models. Using a custom mold and *in situ* fabrication, these "Biovalves" were highly collagenous with a small amount of elastin [107]. Early generations of this TEHV allowed substantial regurgitation in dogs [108], which ultimately led to design changes in the valve mold. The most recent Biovalve incorporated a 3D printed mold and were implanted in the aortic position for one month [107]. Another group implanted an electrospun supramolecular polymer scaffold that was functionalized with biological components to recruit circulating host cells [47]. They reported sustained mechanical and biological function of their TEHV up to 6 month in their preliminary report.

Two different groups have described the fabrication of TEHVs using fibrin scaffolds with complex molds. Flanagan et al. used autologous cell populations (smooth muscle cells and fibroblasts) and bioreactor culture for 4 weeks to generate TEHVs sufficient for implantation [109]. The mature TEHVs were seeded with autologous endothelial cells prior to implantation into the pulmonary position of mature sheep for 3 months. Extensive *in vivo* remodeling resulted in the replacement of the fibrin scaffold with cell-produced extracellular matrix. An endothelium was observed on the valvular

surfaces and there was no evidence of thrombi, calcification, stenosis, or aneurysms. Despite these promising results, valvular function was not maintained due to cell-mediated leaflet shortening.

Another fibrin-based TEHV was fabricated by using human dermal fibroblasts and a cyclic stretch bioreactor [73,110]. Cell-mediated fibrin gel contraction was exploited by this group to dictate collagen fiber alignment and mechanical anisotropy similar to the native heart valve root and leaflets [73,96]. These bileaflet TEHVs were implanted interpositionally into the pulmonary position of sheep after comprising the native pulmonary valve leaflets [110]. A concentric sleeve was placed along the entire root length to mitigate the risk of suture pullout or root rupture.

Echocardiography immediately following implantation showed coapting leaflets with regurgitation, orifice area, and pressure gradients comparable to the native pulmonary valve. However, echocardiography at 4 weeks revealed moderate regurgitation due to significant leaflet shrinkage. Only one shortened leaflet was observed in each of the two valves explanted after 8 weeks. Extensive tissue remodeling and endothelialization was observed following implantation. Elevated collagen and elastin concentrations and minimal calcification were observed.

These studies demonstrated the feasibility of TEHVs, but ultimately failed to due progressive leaflet contraction *in vivo*. Syedain et al. demonstrated that the transplanted fibroblasts maintained a contractile phenotype following implantation. Flanagan et al. also reported that cells in the explanted leaflets expressed alpha smooth muscle actin. Proposed solutions included fabricating TEHVs with additional coaptation area, utilizing stiffer polymers to prevent over compaction, or cell removal following *in vitro* tissue remodeling [55,109,110].

Decellularization has been explored recently as a means to eliminate *in vivo* leaflet shortening by removing the cellular components. It also reduces the immunogenicity of the TEHVs. However, this approach relies on rapid host cell invasion to repopulate the TEHVs so that cell-mediated repair and remodeling (and potentially

growth) can occur. It is imperative that the acellular TEHVs can withstand this initial phase prior to recellularization *in vivo.* Decellularization was first performed on TEHVs fabricated using synthetic polymer scaffolds attached to expandable nitinol stents [94], and subsequently in TEHVs fabricated using a fibrin gel [90].

Decellularized TEHVs implanted into the pulmonary position of sheep exhibited extensive host cell invasion and matrix remodeling. Recellularization was fastest in the valve root, followed by the root/leaflet attachment area and the leaflets. However, mild central regurgitation appeared after 8 weeks and progressed to moderate after 24 weeks [91]. This loss of function was attributed to fusion of the leaflets to the valve root at the leaflet base, as shown in Figure 1-4. Similar results were reported in a senescent non-human primate model [99]. However, the appearance of mild to moderate regurgitation after 8 weeks was attributed to the passive retraction of the extracellular matrix in the primate study.

Another decellularized TEHV has also been reported recently using engineered tubes derived from a sacrificial fibrin scaffold [90]. Following *in vitro* maturation and decellularization, the engineered tubes consisted primarily of cell-produced collagen, which was preferentially aligned in the circumferential direction. The engineered tubes were sewn onto a three-pronged frame to create a tubular heart valve and tested under aortic conditions in an *in vitro* pulse duplicator system [90]. The TEHVs were subsequently implanted into the aortic position of adult sheep for up to 24 weeks [111]. Although there has been one other aortic TEHV study in sheep, it was designed to assess valve delivery, position, and function immediately after implantation [112]. The study by Syedain et al. was the first long term aortic valve study with a traditional TEHV (derived using synthetic or biopolymeric scaffolds) reported.

Full leaflet motion, laminar flow, and maintained effective orifice area were observed throughout the entirety of the implant period [111]. Two of the four valves implanted exhibited trivial to mild aortic insufficiency immediately after implantation. The insufficiency grade in three of the valves increased after 12 weeks, which was

attributed to small matrix tears near the top of the frame struts. However, the aortic insufficiency did not progress further between 12 and 24 weeks. No evidence of calcification was reported in any of the explanted TEHVs. Extensive recellularization was observed near the base of the leaflets after 12 weeks. After 24 weeks, the cells in these regions expressed vimentin and lacked alpha smooth muscle actin, similar to native valve interstitial cells. Increased cell invasion was observed near the leaflet free edge at this time point as well. The invaded cells deposited proteoglycans, elastin, collagen IV, and laminin. An endothelium was similarly forming from the base of the leaflets towards the free edge.

1.7 Remaining Challenges

The prospect of using tissue engineering principles to generate a living heart valve capable of repairing and remodeling itself is promising and exciting. However, there are numerous challenges remaining before a tissue engineered heart valve can be safely translated to the clinic. These heart valves must demonstrate both short and long term function in dynamic mechanical and flow environments. In order to respond to these environments and other biological cues, the correct cells must reside in the TEHV and maintain a homeostatic functional state over an extended period of time [113]. This challenge is exacerbated in pediatric patients who are also undergoing somatic growth.

Due to the breadth of valve fabrication methods (scaffolds, cells, cell stimulation, etc.) continued research is needed to identify the optimal TEHV. The use of animal models will be crucial in order to elucidate the host response to TEHVs and their various components in regards to thrombosis, inflammation, infection, and calcification. Demonstrating repeatable and long term valve function has been a challenge for the field to date.

Since TEHVs depend on resident cells to confer remodeling and somatic growth in response to physiologic cues *in vivo*, it will be crucial to assess their presence and phenotype following implantation. Ensuring cellularity is essential for decellularized valves, which are reliant on host cell invasion to provide durability (via secretion of new

matrix proteins) and hemocompatibility. Demonstrating success in these areas will be critical to the success of the heart valve tissue engineering field.

1.8 Conclusions

There are numerous approaches to developing a TEHV, each with their own advantages and disadvantages. Various cell sources, scaffold materials, and cell stimulation paradigms have been explored with varying levels of success. Ensuring the safety and efficacy of a tissue engineered valve prosthesis will require well designed *in vitro* and *in vivo* studies. Translating tissue engineered heart valves into the clinic is promising, but also challenging, as evidenced by outcomes of *in vivo* TEHV studies to date.

1.9 Chapter 1 Figures and Tables

Table 1-1. Valvular heart disease statistics in 2011

2011 valvular heart disease hospital discharges stratified by procedure type (repair or replacement) and patient age. Bold numbers = Total number of patients for a given subset. Percentages = Number of given subset to the total number of valve procedures (repair & replacement). Adapted from 2011 HCUPnet data.

Note: sum of all age groups does not necessarily equal "all ages" group due to the associated standard errors.

			All Valves		Aortic Valve		Mitral Valve		Pulmonary Valve		Tricuspid Valve	
			Replace	Repair	Replace	Repairs	Replace	Repairs	Replace	Repairs	Replace	Repairs
All ages			**91,803** 83.1%	**18,689** 16.9%	**73,679** 66.7%	**2,279** 2.1%	**15,981** 14.5%	**14,646** 13.3%	**1,418** 1.3%	**375** .3%	**735** .7%	**1,389** 1.3%
Age group	**"Pediatric"**	<1	**57** 0.1%	**681** 0.6%	*	**85** 0.1%	*	**75** 0.1%	**57** 0.1%	**251** 0.2%	*	**270** 0.2%
		1-17	**982** 0.9%	**901** 0.8%	**352** 0.3%	**322** 0.3%	**118** 0.1%	**260** 0.2%	**512** 0.5%	**96** 0.1%	*	**223** 0.2%
	"Adult"	18-44	**5,715** 5.2%	**1,662** 1.5%	**3,629** 3.3%	**373** 0.3%	**1,204** 1.1%	**1,078** 1.0%	**624** 0.6%	*	**258** 0.2%	**211** 0.2%
		45-64	**24,879** 22.5%	**7,099** 6.4%	**18,694** 16.9%	**740** 0.7%	**5,818** 5.3%	**6,062** 5.5%	**157** 0.1%	*	**210** 0.2%	**297** 0.3%
		65-84	**53,279** 58.1%	**7,871** 7.1%	**44,702** 40.5%	**706** 0.6%	**8,390** 7.6%	**6,808** 6.2%	*	*	**205** 0.2%	**357** 0.3%
		85+	**6,694** 6.1%	**411** 0.4%	**6,253** 5.7%	**53** 0.0%	**441** 0.4%	**358** 0.3%	*	*	*	*

ICD-9-CM Codes Used		Aortic Valve	Mitral Valve	Pulmonary Valve	Tricuspid Valve
	Replacement	35.21, 35.22, 35.05, 35.06	35.23, 35.24	35.25, 35.26	35.27, 35.28
	Repair	35.01, 35.11	35.02, 35.12	35.03, 35.13	35.04, 35.14

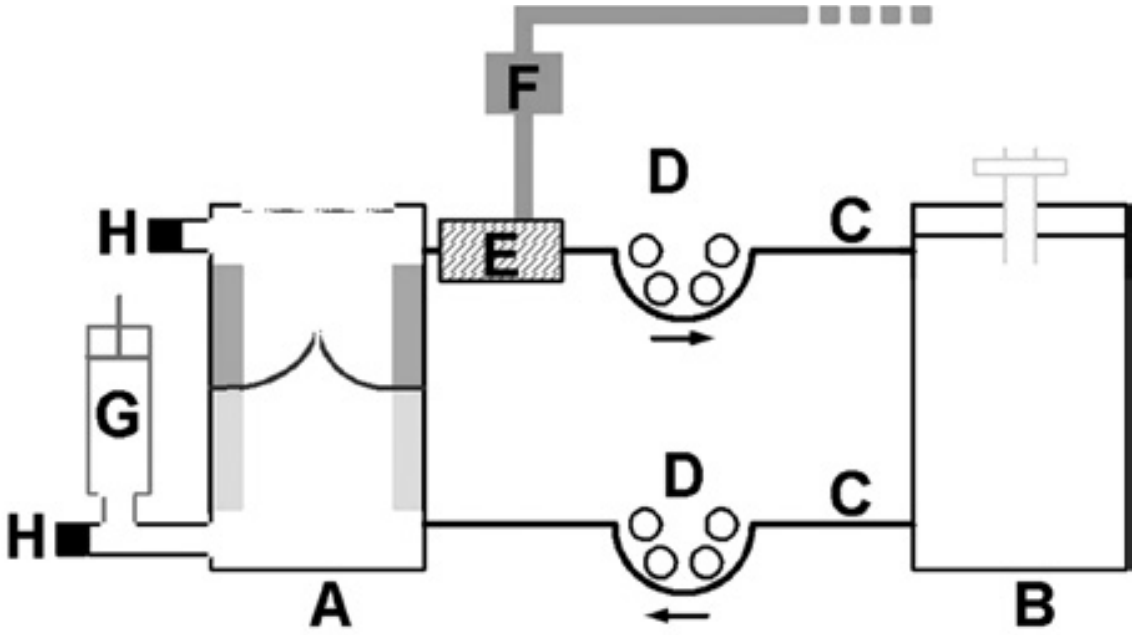

Figure 1-1. Diastolic pulse duplicator system schematic

System consists of (A) bioreactor and a (B) medium chamber. The medium is pumped through the (C) tubing connecting the two chambers using (D) roller pumps. Compressed air is introduced into a (E) polycarbonate cylinder, which encases part of the tubing, using a (F) magnet valve. Compliance is incorporated into the system using a (G) syringe and pressure is measured using (H) sensors on either side of the TEHV. With kind permission from Springer Science+Business Media: <Annals of Biomedical Engineering, Tissue Engineering of Human Heart Valve Leaflets: A Novel Bioreactor for a Strain-Based Conditioning Approach, 33, 2005, 1778-1788, A. Mol, N.J. Driessen, M.C. Rutten, S.P. Hoerstrup, C.V. Bouten, and F.P. Baaijens, Figure 2, [81].

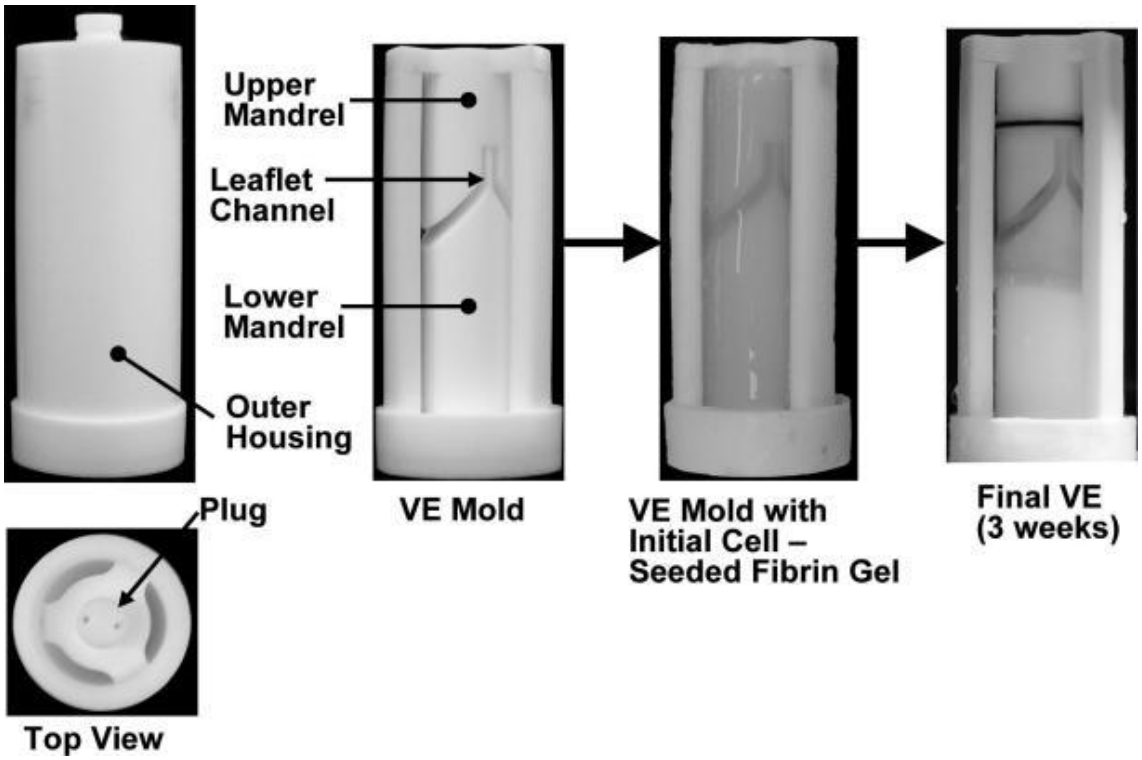

Figure 1-2. Bileaflet valve mold and fabrication procedure

Machined Teflon mold with a leaflet channel for use with a biopolymeric (fibrin) scaffold [73].

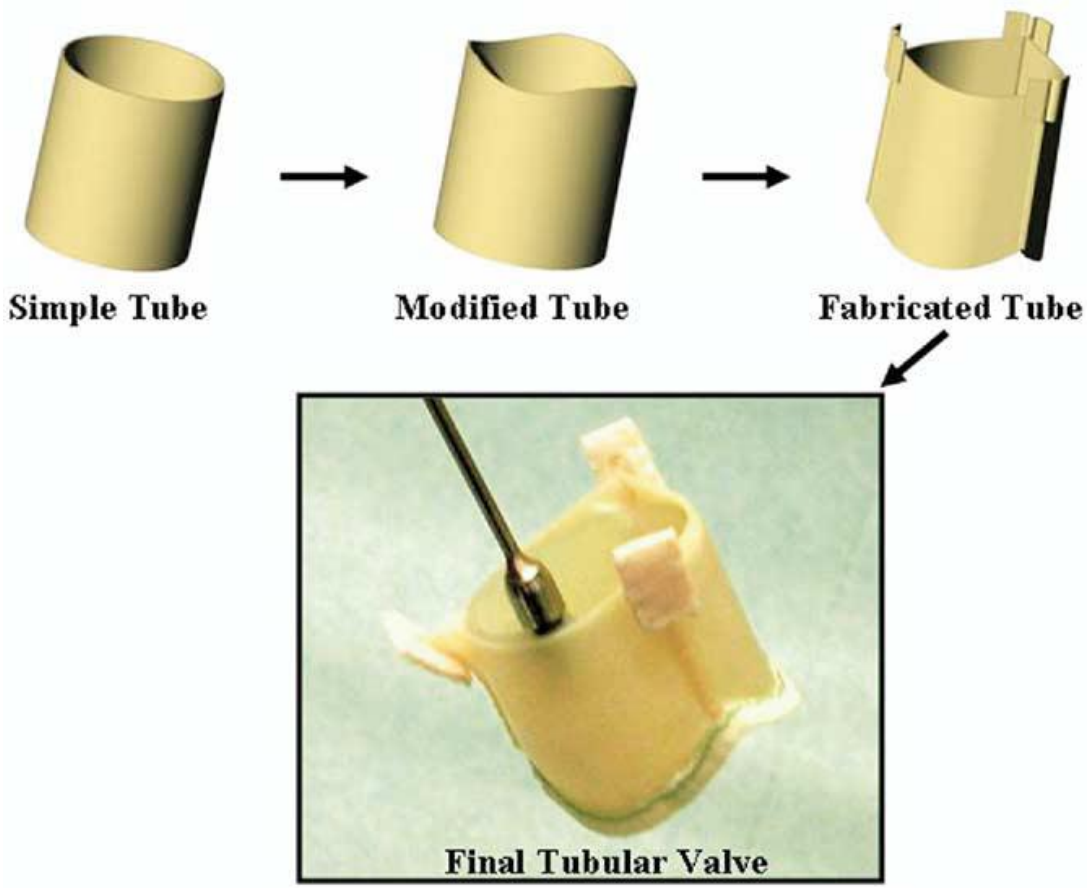

Figure 1-3. Tubular valve concept schematic

Schematic showing the tubular valve design and modification of the Medtronic 3F bioprosthetic valve. During implantation, the fabricated tube is attached around the base and at the three commissural tabs. Exposure to back pressure collapses the tube in the regions in between the commissural tabs, resulting in the formation of leaflets [89]. Reprinted from Journal of Thoracic and Cardiovascular Surgery, Volume 130 / edition 2, James Cox, Niv Ad, Keith Myers, Mortiz Gharib, and R.C. Quijano, Tubular heart valves: A new tissue prosthesis design—Preclinical evaluation of the 3F aortic bioprosthesis, 520-527, Copyright (2005), with permission from Elsevier.

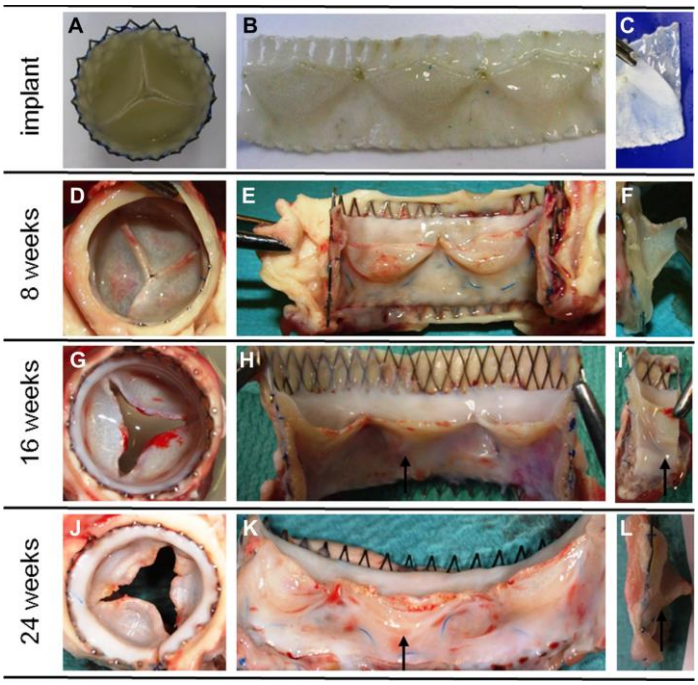

Figure 1-4. Macroscopic appearance of a TEHV before and after implantation

Macroscopic appearance of a decellularized TEHV (derived using synthetic polymers), (A-C) before and after implantation for (D-F) 8, (G-I) 16, and (J-L) 24 weeks. Leaflet coaptation was (D) maintained for 8 weeks, but (G,J) was not evident thereafter. (E,F,H,I,K,L) Leaflet fusion to the root (arrows) progressed upward over time, resulting in smaller leaflets. Reprinted from the Journal of American College of Cardiology, Volume 63/Issue 13, A. Driessen-Mol, M.Y. Emmert, P.E. Dijkman, L. Frese, B. Sanders, B. Weber, N. Cesarovic, M. Sidler, J. Leenders, R. Jenni, J. Grunenfelder, V. Falk, F.P. Baaijens, and S.P. Hoerstrup, Transcatheter Implantation of Homologous “Off-the-Shelf" Tissue-Engineered Heart Valves with Self-Repair Capacity: Long-Term Functionality and Rapid In Vivo Remodeling in sheep. Pages 1320-1329, 2014, with permission from Elsevier. [91].

Chapter 2. Pediatric Tubular Pulmonary Heart Valve from Decellularized Engineered Tissue Tubes

2.1 Summary

Pediatric patients account for a small portion of the heart valve replacements performed, but a pediatric pulmonary valve replacement with growth potential remains an unmet clinical need. Herein we report the first tubular heart valve made from two decellularized, engineered tissue tubes attached with absorbable sutures, which can meet this need, in principle. Engineered tissue tubes were fabricated by allowing ovine dermal fibroblasts to replace a sacrificial fibrin gel with an aligned, cell-produced collagenous matrix, which was subsequently decellularized. Previously, these engineered tubes became extensively recellularized following implantation into the sheep femoral artery. Thus, a tubular valve made from these tubes may be amenable to recellularization and, ideally, somatic growth.

The suture line pattern generated three equi-spaced “leaflets” in the inner tube, which collapsed inward when exposed to back pressure, per tubular valve design. Valve testing was performed in a pulse duplicator system equipped with a secondary flow loop to allow for root distention. All tissue-engineered valves exhibited full leaflet opening and closing, minimal regurgitation (< 5%), and low systolic pressure gradients (< 2.5 mmHg) under pulmonary conditions. Valve performance was maintained under various trans-root pressure gradients and no tissue damage was evident after 2 million cycles of fatigue testing.

Keywords: Tubular Heart Valve; Fibrin; Cardiac Tissue Engineering; Pulse Duplicator; Decellularization

2.2 Introduction

Valvular heart disease affects ~2.5% of the U.S. population and there were more than 110,000 heart valve procedures in 2011 [114,115]. There is a clinical need for a new prosthetic pulmonary valve (PV) despite the fact that this valve accounted for only ~1.3% of all heart valve procedures in the U.S. in 2011 [114]. Current PV prostheses are not ideal for "pediatric patients" (younger than 18 years old) due to their inability to grow. Current commercially-available PV prostheses include homograft valves (cryo-preserved or decellularized) and a chemically-fixed bovine jugular vein graft (trileaflet) [34,116]. Glutaraldehyde-fixation eliminates the immunogenicity of xenogeneic tissue, but also limits cell invasion and ultimately somatic growth [117]. Thus, young patients typically undergo multiple operative procedures in order to replace outgrown PV prostheses during maturation.

Numerous tissue-engineered heart valves (TEHVs) have been explored in hopes of developing "living" valves capable of *in vivo* tissue remodeling and growth [72,77,81,83,109,118]. Various strategies have been used for tissue fabrication, including the use of cell-seeded hydrogels with or without a polymeric co-scaffold. Although initially functional, many of these TEHVs exhibited progressive leaflet retraction during preclinical animal studies [109,119]. This has been attributed to sustained contraction of the transplanted cells, leading researchers to decellularize the tissue prior to implantation [90,91]. Although somatic growth has not yet been demonstrated, there have been several reports of decellularized tissue being recellularized [99,120], which is a necessary precursor to tissue remodeling and growth.

Earlier valve iterations focused on mimicking the shape of natural valve leaflets and often utilized complex molds [83,121,122]. More recently, TEHVs with a tubular leaflet design have been explored that do not rely on complex molds. To date, these tubular TEHVs have all used a single tube – attached to a stent, frame, or within an inert conduit – to generate a valve-like action [88,90,92]. Our group has previously reported a tubular TEHV using a single tube, generated by entrapping fibroblasts in a sacrificial

fibrin gel, onto a PEEK frame [123]. Despite the promising functional performance of this TEHV, its inert frame precludes it from growing and thus renders it suboptimal for pediatric PV replacements.

In this study we report a frameless, tubular TEHV generated from two decellularized engineered tissue tubes (referred to as "engineered tubes" hereafter) sewn together in a specified pattern using degradable sutures. The outer tube serves as the flow conduit and provides the mechanical constraints needed for the inner tube to function as "leaflets", as in classic tubular valve design. The regions of the inner tube not mechanically constrained by the outer tube collapse inward when exposed to back pressure. The engineered tubes were fabricated by entrapping ovine dermal fibroblasts in a tubular fibrin gel, as previously discussed [90]. The entrapped cells replaced the fibrin with a collagenous matrix, which is anisotropic due to the mechanical constraints imposed during the culture period. Collagen production was stimulated by stretching the constructs in a pulsed flow-stretch bioreactor following an initial static culture period. Decellularization in sequential detergent treatments was then used to remove the cellular components.

Following engineered tube and valve fabrication, the TEHVs were functionally tested in a custom pulse duplicator system to assess valve performance and root distention under pulmonary conditions. The durability of the suture line was assessed by fatiguing one TEHV for two weeks. Macroscopic appearance and valve performance metrics were compared before, during, and after fatiguing to assess the TEHV's durability. Valve performance and mechanical properties were compared to those from a commercially-available, pulmonary valve prosthesis (Medtronic Contegra valve).

2.3 Materials and Methods

2.3.1 Tissue Fabrication

A cell-entrapped, isotropic fibrin gel was formed by mixing bovine fibrinogen (Sigma), ovine dermal fibroblasts (Coriell), thrombin (Sigma), and calcium chloride.

Final component concentrations of the gel were as follows: 4 mg/mL fibrinogen, 1 million cells/mL, 0.38 U/mL thrombin, and 5 mM $CaCl_2$. This solution was injected into a tubular mold, formed by inserting a 19 mm glass rod into a concentric, polycarbonate tube (Figure 2-1a). The glass rods were pre-fitted with Dacron© cuffs on either end to aid in handling and pretreated with 5% Pluronic F-127 (Sigma) in double-distilled water.

Following gelation, the glass molds were removed from the polycarbonate outer casings and cultured in DMEM supplemented with 10% fetal bovine serum (FBS, HyClone), 100 U/mL penicillin, 100 μg/mL streptomycin, 0.25 μg/mL amphotericin B, 2 μg/mL insulin, and 50 μg/mL ascorbic acid. After two weeks, the tissue tubes were transferred onto 16 mm latex tubes, attached to custom manifolds, and cyclically stretched in a pulsed-flow-stretch bioreactor for 5 weeks [124]. Construct stretching began at 3% strain and was increased weekly by 1% until a 5% maximum strain was achieved.

2.3.1.1 Tissue Tube Decellularization

The tissue tubes were treated with 1% sodium dodecyl sulfate (SDS, Sigma) in distilled water for 6 hours (replaced after 1, 3, and 5 hours) at room temperature with continuous shaking. Following SDS treatment, the tubes underwent 3 x 10 minute washes in 1% Triton X-100 (Sigma) in distilled water at room temperature. The tubes were extensively rinsed in phosphate buffered saline (PBS) for one week at 4° Celsius before and after overnight incubation in DMEM supplemented with 10% FBS and 2 U/mL deoxyribonuclease (Worthington Biochemical).

2.3.2 Valve Fabrication

Four TEHVs were fabricated, each of which used two 16 mm inner diameter engineered tubes, which were trimmed to an axial length of either ~15 mm or ~12 mm. The tubes were sewn together, with the shorter tube inside of the longer tube, using absorbable 7-0 Maxon CV (Covidien) sutures. The pattern of the first suture line (Figure 2-2a, green dashed line) defined commissure and “leaflet” regions. Independent,

crosshatched suture lines were then added to reinforce each commissure (Figure 2-2a, purple dashed line) on the three subsequent TEHVs.

2.3.3 Pulse Duplicator Testing

Four TEHVs and one commercial pediatric pulmonary valve (Medtronic Contegra, 18 mm ID) were tested in a custom pulse duplicator system. One TEHV (no cross-hatching pattern) was used to assess root strain at different trans-root pressure gradients. These pressure gradients were prescribed by adjusting the ablumenal pressure on the TEHV, while maintaining the lumenal pressure and waveforms (by keeping the pump displacement constant). One TEHV was fatigued at pulmonary pressure conditions for two weeks real-time at 100 cycles/minute and was functionally characterized (with a higher flowrate) before, after 1 week, and at the conclusion of the fatiguing regimen. Two other TEHVs and the Contegra valve were functionally characterized, but not fatigued.

The pulse duplicator system consisted of a pulse generator, compliance chambers, and two flow loops (Figure 2-3a). The pulse generator pumped fluid through an electromagnetic flowmeter (Carolina Medical) and test valve before being returned to the reservoir in the primary flow loop, as previously described [123]. Unidirectional flow was ensured by placing a bileaflet, mechanical valve downstream of the reservoir. For these tests, a secondary flow loop was added that exited from the top of the fluid-filled chamber where the test valve was mounted (Figure 2-3a). A downstream needle valve controlled the trans-root flow and was used to regulate the pressure on the ablumenal surface of the test valve. System compliance, for both flow loops, was modulated by changing the fluid level in air-filled chambers upstream and downstream of the test valve. Additional information on the pulse duplicator system setup can be found in Appendix A.

Transducers (Vivitro Systems) were placed downstream, upstream, and on the ablumenal surface of the test valve to record system pressures. Instantaneous flowrates were measured using an electromagnetic flowmeter (Carolina Medical) placed between the pulse generator and test valve. Flowrates and system pressures were recorded using a custom LabVIEW program and analyzed using a custom Matlab script (see Figure 2-3b

for a representative waveform and Appendix A for the code). All pressure and flow metrics reported in Table 2-2 & Table 2-3 were averaged over 3 cycles for each valve. Diastolic pressure drop was defined as the average difference between the inflow and outflow pressures over the period of the cycle when the flowrate was less than or equal to zero. Systolic pressure drop was defined as the average pressure difference over the period of the cycle when the inflow pressure exceeded the outflow pressure. Mean forward flowrate is the average of the forward flow portion of the flow trace. Regurgitation refers to ratio of total negative flow to the stroke volume, or positive flow, for each cycle. Additional information on these metrics can be found in ISO 5840.

There was a "water hammer" effect during valve closure that resulted in a substantial pressure spike on the inflow side of the valve, though it is noticeable in all three pressure traces (Figure 2-3b). This pressure spike was noticeably larger in one of the TEHVs, which resulted in a higher diastolic pressure drop at the desired mean forward flowrate. The magnitude of the spike was reduced by increasing the ventricular compliance of the system. However, this resulted in a second positive flow pulse after the TEHV closed. Therefore, only the regions before this secondary pulse were used to calculate the mean diastolic pressure drop and regurgitation for this TEHV.

Lumenal and ablumenal videos of the test valve were recorded during testing at 50 fps (Canon Rebel T3i) and analyzed in ImageJ to assess geometric orifice area (GOA) and maximum root strain. GOA is defined as the ratio of the open area during systole to the maximum cross-sectional area of the valve leaflets. For this study, the maximum (viewable) cross-sectional area is dependent on the inner diameter of the silicone tubes (16 mm), which are attached to each end of the test valve and prevent paravalvular leak. Maximum root strain was taken as the natural logarithm of the maximum over the minimum root diameter, as determined in ImageJ.

2.3.4 Macroscopic Tissue Imaging & Histology

Valves were macroscopically visualized using a stereoscope (Leica StereoZoom 4) outfitted with a digital camera (Canon Rebel T3i). Images of the suture lines, as seen

from the ablumenal and lumenal surfaces, were captured before, during, and after valve testing. For histology, tissue strips were cut and fixed in 4% paraformaldehyde at 4° Celsius and frozen in OCT (Tissue-Tek) using liquid nitrogen. 9 μm cross-sections were sliced and stained with Lillie's trichrome and picrosirius red. Images were taken using a color CCD camera from an Olympus IX70 microscope at 4X magnification. For picrosirius red staining, the samples were placed between crossed plane polarizers during imaging.

2.3.5 Tensile Mechanical Testing

Strips, parallel ("circumferential") and orthogonal ("radial") to the circumference of the tubes, were cut (~2 mm x 12 mm) from the engineered tubes and mechanically characterized. Strips from the Contegra valve's leaflets and root were also characterized. The engineered tubes used for the TEHV were fundamentally the same, so separate "root" and "leaflet" mechanical properties were not reported. Sample dimensions were measured prior to testing using a digital caliper.

The strips were mounted in custom grips attached to the tester's actuator arms and straightened with a 0.005 N tensile load. Six preconditioning cycles were performed (0-10% strain) before the samples were strained to failure at 3 mm/min using an Instron MicroBionix (Instron Systems). Strain was calculated by taking the natural logarithm of the sample's deformed length over its initial length. Stress was defined as the force divided by the undeformed, cross-sectional area of the strip. Modulus and ultimate tensile strength (UTS) were taken as the slope of the linear region of the stress-strain curve and the maximum stress recorded, respectively.

2.3.6 Suture Retention Testing

The suture tension properties were also evaluated for the engineered tubes, in accordance with ISO 7198. Briefly, a 6-0 prolene suture was passed through the circumferential strips (~5 mm x 10 mm) 2 mm from the free edge. The suture was tied into a loop and then pulled at a rate of 50 mm/min axially, or orthogonal to the presumed fiber direction, through the strips using the Instron MicroBionix tester.

2.4 Results

2.4.1 Tissue Fabrication and Characterization

Engineered tissue tubes were fabricated by allowing entrapping ovine dermal fibroblast in a cylindrical fibrin gel (Figure 2-1a). The entrapped cells replaced the fibrin (Figure 2-1b, red stain) with circumferentially-aligned, cell-produced collagen (Figure 2-1b, green stain). Decellularization removed cell components, leaving a matrix-only engineered tube, as shown in Figure 2-1b. Collagen fibers were visualized by staining with picrosirius red and imaged under crossed plane polarizers (Figure 2-1c). The intensity of red is directly related to collagen packing and alignment [125].

The engineered tubes were tested for their tensile mechanical properties and compared to those for the Contegra valve, a commercial pediatric pulmonary valve (Table 2-1). The engineered tubes exhibited anisotropy, which is characteristic of native cardiovascular tissues. The thickness of the Contegra valve's leaflets (0.21 ± .03 mm) and root (0.76 ± 0.10 mm) were different than the thickness of the engineered tubes (1.35 ± 0.05 mm). The suture retention strength of the engineered tissue was 175 ± 54 grams force.

2.4.2 Tubular TEHV Fabrication and Characterization

TEHVs were fabricated by sewing 2 concentric, engineered tubes together using absorbable sutures in a prescribed pattern (Figure 2-2a). The geometry of the sewing pattern dictated the behavior of the inner tube when exposed to forward and reverse flow. The tubes were attached around their entire circumference by the first sewing pattern (purple line in Figure 2-2a). The three commissure regions (one is shown in Figure 2-2b) mechanically constrained the inner tube from collapsing near its free edge, analogous to the posts on a framed valve. The three commissure regions were reinforced with a second sewing pattern (green line in Figure 2-2a) to increase the number of anchor points. The three "leaflets", or regions between adjacent commissures on the inner tube, were not mechanically constrained at their free edge and collapsed inward to close the TEHV

when exposed to back pressure (Figure 2-2c). The outer tube functioned as the flow conduit of the valve and provided structural support for the inner tube (Figure 2-2a).

2.4.3 In Vitro Performance Testing

Three TEHVs and a control valve (Contegra valve) were tested in a pulse duplicator system (Figure 2-3a) at pulmonary conditions with a mean forward flowrate of 3.6 ± 0.2 L/min. A representative pressure and flow waveform is shown in Figure 2-3b and their line colors correspond with the pressure and flow sensors shown in Figure 2-3a. Each of the TEHVs tested had lower regurgitation and mean systolic pressure drop compared to the Contegra valve, as seen in Table 2-2. Additionally, the GOA for the Contegra valve (52%) was substantially lower than for the TEHVs (76% ± 15%) despite the Contegra valve's leaflets being much thinner. Representative still frames of the TEHV opening are shown in Figure 2-4. The TEHV fully closed (Figure 2-4a) during diastole and then began to symmetrically open (Figure 2-4b-d) before achieving maximum opening (Figure 2-4e) at peak systole.

2.4.4 Trans-Root Pressure Manipulation

TEHV root distention and valve function were assessed under various trans-root pressure gradients, ranging from 27.2 to 39.1 mmHg (Figure 2-5). Mean diastolic pressure drop and mean forward flowrate were ~15 mmHg and ~1.7 L/min for all cases, respectively. Maximum circumferential root strain ranged from 0.8% to 2.7% and was linearly dependent on the trans-root pressure gradient (Figure 2-5a). TEHV regurgitation and maximum GOA were maintained independent of trans-root pressure gradients (values remained within 4% of each other for all of the test cases reported) as shown in Figure 2-5b and 5c, respectively. These valve performance metrics were normalized by their respective values at maximum root distention (2.7%).

2.4.5 TEHV Fatiguing

One TEHV was fatigued in the pulse duplicator system for 2 weeks at 100 cycles/minute and a mean diastolic pressure drop of 7.4 – 8.7 mmHg. The mean forward

flowrate was only ~1.9 L/min, but the testing conformed to ISO 5840 in that the valve was able to fully open and close during each cycle. The entire TEHV was visually inspected using a stereoscope, but particular attention was given to the commissure regions as seen from the ablumenal and lumenal surfaces (Figure 2-6a). Macroscopic tissue damage was not detected before (Figure 2-6b-c), during (Figure 2-6d-e), or after (Figure 2-6f-g) fatiguing. It did appear that the suture lines, particularly the cross-hatched pattern, became looser over the course of fatiguing (Figure 2-6b, d, and f). However, the inner tube remained firmly attached to the outer tube (Figure 2-6c, e, and g).

TEHV GOA increased from 81% before fatiguing to 89% and 87% after 1 and 2 weeks, respectively (Table 2-3). One leaflet of the TEHV developed a slight prolapse during diastole after the first week of fatiguing. This development was represented by the increase in regurgitation from 3.9% to 12.9% (Table 2-3). However, the prolapse and regurgitation did not progress over the final week of fatiguing and did not lead to any observable tissue damage on the suture line.

2.5 Discussion

We have previously developed a TEHV using a single engineered tube attached to a frame [123]. This valve had characteristic anisotropic leaflet stiffness and performance at physiological conditions with a small systolic pressure drop and trivial regurgitation. However, the engineered tube was mounted onto a non-degradable frame, which made it suboptimal for pediatric patients since it precludes somatic growth. In this iteration of our TEHV, we have developed a frameless valve that is more suitable for pediatric patients since it has the potential to grow and remodel. It consists of two engineered tubes that were sewn together using degradable sutures. Since the sutures will completely degrade, host cell invasion will be critical to the TEHV's *in vivo* growth and remodeling potential.

Previous attempts at developing a valve from a single mold, with fibrin as the scaffold, have been reported by our group and others [81,83,121]. While these valve designs provided a proof of concept, there are several challenges associated with the single mold approach. One major challenge is creating leaflets with the appropriate initial

thickness while ensuring that coaptation and mechanical strength are maintained as the fibrin gel is contracted by the entrapped cells. Further challenges included machining complex molds and high stress on sharp corners of the mold, leading to thinning and tearing in the engineered tissue.

While tubular valve design addresses many of the challenges associated with the single mold design, it relies on the two engineered tubes fusing during *in vivo* remodeling. The sutures in the proposed design were selected based on their slow degradation rate, which will allow them to provide mechanical support during *in vivo* recellularization and tissue remodeling. In previous studies by our group using similarly decellularized tissue implanted as arterial grafts, we showed recellularization spanning the entire length (2-3 cm) of the graft after 8 weeks [126,127]. If the valve leaflets have similar host cell invasion and matrix deposition, then the timing of suture degradation and recellularization would match fairly well.

Demonstrating somatic growth by replacing the pulmonary artery using a vascular graft made from degradable polymers has been tested in a lamb model. In the study by Hoerstrup *et al.*, a degradable polymer graft was seeded with autologous cells from a lamb and evaluated for growth and remodeling [128]. The graft was harvested after 100 weeks and it showed progressive growth, complete degradation of the synthetic polymer, and host tissue replacing the entire structure of the graft. Another study reported remodeling and an increase in size of a synthetic polymer graft seeded with bone marrow mononuclear cells over 6 months implanted into the inferior vena cava of a lamb [129].

Based on these two studies and our previous arterial graft study [126,127], we expect our tissue to be amenable to host cell invasion. To ensure that our proposed valve design is capable of withstanding the initial phase of cellular ingrowth and suture degradation, we performed several *in vitro* tests to assess its durability. The most relevant test was to fatigue the TEHV at pulmonary pressure conditions (i.e. physiologic end-diastolic pressure drop with complete valve opening and closing). This testing was performed for more than 2 million cycles and there was no noticeable change in the

sutures, tearing, or tissue damage. However, one leaflet developed a slight prolapse, possibly due to asymmetry in the "leaflets" as sewn or prolonged exposure to the water-hammer effect, which led to increased regurgitation after 1 week. While longer testing could have been performed, we consider this number of cycles to be sufficient to assess the TEHV's current design. Important questions regarding the TEHV's growth, remodeling, and tissue fusion cannot be answered with *in vitro* fatigue testing.

While this is the first tubular valve design using two completely-biological engineered tubes, other groups have explored tissue-engineered valves with various designs. One design from Weber *et al.* embedded a knitted, non-degradable, synthetic polymer tube within a cell-containing fibrin gel in a tubular geometry [88,92]. These proof of concept studies were done by connecting the fibrin/polymer mesh to a silicone outer tube or nitinol stent to generate "leaflets". The advantage of this approach is that the initial strength of the synthetic polymer provides a durable anchor for attachment, while still providing a biological matrix for cellular remodeling. However, mechanical anisotropy similar to native leaflets was a critical design criterion in our approach and the inclusion of any polymer mesh would preclude fibrin gel compaction and associated mechanical anisotropy. The suture retention strength of our engineered tissue allowed us to sew the tubes together without synthetic polymer reinforcement. Compliance mismatch in a composite structure could also have detrimental effects during fatigue testing or during *in vivo* testing, which was not reported. Moreover, their design using a non-degradable, synthetic polymer tube or inert stent would not be suitable for pediatric applications.

Functionally, we evaluated the tissue-engineered valve in a pulse duplicator and compared the values to a commercial pediatric pulmonary valve (Contegra 18 mm diameter conduit, Medtronic). One of the critical parameters for a pulmonary valve replacement is its systolic pressure drop. While the engineered (ovine) tissue used in this study was much thicker than the Contegra valve's leaflets, the systolic pressure drop of the TEHV was lower than the Contegra's under similar testing conditions. This was

potentially due to the non-fixed, compliant nature of the engineered matrix. Regurgitation (including closing volume) is another critical parameter and was also lower in our TEHV compared to the Contegra valve.

We also evaluated the effects of variable trans-root pressure gradients to ensure that valve coaptation, maximum valve opening, and regurgitation were not adversely affected. This is relevant because certain congenital defects can lead to pulmonary artery hypertension, which is defined as when the mean pulmonary pressure exceeds 25 mmHg *in vivo* [130,131]. Theoretical outer diameters were calculated (data not shown) using the Law of Laplace for thick-walled right cylinders [132], but did not fully agree with the measured values. Several aspects of the test system could account for these differences, such as the "wall" being non-continuous due to the presence of separate inner and outer tubes. Additionally, the relatively small axial length to diameter aspect ratio of the TEHV and the presence of suture lines could account for some of the differences observed.

Overall, the pulse duplicator testing and fatigue testing provide strong evidence that the current valve design will exhibit excellent initial performance in the pulmonary position. Whether the valve remodels to same extent as seen previously in arterial position remains to be seen and will be the focus of a subsequent *in vivo* study.

2.6 Acknowledgement

Authors acknowledge technical assistance from Naomi Ferguson, Sandy Johnson, Susan Saunders, and Jill Schmidt and funding from NIH R01 HL107572 to R.T.T. Reprinted from Biomaterials, 62, J. Reimer, Z. Syedain, B. Haynie, and R. Tranquillo, Development of a Tubular Biological Tissue-Engineered Heart Valve with Growth Potential, Pages 88-94, Copyright (2015), with permission from Elsevier.

2.7 Chapter 2 Figures and Tables

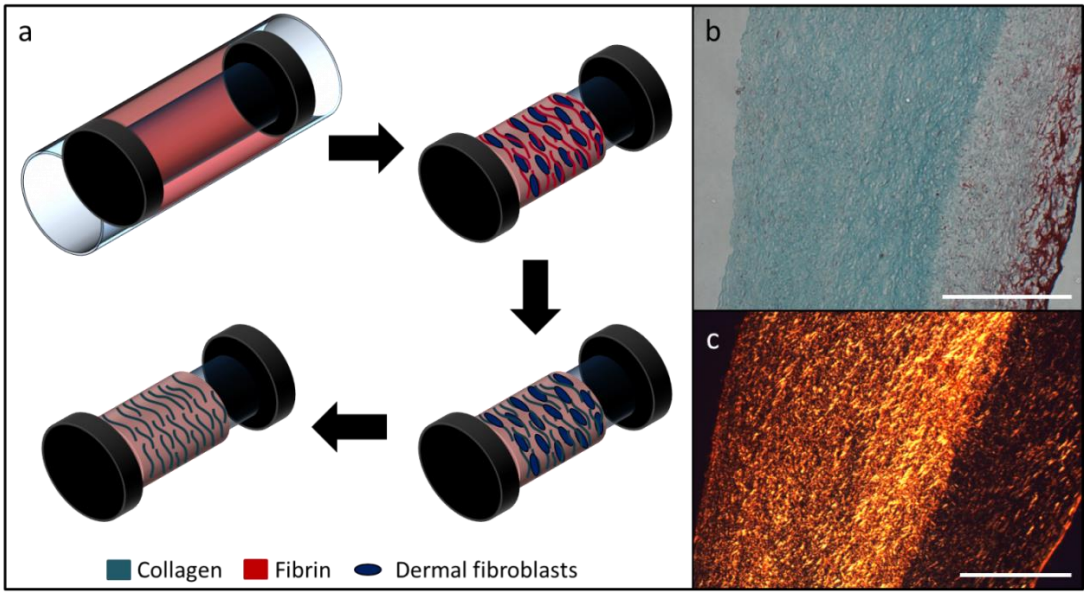

Figure 2-1. *In vitro* tissue fabrication and histology

(a) Tissue tube fabrication schematic. The entrapped dermal fibroblasts replace the initial fibrin gel with an aligned, collagenous matrix. The cell-produced matrix is left intact following decellularization. (b) Trichrome staining showing collagen (green) and non-collagen (fibrin, red) after decellularization. (c) Picrosirius red staining under crossed plane polarizers showing collagen fiber organization. Both scale bars are 500 μm.

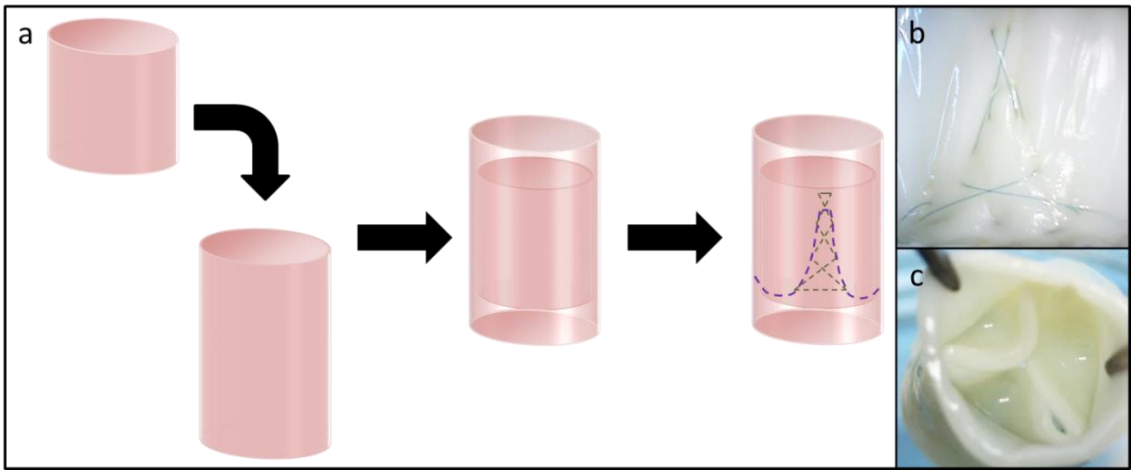

Figure 2-2. Valve fabrication schematic and macroscopic images

(a) Schematic of a frameless tubular heart valve made from two concentric, engineered tissue tubes. They are attached using a degradable suture line (purple) that defines belly and commissure regions. (b) The commissure regions are reinforced with a secondary crosshatching pattern (see also green dashed line in (a)). (c) The inner tube collapses inward between the three commissures when the valve is exposed to back pressure, which generates three "leaflets" and a valve-like action.

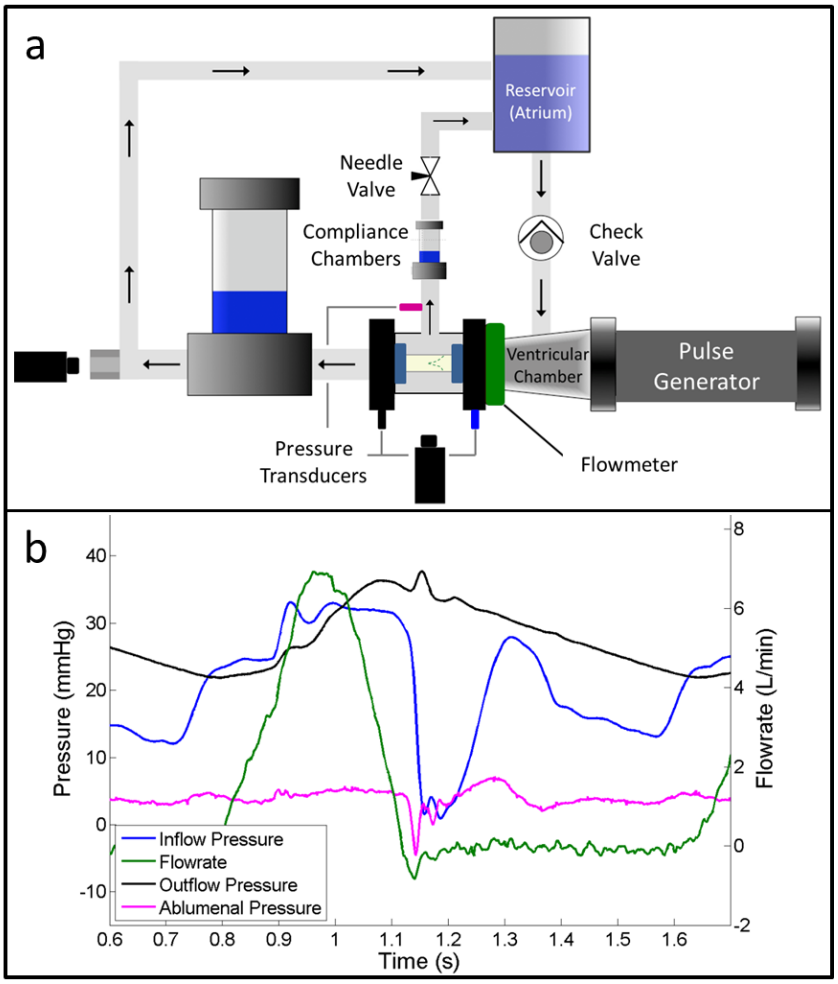

Figure 2-3. Pulse duplicator schematic and waveform

The TEHVs were tested using (a) a custom pulse duplicator system, which allows valve root distention and trans-root flow. The valve test chamber is fluid-filled and is connected to the reservoir through a secondary flow loop. (b) A representative flow-pressure trace is shown under pulmonary conditions. The locations of pressure probes and corresponding pressure traces are color coded in the panels. A water hammer effect typical in pulse duplicator systems affects all of the pressure traces, but is most evident in the inflow pressure (at time = ~1.15s).

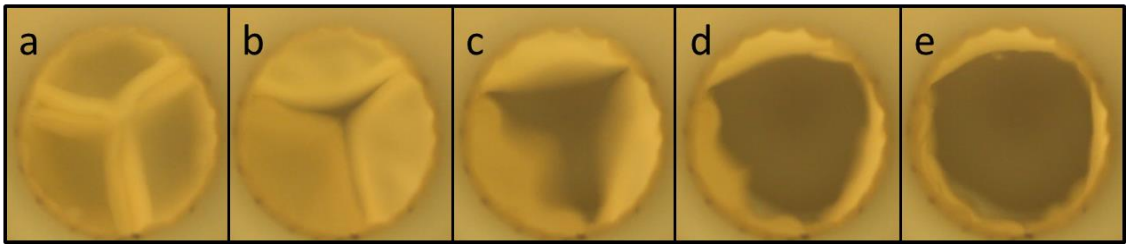

Figure 2-4. Leaflet motion during pulse duplicator testing

Images of leaflet motion during valve testing in a pulse duplicator system under pulmonary flow conditions. (a) Leaflet coaptation is maintained during diastole, but (b-d) rapidly opens as systole begins. (e) Full valve opening is achieved before the leaflets begin to close.

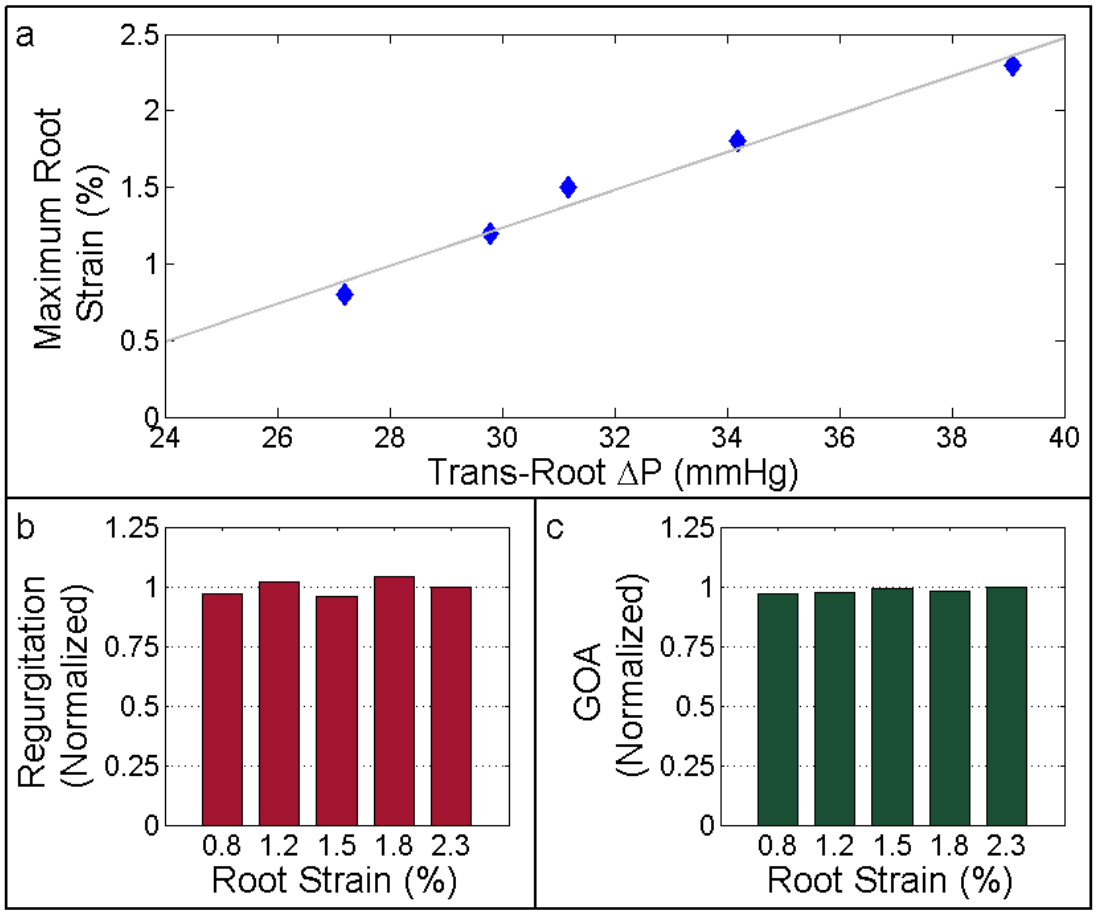

Figure 2-5. *In* vitro TEHV function versus trans-root pressure gradient

Ablumenal pressure was manipulated to assess TEHV performance under various trans-root pressure gradients. (a) TEHV root strain shown as a function of the trans-root pressure gradient. TEHV (b) regurgitation and (c) geometric orifice area are normalized to their respective values using the maximum trans-root strain/pressure gradient case.

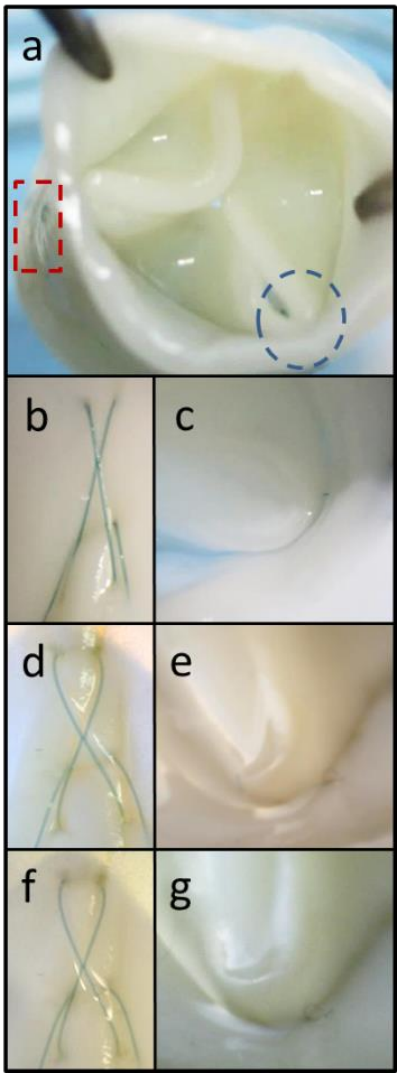

Figure 2-6. Macroscopic images from TEHV fatiguing

Macroscopic images of a TEHV fatigued in the pulse duplicator system for 2 weeks at 100 cycles/minute. Images were taken near the commissures on the (a, rectangle) ablumenal or (a, circle) lumenal surface. The TEHV was macroscopically analyzed at the same locations (b-c) before fatiguing, (d-e) after 1 week, and (f-g) following completion of testing at 2 weeks.

Table 2-1. Tensile mechanical properties of a bioprosthetic commercial valve and engineered tubes

Property	Contegra Valve	Engineered Tubes
Leaflet Thickness (mm)	0.21 ± 0.03	1.35 ± 0.05
Leaflet Circumferential UTS (MPa)	3.3 ± 1.1	1.5 ± 0.4
Leaflet Circumferential Modulus (MPa)	12.6 ± 1.8	5.2 ± 0.6
Leaflet Modulus Anisotropy	N/A	3.8 ± 0.9
Root Thickness (mm)	0.76 ± 0.10	1.35 ± 0.05
Root Circumferential UTS (MPa)	3.4 ± 0.3	1.5 ± 0.4
Root Circumferential Modulus (MPa)	6.5 ± 0.1	5.2 ± 0.6
Root Modulus Anisotropy	1.0 ± 0.1	3.8 ± 0.9

Table 2-2. Pulse duplicator testing of TEHVs compared to a commercial bioprosthetic valve

Property	Contegra Valve	TEHVs (n=3)
Mean Diastolic ΔP (mmHg)	16.5	14.5 ± 3.7
Mean Systolic ΔP (mmHg)	3.3	2.4 ± 0.1
Mean Ablumenal Pressure (mmHg)	4.3	3.5 ± 0.7
Mean Forward Flow Rate (L/min)	3.4	3.6 ± 0.2
Regurgitant Fraction	7.3%	4.8% ± 0.8%
Geometric Orifice Area	52%	76% ± 15%

Table 2-3. Pulse duplicator testing before, during, and after TEHV fatiguing

Property	T = 0 weeks	T = 1 Week	T = 2 weeks
Mean Diastolic ΔP (mmHg)	13.2	11.9	11.4
Mean Systolic ΔP (mmHg)	2.5	1.8	3.1
Mean Ablumenal Pressure (mmHg)	4.0	3.0	1.4
Mean Forward Flow Rate (L/min)	3.6	3.2	3.8
Regurgitant Fraction	3.9%	12.9%	13.8%
Geometric Orifice Area	81%	89%	87%

Chapter 3. Somatic Growth of "Off-the-Shelf" Tissue-Engineered Pediatric Conduit in the Lamb

3.1 Summary

Treatment of congenital heart defects requiring right ventricular outflow tract (RVOT) reconstruction typically involves multiple open-heart surgeries for growing patients. We developed an “off-the-shelf” (acellular) tissue-engineered vascular graft to address this critical unmet need. The grafts were implanted as a pulmonary artery replacement in young lambs and evaluated to adulthood. Longitudinal ultrasounds showed dimensional growth with laminar flow, no pressure gradient, and normal right heart function. Body weight increased 366%, while graft diameter and volume increased by 56% and 216%, respectively. Explanted grafts had physiological strength and stiffness with anisotropic mechanical properties due to designed circumferential matrix alignment. The total collagen content increased by 465%, with substantial elastin deposition. Grafts developed complete endothelialization of the lumen and were extensively populated by mature smooth muscle cells. Further, the grafts showed no evidence of calcification, aneurysm, or stenosis. Collectively the data support somatic growth of this completely biological graft grown from cells.

3.2 Introduction

Surgical correction of congenital heart defects has increased dramatically over the last several decades. These defects, considered fatal just 30 years ago, can now often be successfully corrected with overall operative mortality of less than 2 % [133,134]. Reconstruction or replacement of blood vessels, valves, and cardiac chambers is often required to repair or reform the appropriate anatomic configuration. The use of synthetic materials, with zero growth potential and unpredictable durability, is often the only way to achieve these operative goals. The availability of tissue-engineered material, with the ability to grow, heal, and provide long-term durability, would revolutionize the practice of congenital heart surgery.

Tetralogy of Fallot and pulmonary atresia with ventricular septal defect are just two examples of cardiac defects that, although long-term survival is excellent, will often require multiple operative procedures to replace the reconstructed connection between the right ventricle and pulmonary artery (PA). Currently, homograft pulmonary artery conduits or bovine jugular vein grafts are the only materials sufficient to create this connection. These conduits have zero ability to grow and remodel with the somatic growth of the child. Additionally, an intense inflammatory reaction to these materials often occurs, resulting in early calcification and failure [135]. Thus, these patients will sometimes require 5 to 7 operative procedures during their lifetimes even with a "successful" corrective procedure [136]. While a valved conduit would benefit a larger patient population, and several researcher groups are working on such grafts [93,99,118,137-139], a conduit with the ability to grow somatically would suffice for many patients with competent valves but requiring cardiopulmonary vascular reconstruction. It might also possibly be a compromise solution for patients in need of a valved conduit absent the availability of one with growth potential.

The application of a competent, readily available conduit, with the ability to grow with the child, would eliminate the need for multiple operations and the morbidities associated with these procedures. It could benefit more than 1,000 pediatric patients

annually in the US [136]. It would also dramatically reduce the financial burden on the health care system associated with currently used conduits that require periodic replacement to accommodate child growth.

Pioneering research in this field has been conducted by Shin'oka, Breuer, and colleagues with the landmark report of reconstruction of an occluded pulmonary artery in a 4-year old patient with a degradable synthetic polymer tube (PLA/PCL) seeded with autologous cells [140]. In a subsequent clinical trial, similar grafts seeded with autologous bone marrow mononuclear cells were implanted into 42 patients (median age 5.5 years) [141]. There was no graft-related mortality with mean follow-up of 5.8 years although one patient had a partial mural thrombosis, and four patients had graft stenosis [142]. Recently, they reported histological examination of one graft evaluated after 12 years in a patient (implanted at age 4 years), showing graft remodeling with complete lumen endothelialization and a mature smooth muscle wall [143]. In addition, investigators have conducted extensive research in the mouse model to elucidate the role of the seeded cells and the host response [129,144-150].

In another sheep study, again using autologous cells seeded on a synthetic polymer scaffold, Hoerstrup and colleagues implanted 18 mm diameter PGA/P4HB tubes seeded with autologous myofibroblasts into lambs as arterial replacements for up to 240 weeks [128,151]. Longitudinal CT imaging and explant histology revealed extensive remodeling and graft growth.

Both of the above approaches, while successful in pre-clinical and clinical studies, respectively, require autologous cells to be isolated from the patient and expanded prior to implantation. An "off-the-shelf" graft that is both acellular and possesses growth potential via host cell invasion post-implantation, as reported herein would be a significant clinical advancement. In addition, an acellular graft would eliminate the need to develop a manufacturing process to isolate autologous cells and reliably seed them onto the scaffold in order to translate the technology into the clinic.

The goal of this study was to demonstrate proof-of-principle for an "off-the-shelf" graft that is capable of somatic growth. The completely-biological tubular grafts, consisting primarily of cell-produced collagen, were derived from a sacrificial fibrin gel, which was remodeled in a bioreactor by entrapped dermal fibroblasts. Following this remodeling, the tubes were decellularized, which, when done effectively, removes the need for immunosuppression, but maintains the cell-produced matrix. The graft was grown to be strongly aligned in the circumferential direction in order to mimic the mechanical anisotropy associated with native arteries. These 16 mm diameter acellular allografts were characterized, stored, and then implanted into 3 lambs (average age 8 weeks), tracked longitudinally with ultrasound, and then explanted after the lambs reached adult size (age 50 weeks) for mechanical, biochemical, and histological characterization.

3.3 Methods

3.3.1 Engineered Tissue Tubes

Ovine dermal fibroblast (oDF)-seeded fibrin gels were formed by adding thrombin (Sigma) and calcium chloride in 20 mM HEPES-buffered saline to a suspension of cells (oDF from Coriell) and bovine fibrinogen (Sigma). The final component concentrations of the suspension were as follows: 4mg/ml fibrinogen, 0.38U/ml thrombin, 5.0 mM Ca^{++}, and 1 million cells/ml. The suspensions were mixed and injected into a tubular glass mold. The tubular grafts were cultured statically for 2-weeks and then transferred to custom pulsed-flow-stretch bioreactors for an additional 5-week maturation period as previously described [124].

Following bioreactor conditioning, the tubes were decellularized. First the tubes were placed on an orbital shaker at room temperature for 6 hr with 1% sodium dodecyl sulfate (SDS, Sigma) followed by 1% Triton X-100 (Sigma) for 30 min, extensively washed with PBS for 2 weeks at 4C, and then incubated at 37C in 2U/ml

deoxyribonuclease (Worthington Biochemical, DR1) in DMEM supplemented with 10% FBS overnight. Grafts were sterilely stored at 4C until use in phosphate buffer solution.

3.3.2 Graft Implant in Growing Lamb Model

Tissue-engineered ovine grafts were implanted as pulmonary artery replacements in n=3 Dorset lambs (average weight 15.3 kg, age at implant: 8.4 weeks). All protocols were approved by the Institutional Animal Care and Use Committee of the University of Minnesota and conform to NIH guidelines on Care and Use of Laboratory Animals. The surgeries were performed by the University of Minnesota's Experimental Surgical Services. For all animals, anesthesia was induced by administering 10mg/kg Ketamine (IM) and 2-6 mg/kg propofol (IV). Animals were then intubated and maintained on isoflurane at 1-3% for the duration of surgery and monitored for heart rate, mean blood pressure, fixed pupil location, corneal reflex absence, and oxygen saturation to ensure proper anesthesia. The heart was exposed by a left lateral thoracotomy with dissection through the intercostal space. The animal was heparinized (250IU/kg, IV) and placed on cardiopulmonary bypass. The grafts were implanted interpositionally using continuous 5-0 Maxon CV (Covidien) degradable sutures after excising a similar length of the native main pulmonary artery. The native pulmonary valve was left intact. In addition, prolene sutures were used to attach two silver clips on the native pulmonary artery near the anastomoses to serve as markers (Fig 1f).

Post-surgery, animals received subcutaneous 750IU heparin BID for the duration of the study. For pain, animal received ketoprofen 1-2mg/kg (IM) every 12-24 hours as directed by the post-operative veterinarian. Additionally slow release buphenorphine 0.27 mg/kg (SQ) was given prior to induction of anesthesia. Animals for the study were numbered as PAC1, PAC2, and PAC3. The first ultrasound was performed 8 weeks following implantation. The second and third ultrasounds were done when the animals were 30 weeks old and prior to euthanasia at 50 weeks of age, respectively Conduit dimensions, pressure drop, flow velocity and flow profile (laminar or turbulent characteristics) were measured from the ultrasound. Animals were heparinized

(300IU/kg, IV) and then euthanized with beuthanasia given intravenously at 87-90 mg/kg. Explanted grafts were photographed, and then dissected into strips for histological, biochemical, and mechanical characterization.

3.3.3 Mechanical Testing

Tissue strips were cut from the engineered tissue tube and native pulmonary artery prior to implant and following explant with dimensions of ~2 mm x 10 mm in both the circumferential and axial directions. Following explant, additional axial strips were cut that consisted of half native pulmonary artery and half engineered tissue from the anastomotic regions. All samples were measured for dimensions and then tested for tensile mechanical properties using an Instron mechanical testing system and compression grips. The tangent modulus (E) was defined as the slope of the linear region of the stress-strain curve prior to failure. The peak stress was defined as ultimate tensile strength (UTS). Mechanical anisotropy was defined as the ratio of the modulus of tissue samples cut in the circumferential direction to the modulus of samples cut from the tissue in the axial direction.

3.3.4 Tissue Composition and DNA Analysis

The collagen mass content was quantified using a hydroxyproline assay previously described [152] assuming 7.46 mg of collagen per 1 mg of hydroxyproline. Insoluble elastin was measured by dissolving tissue samples in NaOH and using a modified ninhydrin assay to measure elastin [153]. The total protein content was measured using the ninhydrin assay [121]. The tissue volume was calculated using the measured length, width, and thickness of the samples. For total collagen content of the graft, length, width and thickness of implanted and explanted construct were used to measure total volume of the graft. Average collagen concentration for each graft, obtained from the tissue strips, was used to estimate total collagen, protein and elastin contents. The DNA content was quantified with a modified Hoechst assay for total DNA [154].

3.3.5 Histology and Immunostaining

Each explanted graft was histologically and immunologically stained; multiple strips were cut to cover all regions of interest. Circumferential and axial tissue strips of pre-implant and explanted grafts were fixed in 4% paraformaldehyde, embedded in OCT (Tissue-Tek), and frozen in liquid N_2. Cross sections of 9-μm thickness were stained with Lillie's trichrome, Verhoeff-Van Gieson elastin stain, and picrosirius red stain. Histological sections were also immunostained for αSMA (Sigma, A5228), Calponin (Abcam ab46794), vimentin (Abcam, ab80667), Von Willebrand Factor vWF (Abcam ab6994), CD45 (US Biological C2399-07B), elastin (Abcam ab21599), and collagen IV (Abcam, ab6586). All samples were blocked with 5% normal donkey serum, incubated in primary antibody at 2.5-5ug/ml and stained with a Cy5-conjugated, species-matched secondary antibody (Jackson Immunoresearch). Nuclei were counterstained with Hoechst 33342 (Invitrogen H3570).

3.3.6 Statistics

Statistical significance for differences between two groups was determined using Student's t-test when comparing two groups and ANOVA with tukey post-hoc analysis for more than two groups. Paired symbols are used in figures to represent statistical difference. Any reference to a difference in the Results and Discussion sections implies statistical significance at the level $p< 0.05$.

3.4 Results

3.4.1 Tissue-engineered Arterial Graft

Decellularized tissue-engineered tubes (16mm inner diameter), were evaluated for tensile mechanical and biochemical properties. The resulting tubular grafts had thicknesses of 1.21±0.03 mm, which was comparable to the pulmonary artery (1.15±0.20 mm). A representative end and side view of the graft are shown Figure 3-1a,b. Histologically, the grafts were predominantly collagen with a layer of residual fibrin on the lumenal surface (Figure 3-1c). Stretch-to-failure testing showed the grafts possessed

an ultimate tensile strength of 1.9±0.2 MPa and stiffness of 3.6±1.2 MPa (Figure 3-1d) in the circumferential direction. The tissue tubes also possessed mechanical anisotropy, with stiffness being 4.5-fold higher in the circumferential direction than the axial direction. All of these values compared favorably to the ovine pulmonary artery. The total collagen concentration prior to implantation was 38±5 mg/ml (Figure 3-1e). The DNA content after decellularization was less than 99% compared to the graft before decellularization.

The grafts were implanted interpositionally into to the pulmonary artery (Figure 3-1f), following resection of a similar length of native artery, in three lambs. 5-0 Maxon™ CV biodegradable sutures (*in vivo* strength half-life of 4 weeks) were used to attach the graft to the pulmonary artery at the anastomoses. In addition, to ensure anastomoses could be identified at explant, silver clips were sewn on top of the native artery near each anastomosis (Figure 3-1f).

3.4.2 Growth Evaluation of Pulmonary Artery Graft with Ultrasound

All animals were first evaluated with ultrasound at 8 weeks following implantation to access graft diameter, graft length, blood velocity in the graft, and right heart function. Figure 3-2a shows a representative image of the graft 8 weeks after implant with red arrows indicating the anastomoses. The grafts, although originally implanted as straight tubes, showed curvature similar to the native pulmonary artery after 8 weeks. The second and third ultrasounds were performed when the lambs reached the age of 30 and 50 weeks, respectively. Figure 3-2b shows a representative image of the grafts at 50 weeks, with prominent curvature, no indication of calcification (speckles in ultrasound), and no evidence of graft stenosis or aneurysm. This was true for all three grafts (Supplemental Figure 3-1). All animals had healthy weight gains with an increase of 340% over the course of study (Figure 3-2c). The mid-graft diameter increased over the course of implantation by 56% (Figure 3-2d) and total volume of the graft increased by 216%, as determined by measurements in ultrasound (Figure 3-2e). There was no pathological increase in flow velocity measured within the graft during the study

duration, indicating a lack of stenosis (Figure 3-2f). The flow though the graft was laminar throughout the course of the study with no pressure gradient across the graft. The right heart function was also normal with no change in wall motion or pulmonary valve function.

3.4.3 Explanted Graft Gross Pathology

All grafts were explanted when the animals were anatomically mature at age of 50 weeks. Grossly, the explanted grafts looked larger in both diameter and length when compared to the pre-implant graft. Figure 3-3a,b shows the pre-implanted and explanted rafts at the same scale (Supplemental Figure 3-2 shows images of all grafts at implant and explant). The measured diameter and length of each graft at implant and explant is reported in Table 3-1.

The explanted grafts had a diameter consistent with the adjacent pulmonary artery (Figure 3-3b). The average wall thickness of the right ventricle was 6.3±0.6 mm (Figure 3-3c). Cross-sections of the explanted graft showed homogeneous thickness across the length (Figure 3-3d, red arrows indicating lumenal and ablumenal surfaces). The anastomotic regions had no scarring or stenotic tissue and the lumenal surface transitioned smoothly from the native artery to the engineered graft.

3.4.4 Explanted Graft Mechanical and Biochemical Properties

The explanted grafts were cut into strips and stretched-to-failure. Graft thickness was 0.85±0.09 mm as compared to pulmonary artery thickness of 1.15±0.2 mm. The explanted graft stress-strain curves in the circumferential and axial directions, along with the pre-implant graft curves, are shown in Figure 3-3e. The graft UTS and modulus in the circumferential direction were 1.5-2 fold higher than pulmonary artery (Figure 3-3f,g) with UTS in the circumferential direction of 1.6±0.5 MPa and modulus of 3.3±0.8 MPa. The modulus was 1.8 fold higher in the circumferential direction compared to the axial direction. In order to assess how mechanically robust the fusion at the anastomoses was and any influence of scar tissue formation, axial strips from this region were compared to axial strips from the graft and the adjacent pulmonary artery (Figure 3-4a). UTS,

maximum tension, and modulus were not different between the three regions (Figure 3-4b-d).

The explanted graft DNA content was 58% of the pulmonary artery value, corresponding to a cell concentration of 119±15 million cells/ml (Figure 3-4e). The total collagen and elastin content in the grafts were 180% and 49% of the pulmonary artery, respectively (Figure 3-4f). The total protein content was 80% of the pulmonary artery (Figure 3-4f). Based on collagen concentration, total surface area, and thickness measured for implanted and explanted grafts, the total collagen content of the explanted grafts was 224±51 mg, which was 465% higher than total collagen content of the pre-implanted grafts (40±7 mg). There was also 277% increase in total protein content of tissue. Compared with pre-implant grafts, which had no detectable level of elastin, explanted grafts contained substantial elastin (Figure 3-4g).

3.4.5 Explanted Graft Histological Analysis

The explanted graft and pulmonary artery sections were stained to visualize the matrix composition. Trichrome staining showed complete remodeling of the lumenal fibrin layer into a dense collagen network and evidence of recellularization along the entire graft's length (Figure 3-5e). Further characterization with picrosirius red staining imaged under polarized light showed crimped collagen fibers similar to the pulmonary artery (Figure 3-5b,f). Elastin was present throughout the entire pulmonary artery (Figure 3-5i) and graft (Figure 3-5j), with evidence of mature elastin near the lumenal surface of the graft (Figure 3-5g), The basement membrane protein collagen IV was strongly expressed at the lumenal surface of the pulmonary artery (Figure 3-5d) and the graft (Figure 3-5h). Von Kossa staining showed no evidence of calcification along the entire length of the grafts (Figure 3-5k), except at localized sites near the anastomoses in the adjacent pulmonary artery where the sutures had degraded.

Immunostaining was performed in order identify the phenotype of the invaded host cells and then counterstained with Hoechst. Complete recellularization across the entire thickness and length of the grafts was observed (Figure 3-6). The absence of

CD45-expressing cells indicated a lack of immune cell types in the pulmonary artery (Figure 3-6a) and the explanted graft (Figure 3-6b).

The majority of the cells present stained positive for α-smooth muscle actin (α-SMA) and calponin (Figure 3-6c-f), which are two markers for smooth muscle cells. The grafts had a complete endothelial cell layer, as evidenced by the uniform expression of Von Willebrand factor (vWF) along both the pulmonary artery (Figure 3-6g) and the entire length of the graft (Figure 3-6h). Further evidence of native-like tissue organization was observed when cells were imaged for calponin in both the circumferential and axial directions, showing elongated cells aligned in the circumferential direction (Supplemental Figure 3-3).

3.5 Discussion

Tissue engineering has the potential to overcome the limitations of existing treatments for congenital cardiovascular defects. An ideal treatment option would be durable, not prone to calcification, and possess the potential to somatic growth. To this end, two groups have previously demonstrated growth potential of synthetic biodegradable grafts seeded with autologous cells [128,129,151,155]. The studies by Shin'oka *et al* led to a clinical trial in which 24 patients were enrolled [141]. While they have shown promising results, their approach relies on isolating and seeding the conduits with autologous cells prior to implantation. If growth and remodeling could be demonstrated with an "off-the-shelf" (acellular) conduit, this would simplify the procedure and the GMP-regulated manufacturing processes to prepare the grafts for clinical use.

Herein, we report an "off-the-shelf" pulmonary artery replacement capable of growing and remodeling. This study builds on our prior research, which used decellularized engineered tissue tubes as femoral artery grafts and tubular aortic heart valves in an adult sheep model. Both studies demonstrated excellent graft remodeling and function out to 24 weeks [111,126]. Based on the complete recellularization and mechanical durability of the completely biological matrices found in these studies, we

undertook this study to investigate the growth potential of the matrix by implanting anatomically-matched 16 mm diameter grafts as a pulmonary artery replacement in lambs. The animals were evaluated from average ages of 8 weeks to 50 weeks, with maximum graft implant duration of 44 weeks.

Over the course of the study, all animals were asymptomatic and showed healthy weight gain. To reduce the risk of clotting as a potential failure mode in our assessment of somatic growth potential of our tissue-engineered matrix, subdermal heparin was utilized for the duration of this study, based on our prior aortic valve implant experience [111]. No complications, bruising, or bleeding were seen in any animal with anticoagulant therapy for the duration of study. Normal right heart function was observed with ultrasound 8 weeks post-surgery and at animal ages of 30 and 50 weeks.

Since we used biodegradable sutures that have a 4 week half-life, rapid host cell invasion and subsequent matrix deposition were necessary to fuse the anastomoses. Since we saw a uniform flow tract in all animals at all time points, it was apparent that the matrix fused with the pulmonary artery at the anastomoses prior to suture degradation. Although the exact timeline of cell invasion and fusion isn't known for this study, we have previously shown that grafts harvested after 8 weeks in the femoral artery position had complete endothelial coverage near the anastomoses and invasion of α-SMA positive cells from the surrounding tissue [126]. Hence, it was not surprising in this study that sufficient extracellular matrix was deposited to ensure fusion at the anastomoses before the critical suture degradation point.

While the grafts were implanted as straight tubes, curvature around the aorta (as seen in the native pulmonary artery) was observed in the first ultrasound following implantation (8 weeks). Initially, this would most likely be due to physical forces on the graft; however, the cells invading the matrix remodeled the graft over time, while maintaining this physiological geometry.

Importantly, graft diameter and length increased over the duration of implantation to the same degree as seen in the adjacent pulmonary artery. The uniform growth of the

graft in all three animals contributed to the laminar flow profiles and no pathological pressure gradient across the grafts based on ultrasound examination. For comparison, in a growing lamb study using synthetic PTFE conduits, a 20 mmHg increase in pressure gradient developed within one year of implantation [156]. At the 50 week ultrasounds, it was challenging to visually discern the actual anastomotic locations as there was no narrowing, dilation, or other markings to differentiate the graft and pulmonary artery, which had indistinguishable diameters. Evaluation of the explanted grafts confirmed uniform growth with diameters matching the adjacent artery and no difference in axial mechanical properties between the native artery above the graft, the anastomotic region, and the graft.

The explant graft volume increased by 216% over the course of implant, which was comparable to 244% volumetric increase of the pulmonary artery measured by Gottlieb *et al* with MRI [101]. For animal weight gains from 15 kg to 65 kg, they also reported cross-sectional area of the pulmonary artery increased from ~300mm^2 to ~600mm^2, or a ~42% increase in diameter, which is also comparable to the 56% increase in diameter observed for our graft.

The strongest evidence of growth was seen when evaluating the mechanical property measurements and total collagen content together. No substantial change in mechanical properties between pre-implant and post-implant graft was seen even though the graft volume increased by 216%. This was most likely due to 465% more collagen measured in the explanted grafts, which appeared highly organized. Additionally, the new collagen was apparently deposited with the same circumferential alignment as the pre-implant graft, since strong mechanical anisotropy existed in the explanted tissue. In comparison, autologous cell-seeded polymeric grafts implanted by Hoerstrup *et al* showed significantly higher stiffness of explanted grafts compared with pulmonary artery; however, no anisotropic properties were reported [128].

Histologically, the graft exhibited substantial host cell invasion and deposition of matrix proteins comparable to the pulmonary artery. Although the pulmonary artery had

~42% more cells, histological comparisons showed that the explanted grafts also contained mature, circumferentially-aligned smooth muscle cells and a complete endothelium and basement membrane.

In our explanted grafts, elastin content was at 49% compared to pulmonary artery, with mature elastic fibers visible with Verhoeff's stain. In a previous growing lamb model, Hoerstrup *et al* did not measure elastin and detected none via histology [128]. Brennan *et al* showed 47.2% more elastin deposition when synthetic polymer scaffold was pre-seeded with autologous cells compared to a cell-free scaffold [129]. In comparison to pulmonary artery, Brennan *et al* reported elastin content at 51% in their pre-seeded grafts after 26 weeks of implantation [129]. Taking mature elastin as a marker for positive growth and remodeling, this acellular cell-produced matrix tube can thus remodel similar to pre-cellularized polymer grafts reported in previous studies.

Overall, this is the first report of an "off-the-shelf"' tissue-engineered vascular graft implanted in a growing lamb model that exhibited somatic growth and normal physiological function for nearly one year. All three implanted grafts were extensively recellularized (including complete endothelialization), with organized collagen and elastin deposition, and no evidence of calcification or aneurysm. They may thus serve as permanent conduits for RVOT repair.

3.6 Acknowledgements

Authors will like to acknowledge technical assistance of Naomi Ferguson, Sandra Johnson, Susan Saunders, and staff of the UMN Experimental Surgical Services.

3.7 Funding

Funding support for this work was provided by the University of Minnesota Clinical and Translational Science Institute and NIH HL107572 (to R.T.T).

3.8 Chapter 3 Figures and Tables

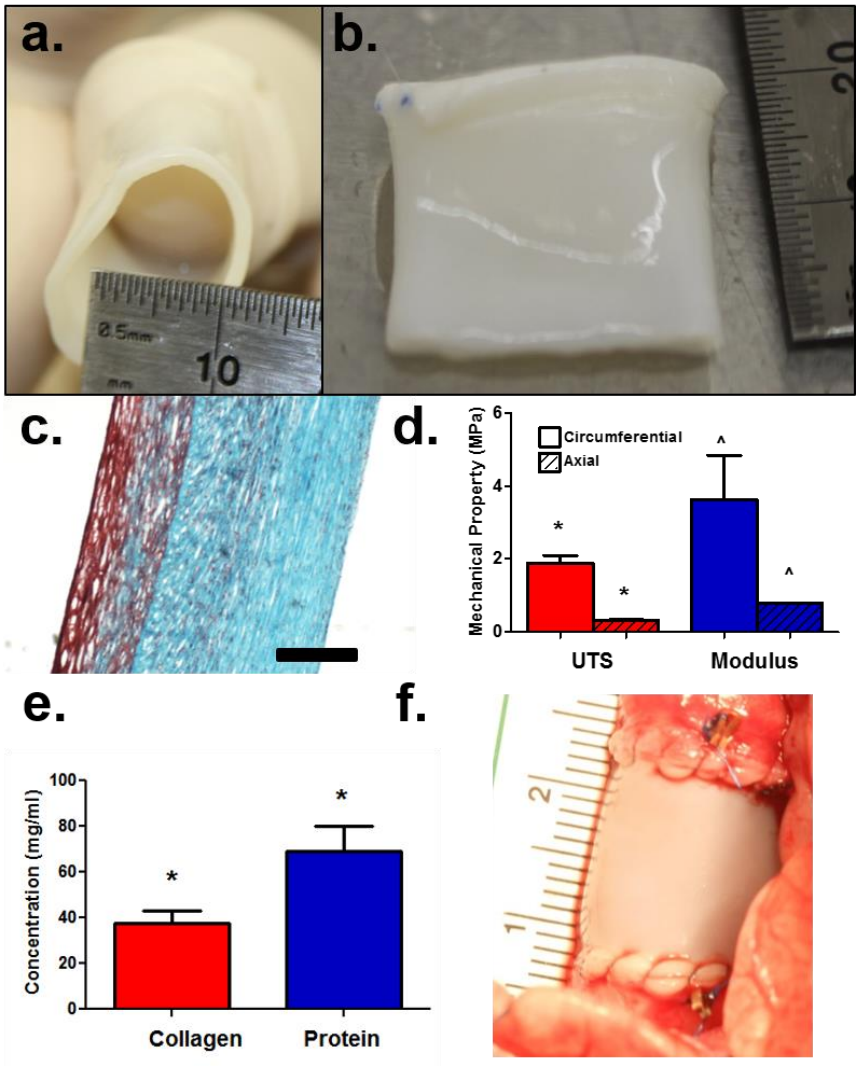

Figure 3-1. Engineered tissue tube *in vitro* characterization

(a) End-on view and (b) side view images of decellularized tissue-engineered graft. (c) Trichrome stained cross-section image of the graft (200 μm scale bar in black). (d) Tensile mechanical properties of the graft in the circumferential (solid) and axial (dashed) directions. (e) Collagen and total protein concentrations of the graft prior to implantation. (f) Image of graft implanted in the ovine pulmonary artery with biodegradable sutures and silver clip markers near the anastomoses.

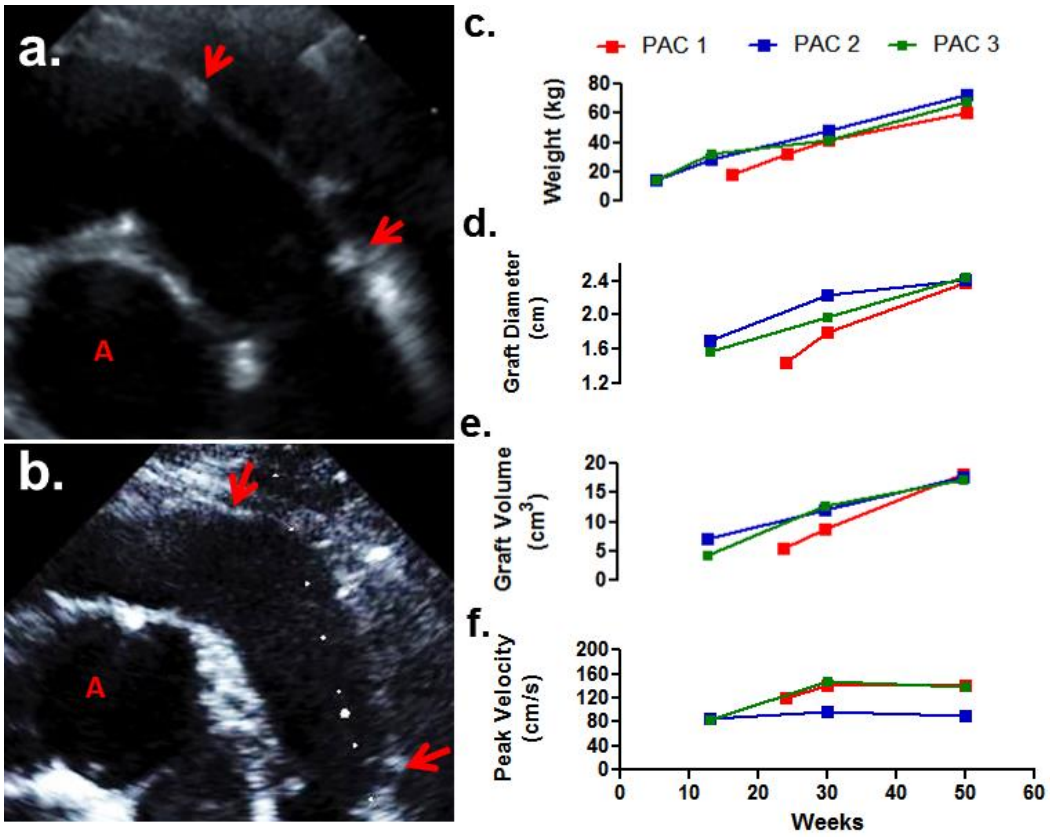

Figure 3-2. Representative ultrasound images and quantified data

Representative ultrasound image of the grafts after (a) 8 weeks implantation and (b) at animal age of 50 weeks, with red arrows pointing to the anastomoses and the 'A' indicating the cross-section of the aorta. (c) Animal weights and ultrasound measurements for (d) mid-graft diameter, (e) graft volume, and (f) peak blood velocity in the graft as a function of animal age.

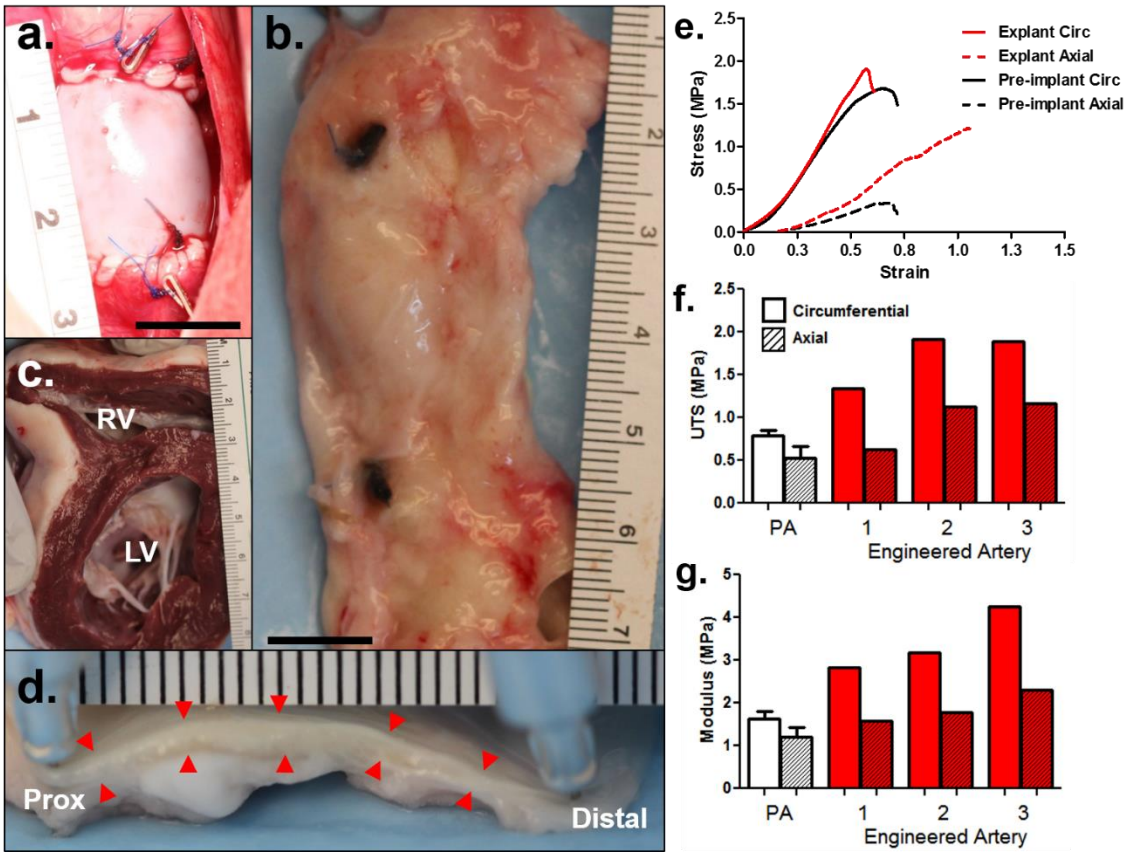

Figure 3-3. Macroscopic and mechanical characterization at explant

Macroscopic images at the same magnification scaled (a) after implantation and (b) after explantation showing anatomical growth. (c) Cross-section of the explanted heart showing normal right ventricular wall thickness. (d) Side view of the explanted graft showing uniform thickness (red arrows point to the lumenal and ablumenal surfaces). (e) Stress-stain plots of representative pre-implant (black line) and explanted grafts in the circumferential (solid) and axial (hashed) directions, and (f) UTS and (g) Modulus for the three explanted grafts and the adjacent pulmonary artery in the circumferential (solid) and axial (dashed) directions.

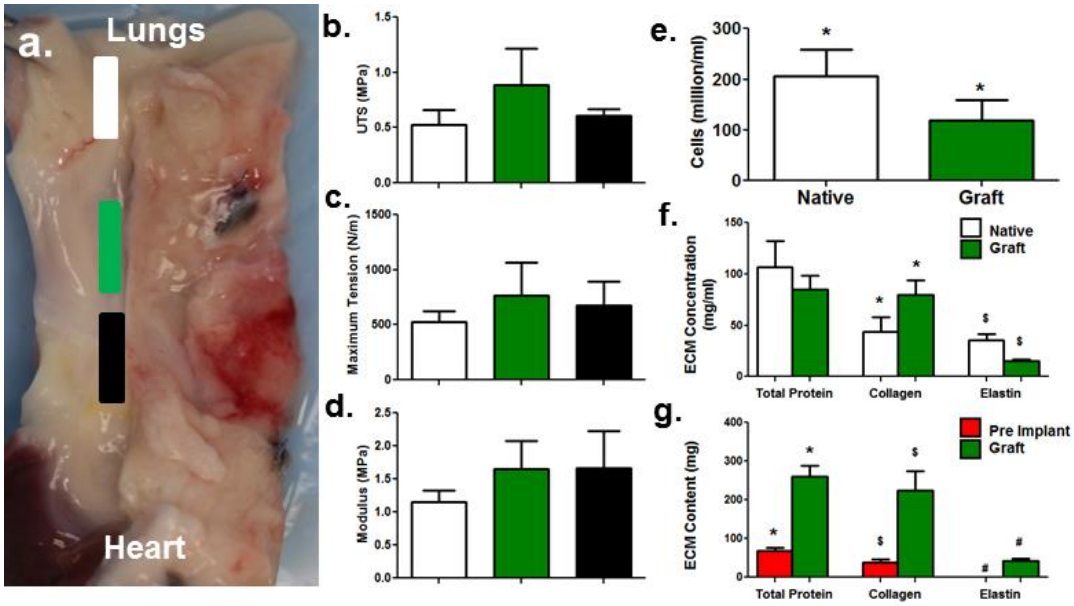

Figure 3-4. Tensile mechanical properties at explant

Tensile mechanical properties in the axial direction with strips tested from (a) adjacent pulmonary artery (white), region encompassing the anastomosis (green), and engineered graft (black). Measured properties from all three grafts are averaged for (b) UTS, (c) Maximum tension, and (d) Modulus. Comparison between the native pulmonary artery and the explanted grafts of (e) cellularity and (f) Extracellular matrix (ECM) protein concentrations. (g) Total protein, collagen, and elastin content in the engineered grafts before and after implantation.

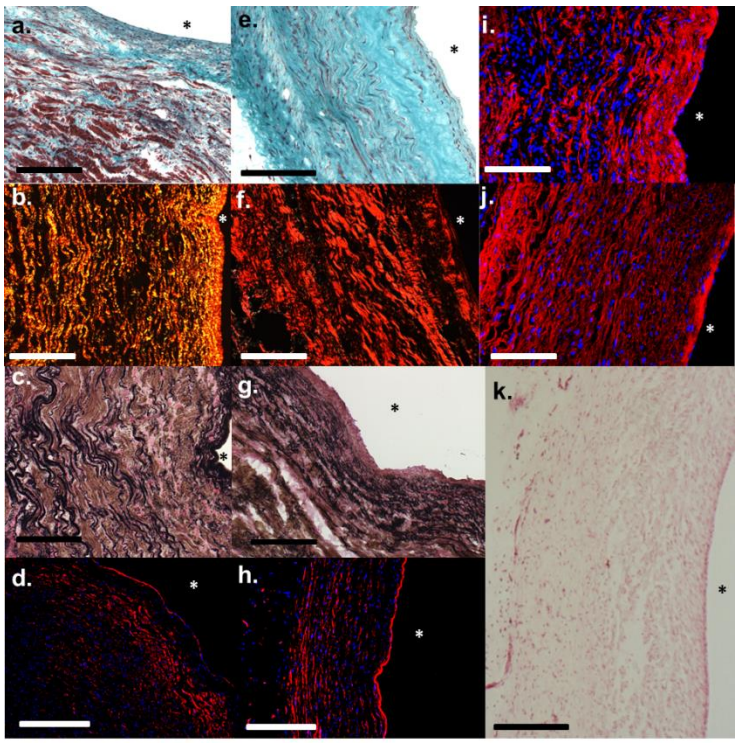

Figure 3-5. Histological characterization of the explanted tissue

Histological images of the engineered graft and adjacent pulmonary artery following explant. Trichrome images of the (a) artery and the (e) graft showing uniform cell density and abundant collagen staining. Picrosirius red staining imaged under polarized light shows collagen crimping both in the (b) artery and (f) graft. Verhoeff stain for elastin showing mature fibers near the lumenal surface in black both for (c) artery and (g) graft. Collagen IV immunostaining at the lumenal surface both for the (d) artery and (h) graft. Elastin immunostaining showing the presence of elastin across the entire thickness of both the (i) artery and (j) graft. (k) No calcification was observed in the graft as visualized by Von Kossa staining. 200 μm scale bar in black or white is shown. Lumenal surface is marked with '*'.

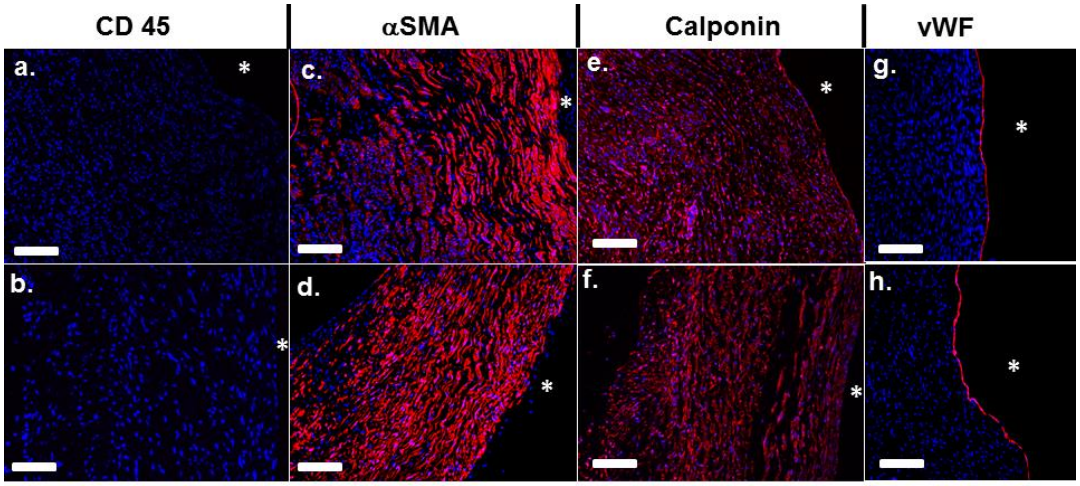

Figure 3-6. Immunostaining for cell marker in the explanted tissue

Immunostaining for cell markers in the (a,c,e,g) pulmonary artery and the (b,d,f,h) explanted engineered graft. Specific cell markers stained include (a,b) CD45, (c,d) αSMA, (e,f) calponin, and (g,h) Von Willebrand factor (vWF). 200 μm scale bar in white is shown. Lumenal surface is marked with '*'.

Table 3-1. Measured dimensions of grafts at implant and explant

Graft	Implant Diameter (mm)	Explant Diameter (mm)	Implant Length (mm)	Explant Length (mm)
PAC1	16	24.7	19	41
PAC2	16	24.1	16	39
PAC3	16	24.0	16	37

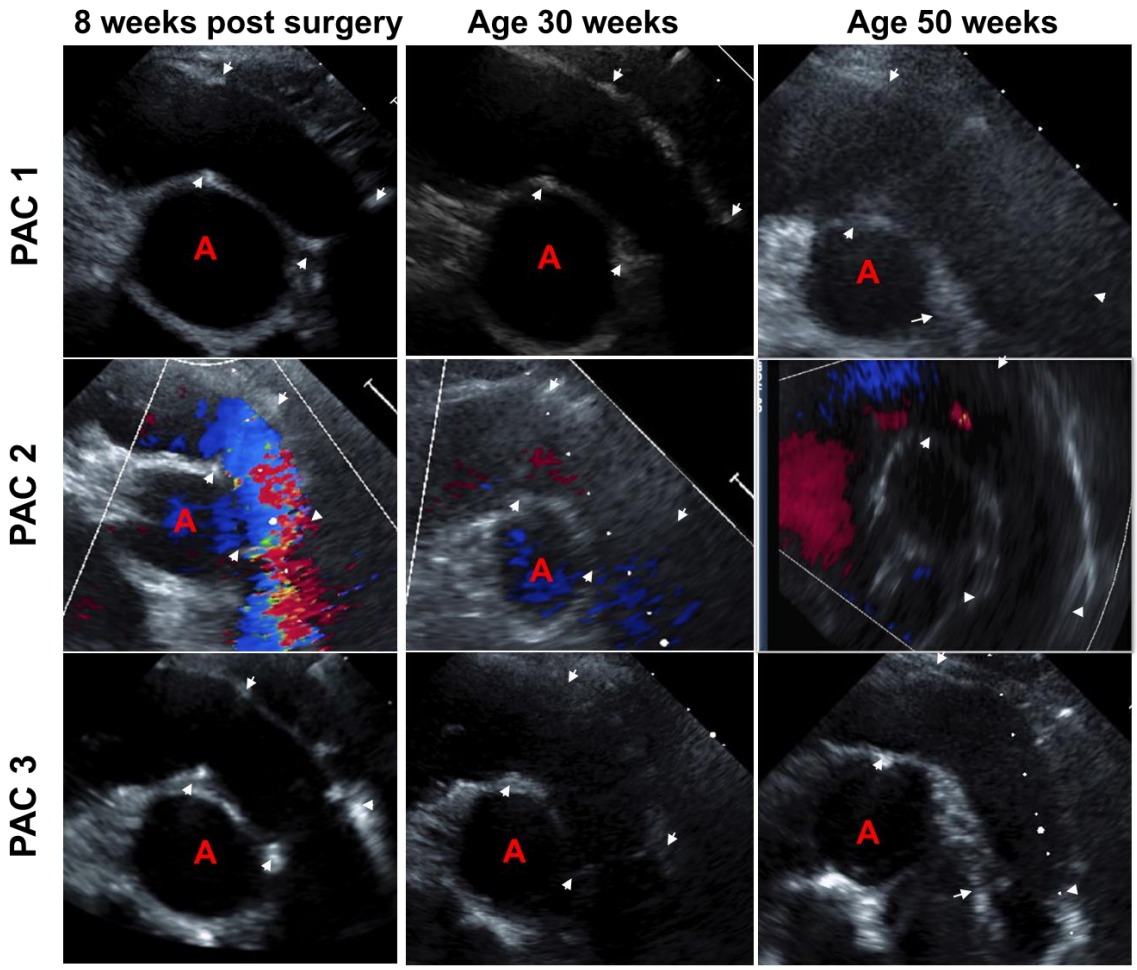

Supplemental Figure 3-1. Ultrasound images of the implanted grafts

Ultrasound images of the graft for PAC1 (top panel), PAC2 (middle panel) and PAC3 (bottom panel) at 8 weeks after surgery and at animal age of 30 and 50 weeks. White arrows mark the anastomotic positions. 'A' marks the lumen of the aorta.

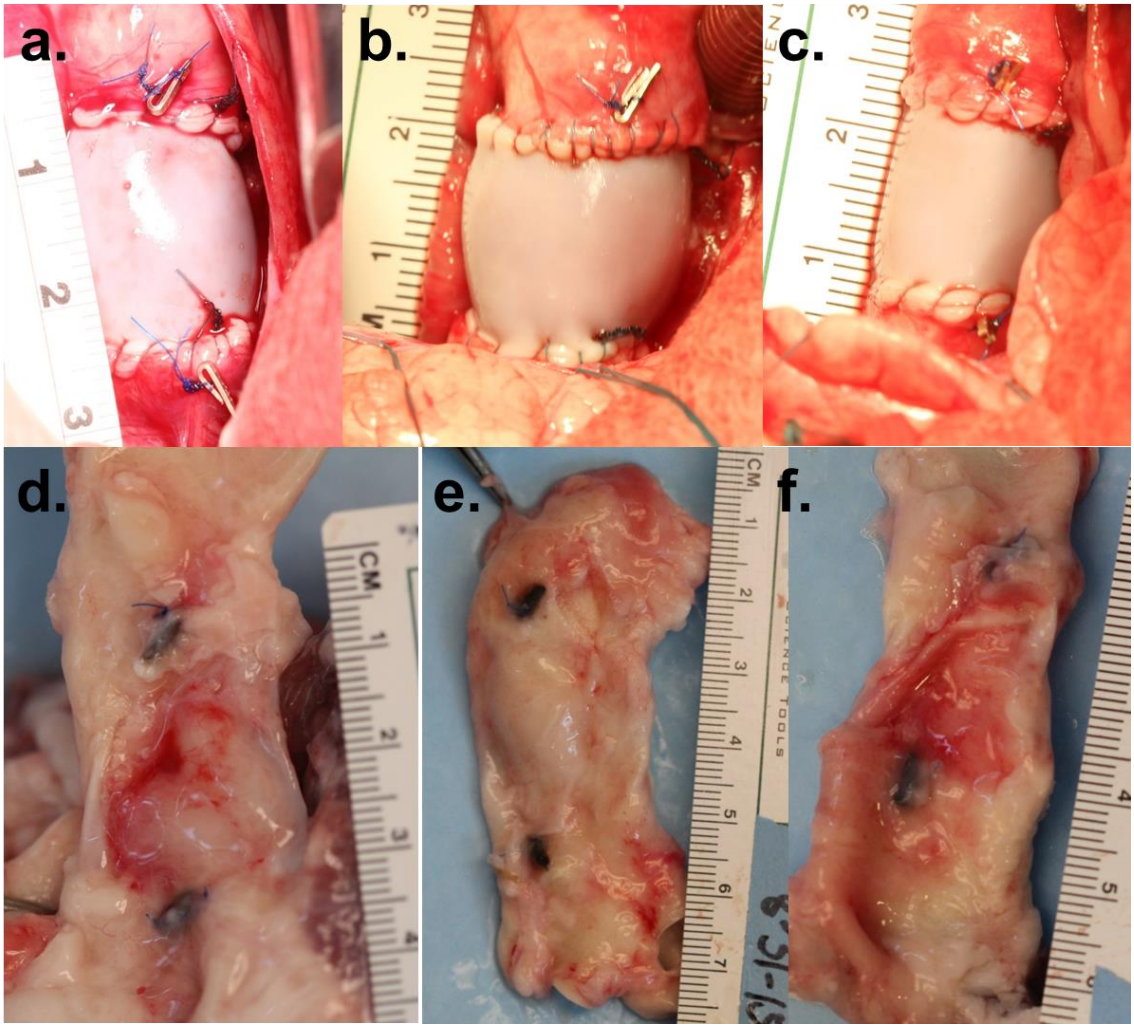

Supplemental Figure 3-2. Macroscopic images of the grafts

Images of the grafts at implant (a) PAC1, (b) PAC2, and (c) PAC3, at explant (d) PAC1, (e) PAC2 and (f) PAC3.

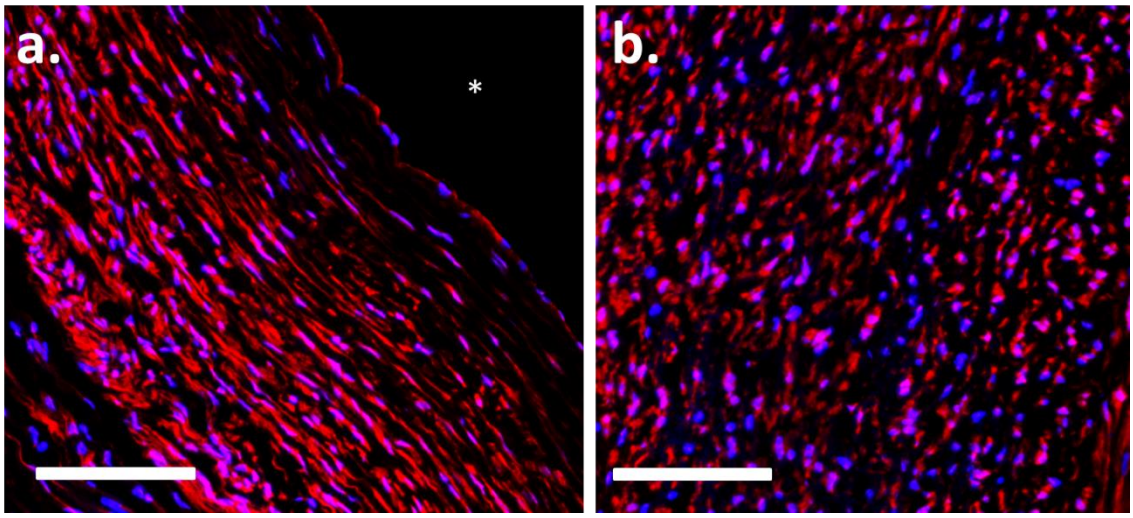

Supplemental Figure 3-3. Immunohistochemical images of cell elongation

Calponin immunostaining of the explanted graft in the (a) circumferential and (b) axial directions showing elongated cells in the circumferential direction. 200 μm scale bar shown and '*' marks the lumenal side.

Chapter 4. Implantation of a Tissue-Engineered Tubular Heart Valve in Growing Lambs

Annals of Biomedical Engineering, Implantation of a Tissue-Engineered Tubular Heart Valve in Growing Lambs, 2016, pages 1-13. J. Reimer, Z. Syedain, B. Haynie, M. Lahti, J. Berry, and R. Tranquillo. With permission of Springer."

4.1 Summary

Current pediatric heart valve replacement options are suboptimal because they are incapable of somatic growth. Thus, children typically have multiple surgeries to replace outgrown valves. In this study, we present the *in vivo* function and growth potential of our tissue-engineered pediatric tubular valve. The valves were fabricated by sewing two decellularized engineered tissue tubes together in a prescribed pattern using degradable sutures and subsequently implanted into the main pulmonary artery of growing lambs.

Valve function was monitored using periodic ultrasounds after implantation throughout the duration of the study. The valves functioned well up to eight weeks, four weeks beyond the suture strength half-life, after which their insufficiency index worsened. Histology from the explanted valves revealed extensive host cell invasion within the engineered root and commencing from the leaflet surfaces. These cells expressed multiple phenotypes, including endothelial, and deposited elastin and collagen IV. Although the tubes fused together along the degradable suture line as designed, the leaflets shortened compared to their original height. This shortening is hypothesized to result from inadequate fusion at the commissures prior to suture degradation. With appropriate commissure reinforcement, this novel heart valve may provide the somatic growth potential desired for a pediatric valve replacement.

4.2 Introduction

The pulmonary valve is the heart valve most frequently afflicted by congenital heart defects, and there is a clinical need for a pulmonary valve replacement in pediatric patients. While this patient population is relatively small (~600/year in the U.S.) [1,114], the need is dire because treatment can require multiple surgeries until adulthood to replace degenerated or outgrown valves [136]. Current replacement options for these children include glutaraldehyde-fixed xenografts, as well as decellularized or cryo-preserved homografts [34,116]. Although there have been some improved preclinical and clinical outcomes [30,157], these valve replacement options traditionally have been prone to valve failure due to calcification, structural degeneration, and limited availability [22]. Additionally, these prosthetic valves are unable to grow with the patient and, consequentially, multiple valve replacements are often needed [158].

Numerous tissue-engineered heart valve (TEHV) approaches have been explored that aim to produce a "living" valve capable of *in vivo* remodeling, repair, and ultimately somatic growth [41]. Although initially functional, most of these valves eventually failed due to leaflet shortening or fusion with the valve root, leading to an unacceptable level of regurgitation [91,105,109,110,118]. Most TEHV studies have utilized adult sheep, but studies with juvenile sheep have been reported [55,118]. Two of these TEHVs contained cells at implant and ultimately failed due to leaflet shortening [118] and/or too much enlargement of the valve root [55]. Decellularization has been investigated as a way to reduce cell-mediated leaflet shortening and to increase their shelf-life [88,90,91]. Significantly, these approaches have demonstrated the feasibility of host cell invasion and matrix remodeling in both the pulmonary and aortic position [91,111]. However, long term function and growth of a TEHV has not yet been demonstrated.

Our group previously reported excellent hemodynamic performance of our decellularized TEHV in a pulse duplicator [93]. It is a tubular heart valve, comprised of two tubes of cell-produced matrix grown *in vitro* held together with degradable sutures [93]. These sutures are reported to maintain 50% of their initial strength after 4 weeks *in*

vivo [159]. We have recently shown that single tubes implanted into young lambs as a pulmonary artery replacement with this suture exhibit somatic growth [160]. Thus, if the two tubes fuse with one another along the degrading suture line on a sufficient time scale by invading host cells, this valve should remain competent and possess growth potential.

The goal of this study was to evaluate the valve function and growth potential in a growing lamb model. Periodic ultrasounds were performed to evaluate valve function and growth before and after the expected time of suture degradation. Explanted valves were macroscopically, mechanically, histologically, and biochemically analyzed to assess tube fusion, recellularization, and new extracellular matrix deposition.

4.3 Materials and Methods

4.3.1 Tissue Fabrication

Tubular, cell-seeded fibrin gels were fabricated by mixing aqueous solutions of ovine dermal fibroblasts (ODFs, Coriell), bovine fibrinogen (Sigma), thrombin (Sigma), and calcium chloride. The final component concentrations were as follows: 1 million ODFs/mL, 4 mg/mL fibrinogen, 0.38 U/mL thrombin, and 5.0 mM Ca^{++}. The mixed solutions were injected into tubular glass molds which had a 19 mm inner diameter mandrel, a 4.5 mm annulus, and were ~9 cm in total length.

Following gelation, the tubular fibrin gels and glass mandrels were cultured in DMEM + 10% fetal bovine serum (FBS, Hyclone), 100 U/mL penicillin, 100 μg/mL streptomycin, 0.25 μg/mL amphotericin B,2 μg/mL insulin, and 50 μg/mL ascorbic acid. Culture medium was changed 3X per week for 2 weeks while allowing the longitudinal shortening of the gels. The tissue tubes were then removed from the glass rods and transferred onto 16 mm diameter latex tubes, which were attached to custom manifolds. Additional details on this pulsed-flow-stretch bioreactor have been previously reported [124]. Construct strain began at 3% and was incremented weekly by 1% until a 5% maximum strain was reached.

Following maturation, the engineered tubes were decellularized by immersion in 1% sodium dodecyl sulfate (SDS, Sigma) and 1% Triton X-100 (Sigma) for 6 hours and 30 minutes, respectively, at room temperature with continuous shaking. The tubes were then extensively rinsed in 1X phosphate buffered saline before and after overnight incubation in culture medium plus 2 U/mL deoxyribonuclease (Worthington Biochemical).

4.3.2 Valve Fabrication

Valves were fabricated using two 16 mm diameter engineered tubes, as previously described [93]. Briefly, the tubes were sutured together using 7-0 degradable sutures (Covidien Maxon CV) in 2 distinct patterns. The first suture line encompassed the entire circumference of the tubes and defined leaflet and commissure regions. A second suture line was added to reinforce each of the three commissure regions. On some valves, a single permanent suture (7-0 prolene) was then added to each commissure near the free edge.

4.3.3 Implantation Procedure in a Growing Lamb Model

The fabricated valves were implanted as pulmonary valve replacements in n=8 Dorset lambs (average age = 5.5 ± 0.8 weeks, average weight = 12.7 ± 0.5 kg). All protocols were approved by the Institutional Animal Care and Use Committee (IACUC) and performed by the University of Minnesota's Experimental Surgical Services. All animals were anesthetized using 10 mg/kg Ketamine and 2-6 mg/kg propofol and maintained on 2-4% isoflurane for the duration of the procedure. The heart was exposed via a left lateral thoracotomy with dissection through the intercostal space. Following surgery, animals received subcutaneous injections of 750IU heparin BID for the duration of the study. Animals were euthanized with beuthanasia given intravenously at 87-90 mg/kg.

Animals for the study were numbered as PACV1-8. The valves implanted in PACV1-2 did not utilize the single permanent sutures near the commissures, while PACV3-8 did. All tissue engineered valves were implanted interpositionally using 5-0

degradable sutures (Maxon CV, Covidien) in the main pulmonary artery after compromising the native pulmonary valve. A segment of the native pulmonary artery that matched the length of the implanted valve was also excised. Silver clips were attached on the ablumenal surface of the native pulmonary artery near the distal and proximal anastomoses to serve as markers (Figure 4-4a).

Valve function, flow velocity and profiles, pressure drop, and conduit dimensions were assessed from periodic transthoracic echocardiograms. The echocardiograms were first performed approximately 1 week after implantation and then monthly for the duration of the study. Explanted valves were photographed and then dissected into strips for histological, biochemical, and mechanical characterization.

4.3.4 Tensile Mechanical Testing

Strips parallel ("circumferential") and orthogonal ("axial") to the circumference of engineered tubes and the native pulmonary artery were cut (~2 mm x 12 mm) and mechanically characterized using an Instron Biaxial tester. Strips were tested prior to implantation and after explantation. Strips were mounted in custom grips and straightened with a 0.005 N tensile load. Following 6 preconditioning cycles (0-10% strain), the samples were uniaxially strained to failure at 3 mm/min. Strain was calculated as the natural logarithm of the sample's deformed length divided by its initial length. Ultimate tensile stress (UTS) and modulus were defined as the maximum stress recorded and the slope of the linear region of the stress-strain curve, respectively. Representative stress-strain curves for the engineered tissue prior to and following implantation are shown in Supplemental Figure 4-1. Sample dimensions for calculating stress were measured using a digital caliper prior to testing.

4.3.5 Tissue Composition and DNA Quantification

The collagen mass content was determined using a hydroxyproline assay assuming 7.46 mg of collagen per 1 mg of hydroxyproline, as previously described [161]. Insoluble elastin was measured by dissolving the samples in NaOH and quantified using a modified ninhydrin assay [153]. The cell content was measured using a modified

Hoechst assay for DNA assuming 7.6 pg of DNA per cell and reported as cell concentration [154]. Tissue volume for these tests was calculated using measured length, width, and thickness using a digital caliper.

4.3.6 Histology and Immunohistochemistry

Explanted valves were histologically and immunohistochemically stained using longitudinal strips that included the root, leaflets, and native pulmonary artery at each end. All samples were fixed in 4% paraformaldehyde, embedded in OCT (Tissue-Tek), frozen in liquid Nitrogen, and cut into 9 μm thick sections. Images were taken at 4x, 10x, or 20x magnification. Histological sections were stained with Lillie's trichrome, Verhoeff-Van Gieson, and Von Kossa stains. Immunohistochemical samples were blocked with 5% normal donkey serum, incubated in the primary antibody (2.5-5 μg/mL), and stained with a Cy5-conjugated, species-matched secondary antibody (Jackson Immunoresearch). Primary antibodies for this study included α-smooth muscle actin (α-SMA, Sigma, A5228), Von Willebrand Factor (vWF, Abcam ab6994), CD45 (US Biological C2399-07B), elastin (Abcam ab21599), and collagen IV (Abcam, ab6586). Nuclei were counterstained with Hoechst 33342 (Invitrogen H3570).

4.3.7 Statistics

Statistical significance was determined between two groups using Student's t-test and between multiple groups using ANOVA with a Games-Howell post-hoc test. Paired symbols in figures are used to represent statistical difference and a p-value < 0.05. All error bars are represented as the standard deviation of the group.

4.4 Results

4.4.1 Tissue Engineered Heart Valve

Completely biological heart valves (n=8, Figure 4-1a) were fabricated by sewing two decellularized engineered tubes together using 7-0 Maxon™ degradable sutures, as previously described [93]. The suture pattern was designed such that there were three

commissures and three leaflets that collapse inward and close the valve when exposed to backpressure (Figure 4-1b), utilizing the principle of tubular heart valve design [89]. The engineered tubes used to make the valve consisted primarily of cell-produced collagen and other extracellular matrix proteins, although a residual fibrin layer remained on the lumenal surface following in vitro culture, as revealed by trichrome staining (Figure 4-1c).

Uniaxial strain-to-failure tests showed that the engineered tubes possessed an ultimate tensile stress (UTS) and modulus of 1.33 ± 0.16 MPa and 4.41 ± 0.82 MPa in the circumferential direction, respectively (Figure 4-1d,e). Mechanical tests in the orthogonal direction revealed that the engineered tubes were mechanically anisotropic, with the modulus being ~4 times stiffer in the circumferential direction. For comparison, mechanical testing was performed on excised native pulmonary valve leaflets and pulmonary artery (Figure 4-1d,e). The UTS and modulus of the engineered tissue were similar to values for the native pulmonary valve leaflets in both the circumferential and axial directions at the time of implant. The UTS and modulus of the native pulmonary artery were ~2.5 times lower compared to the engineered tissue values in the circumferential direction.

4.4.2 Valve Implantation

The valves were implanted into the main pulmonary artery of lambs (average weight = 12.7 ± 0.5 kg, average age = 5.5 ± 0.8 weeks) after resecting the native pulmonary valve leaflets and a length-matched section of the pulmonary artery (Figure 4-4a). The first two valves implanted contained only degradable sutures, while the subsequent 6 incorporated a single 7-0 prolene suture near the top of each commissure. The degradable suture lines used to fabricate the valve and the anastomoses are visible in Figure 4-4a.

All animals survived the implant procedure and no perioperative deaths occurred, although three of the studies were ended prematurely. One animal did not recover well following surgery due to an atrial-septal defect. Two other valves were explanted due to

inadequate initial valve function. In one animal, one leaflet was immobile immediately after implantation; the other animal developed extensive calcific nodules along the degradable suture line shortly after implantation. Since these studies were ended prematurely, and the purpose of this study was to assess long term valve function and remodeling, their outcomes will not be discussed further.

4.4.3 Valve Performance Evaluation with Ultrasound

Valve function and geometrical dimensions were assessed longitudinally using monthly ultrasounds (Figure 4-2). The first was performed 1.3 ± 0.3 weeks after implantation; full valve opening (Figure 4-2a) and closing (Figure 4-2b) were observed. Representative images at 8.1 ± 0.6 weeks (Figure 4-2c) and 21.1 weeks (Figure 4-2e) also demonstrated full leaflet opening. Coaptation was adequate after 8 weeks (Figure 4-2d), but had decreased at the later time points based on regurgitant flow (Figure 4-2f).

All animals exhibited healthy weight gain over the course of the study (Figure 4-3a). In general, the insufficiency index increased over the duration of the study, particularly after the 8 week follow up time point (Figure 4-3b). A value of 1 on the insufficiency index indicates trivial regurgitation and higher values correlate to increased levels of regurgitation (2 = mild, 3 = moderate, 4 = severe). The diameter of the valves also increased over time (Figure 4-3c) and generally matched the neighboring pulmonary artery well. The mean and maximum (~1 week post implant = 11.6 ± 12.8 mmHg; ~16 weeks = 16.3 ± 11.0 mmHg) transvalvular pressure gradients also measured from the pulmonary valve velocity-time integral (PV VTI, Supplemental Figure 4-2).

The endpoint for each animal was dependent on animal health and overall valve function. Thus, the numbers of data points are not equal across all of the study time points; there are less data points at the later time points due to deteriorated valve function. The shortest and longest implantation periods included in the data quantification were 11.9 and 21.9 weeks, respectively. The other valves were explanted after 16.1, 19.1, and 19.4 weeks when adequate leaflet motion and coaptation was no longer apparent and the insufficiency index increased.

4.4.4 Explanted Valve Gross Pathology

At the endpoints, the explanted hearts and valves were analyzed to determine their integration and pathological abnormalities. Representative images of a valve at implant (Figure 4-4a) and explant (Figure 4-4b) are shown, with the clips demarcating the initial anastomoses, which became indistinguishable from the native pulmonary artery. All explanted valves were well integrated with the native pulmonary artery and excessive overgrowth or encapsulation was not present on the ablumenal surface (Figure 4-4b). The pre- and post-implant images are shown using the same scale to demonstrate the increase in root diameter and length during implantation. As observed at implantation (Figure 4-4a) and in subsequent ultrasounds, the valve diameter matched that of the surrounding native pulmonary artery well (Figure 4-4b). Further investigation of the heart revealed normal thickness and appearance of the right ventricle (Figure 4-4c).

The valves were excised from the pulmonary artery and cut longitudinally so that the lumenal surface could be visualized (Figure 4-4d). The lumenal surface was generally clean, although isolated nodules were present near one commissure on two of the five reported valves near the degradable suture line. As observed from the ablumenal surface, there was no clear anastomotic region; rather the native pulmonary artery and engineered root were seamlessly integrated. Importantly, there was also fusion along the original suture line between the two engineered tubes that formed the valve root and leaflets. However, the commissures were not stable relative to their position at implantation, indicated by the asterisks in Figure 4-4d. This instability allowed the leaflets to shorten by 43.3 ± 13.3% compared to their lengths at implantation (Figure 4-3d). In two of the valves, this instability resulted in the complete disappearance of the leaflet. One inspected valve also exhibited some fusion from the leaflet belly towards the free edge. The remaining leaflets generally were thin, pliable, and maintained the initial geometry prescribed by the suture pattern (Figure 4-4e).

4.4.5 Explanted Valve Mechanical Characterization

Strips cut from the explanted valve root, leaflet, and pulmonary artery were strained to failure to assess their tensile mechanical properties (Table 4-1). The thicknesses of the leaflet (0.58 ± 0.12 mm) and root (0.93 ± 0.12 mm) showed a reduction compared to the native pulmonary artery (1.30 ± 0.23 mm). The UTS and modulus in the circumferential direction were 1.75-4 times higher than the orthogonal (axial) direction. The circumferential UTS of the explanted valve root and leaflet were 1.27 ± 0.20 MPa and 2.54 ± 0.77, respectively, compared to the native pulmonary artery (0.28 ± 0.03 MPa). Additionally, strips incorporating both the pulmonary artery and root were taken in order to assess the strength of fusion and any influence of scar tissue at the anastomoses. UTS and modulus were comparable in the axial direction between these strips, the explanted valve root and leaflets, and native pulmonary artery (Table 4-1).

4.4.6 Explanted Valve Histological & Biochemical Analysis

Longitudinal strips were fixed, frozen, and included the proximal and distal pulmonary artery, root, and leaflet. The cross-sections in Figure 4-5 were taken from the middle of the leaflet free edge and stained with Lillie's trichrome, Von Kossa, and Verhoeff's stain. Following implantation, the leaflet and root tubes fused along the degradable suture line, as visualized in the trichrome image near this junction region (Figure 4-5a). Trichrome staining also revealed a cellular, collagenous matrix throughout the entire root and leaflet (Figure 4-5a-c). Immunostaining revealed Collagen IV deposition in the valve root and leaflets after 12 and 22 weeks (Figure 4-6e-h). Calcification was not observed in the engineered root or leaflets (Figure 4-5d-f), though small regions were observed near some anastomoses in proximity to the degraded sutures. Elastin was detected by immunostaining after 12 and 22 weeks in the root and leaflet sections (Figure 4-6a-d). Mature elastin can be detected using Verhoeff's stain and is manifested by black coloration (Figure 4-5g). Mature elastin was not observed in the leaflet sections (Figure 4-5h), but there were some mature fibers near the lumenal surface of the explanted root (Figure 4-5i).

Immunostaining was performed in order to identify the degree, location, and phenotypes of the invaded host cells at the shortest (~12 weeks) and longest (~22 weeks) time points. Complete recellularization of the root was observed at both time points as evidenced by the presence of nuclei (blue) throughout the entire length and thickness. Leaflet recellularization was sparser at both time points, although more nuclei were observed within the leaflets after 22 weeks. The majority of cells after 12 weeks, both within the root and on the leaflet surfaces, stained positive for α-SMA (Figure 4-6i,k). After 22 weeks, α-SMA was primarily expressed near the lumenal surface (indicated by the stars in Figure 4-6) of the root (Figure 4-6j) and partially on the leaflet surfaces (Figure 4-6l).

A complete endothelial layer, as evidenced by positive vWF staining, was observed on the lumenal surface of the root after both 12 and 22 weeks (Figure 4-6m,n). The leaflets were incompletely endothelialized after both 12 and 22 weeks (Figure 4-6o,p), though positive staining was observed up to the leaflet free edge. Evidence of inflammatory and/or immune cells by CD45 expression was observed in the valves. CD45-positive cells were evident throughout the entire thickness of the root after 12 and 22 weeks (Figure 4-6q,r). Fewer CD45-positive cells were observed in the leaflets (Figure 4-6s,t). DNA quantification confirmed the presence of cells in the explanted engineered tissue, though not to the same degree as in the surrounding pulmonary artery (Table 4-1). The cell density in the explanted root was ~5.3 times higher compared to the leaflets (Table 4-2).

Collagen, elastin, and cellularity of the pre-implant tissue, explanted root, leaflet, and native pulmonary were quantified and compared (Table 4-2). Higher collagen and elastin density were observed following implantation compared to pre-implant tissue. Although higher than values at implantation, the elastin concentration in the engineered tissue was lower than that in the native pulmonary artery (Table 4-2). Prior to implantation, we previously reported a collagen concentration of 38 ± 4 mg/cm^3 for similar engineered tubes, which possessed negligible elastin content [111]. Total collagen

content was estimated using the average collagen concentrations for the engineered root and leaflet regions. The total collagen was higher in the explanted root (81.2 ± 26.5 mg) compared to implant (49.1 ± 2.04 mg). The total collagen content in the leaflets was 15.2 ± 0.5 mg and 4.2 ± 1.8 mg before and after implantation, respectively.

4.5 Discussion

A pediatric heart valve capable of growth and remodeling has long been a goal of heart valve tissue engineering, but it has not yet been demonstrated. An ideal valve would be durable, hemocompatible, not prone to calcification, and possess the potential to grow with the patient. All of these characteristics functionally extend the life of a pediatric prosthetic valve and thus limit the need for subsequent surgeries to replace defective or outgrown valves. In light of this clinical need, we have developed a completely biological pediatric pulmonary valve using two decellularized, engineered tubes and degradable sutures. We previously reported the material and hemodynamic properties of these valves under simulated pulmonary valve conditions *in vitro* [93].

Herein, we report the results of an *in vivo* study designed to assess long term valve function, tissue remodeling, and growth potential. All valves were implanted into the main pulmonary artery of lambs (average age = 5.5 ± 0.8 weeks) after excising the native pulmonary valve leaflets and a length-matched segment of the pulmonary artery. Although no perioperative deaths occurred, the implant procedure was refined over time. This included sewing the proximal anastomosis first and keeping the valve hydrated in order to better purge bubbles and avoid tissue sticking, respectively. The animals were evaluated monthly after implant using ultrasound until valve function deteriorated. The minimum and maximum implant durations of the 5 lambs studied were 11.9 and 21.9 weeks, respectively.

Overall, the valves performed well immediately and up to 8 weeks after implantation. This sustained function indicated that the critical process of fusion between the two engineered tubes had occurred along the degrading suture line given that it reportedly retains 50% of its original tensile strength after 4 weeks *in vivo*. However,

valve function deteriorated thereafter as evident from the insufficiency index (Figure 4-3b). The reasons for declining valve function are convoluted due to the fact that the root was enlarging (Figure 4-3c) and the sutures were further degraded and do not provide indefinite support. Thus, valve incompetence could arise from the enlargement of the root, without corresponding growth of the leaflets, or leaflet shortening due to inadequate fusion between the two tubes at the commissures prior to suture degradation.

Discerning between these two causes is complicated by animal growth, as Hoerstrup et al. also concluded [55]. In order to mitigate leaflet shortening, a single permanent suture was added to each commissure to provide long term support in these regions in the event that inadequate fusion was achieved. However, this approach did not prove successful (Figure 4-3d).

The engineered root diameter increased over time and matched the native pulmonary artery well, as observed from ultrasound. The engineered root diameter increased 126.3% from the first (age = 6.9 ± 1.0 weeks, weight = 15.3 ± 1.9 kg) to the last (age = 25.4 weeks, weight = 47.0 kg) echocardiogram. The lack of elevated mean and maximum transvalvular pressure gradients supports this observation (Supplemental Figure 4-2). In comparison, Gottlieb *et al.* studied the growth of the main pulmonary artery and reported an increase of only 31.4% for the pulmonary sinus diameter over the same weight range in Dorset sheep [101]. Interestingly, the percent increase in diameter of our TEHV root was comparable to the main pulmonary artery, as reported by Gottlieb et al., at earlier time points. The engineered root diameter increased only 6.9% and 18.2% from 1.4 to 4.3 and 8.0 weeks, respectively. Gottlieb *et al.* reported an increase of ~6.2% and ~12.8% in sheep between the same weight ranges [101]. The divergence of the increases in the diameter at longer time points is likely related to the elevated pulmonary insufficiency observed in the engineered valves at later time points. Pulmonary root dilation is known to result from pulmonary hypertension and abnormal hemodynamics, which are often byproducts of pulmonary insufficiency [162]. Notably, our group has

previously reported somatic growth of a single engineered tube when implanted as a pulmonary artery replacement, without compromising the native pulmonary valve [160].

After the valves became incompetent, they were explanted and subjected to macroscopic, mechanical, and histological analysis. There was no excessive overgrowth on the ablumenal surface of the valve and its diameter matched that of the surrounding vasculature, both of which were larger than at the time of implant (Figure 4-4a,b). The valves became integrated into the heart and were generally indistinguishable from the native pulmonary artery despite the degradation of the anastomotic sutures. Additionally, the two engineered tubes also fused along the degradable suture line and thereby formed leaflets *in situ* (Figure 4-4e). Significantly, tissue integration at the anastomoses appeared mechanically robust, based on their similar tensile failure mechanics compared to the surrounding tissue (Table 4-1).

Leaflet shortening (Figure 4-3d) was observed after implantation (Figure 4-4d), regardless of whether a permanent suture at the commissures was used or not. Since the leaflets were not extensively repopulated by α-SMA-positive cells, this shortening is likely due to commissure instability resulting from diastolic forces disrupting tissue fusion at the commissures. Leaflet fusion to the root from the belly region upwards, as reported by Driessen-Mol *et al.* [91], was only observed once in our study. Valve failure due to leaflet shortening has been reported previously, especially for pre-cellularized TEHVs [55,91,106,109,110,118]. Gottlieb *et al*. reported elevated pulmonary insufficiency after 12 and 20 weeks [118]. They observed dimensional leaflet changes and reported that leaflet heights decreased by ~47% and 78.5% after implantation for 12 and 20 weeks, respectively. We observed shortening by 43.3 ± 13.3% compared to pre-implant values with no clear temporal dependence.

Recellularization is a crucial requirement for this approach, since the engineered tubes are acellular prior to valve fabrication and implantation. Although the integration of the tissue tubes along the degradable suture lines provide evidence of host cell invasion, more extensive characterization was necessary. Histology revealed uniform and complete

recellularization throughout the engineered root and partial recellularization in the leaflet. Total cell number was quantified and was ~5.3 times higher in the engineer root compared to the leaflet (Table 4-2). Inflammatory and/or immune cells were observed by positive CD45 staining (Figure 4-6). It is expected that these cells would be absent after longer implantation times as seen in a study previously published by our group [111]. However the expected time scale is unknown since the current study was performed in a growing, as opposed to an adult animal. Other cell types present included endothelial cells on the surface and interstitial cells within the matrix. Driessen-Mol *et al*. reported similar recellularization patterns with their TEHV in adult sheep [91]. They also reported repopulation of endothelial and α-SMA positive cells in the root, and subsequently in the leaflets, over time. After 24 weeks, however, they reported that DNA content in their TEHV was similar to the native ovine valve leaflets, with homogeneous recellularization of the leaflets. In contrast, we observed cells primarily on the leaflet surfaces, but with an increasing number of cells within the leaflet matrix from 12 to 22 weeks of implantation.

The recellularization pattern observed in this study contrasts with our observations from our aortic valve study in adult sheep. Previously, leaflet recellularization appeared to proceed with cells invading the base from the adjacent root and then migrating towards the leaflet free edge [111]. There were few cells present near the free edge even after 22 weeks [111]. In the present study, however, cells were observed on surface of the leaflets, including the free edge, as early as 12 weeks after implantation. These cells on were distributed fairly uniformly from the base to the free edge, with more cells invading from the leaflet surfaces at 22 weeks. These observations suggest that, in this study, the majority of cells repopulating the leaflets originated from the blood instead of the adjacent root. However, we cannot discount the possibility that cells from the root very rapidly migrated over the surface and more slowly invaded from the surface.

In an attempt to distinguish between passive stretching and tissue growth, the total collagen content in the root and leaflets were compared before and after implantation.

The total collagen content increased ~65% in the root while decreasing ~72% in the leaflets. The decrease in the leaflets is attributed to the decrease in leaflet height (and thus smaller volume) since the collagen concentration increased in both the root and leaflet regions (Table 4-2) [111]. Histology revealed that the invading cells deposited elastin and collagen IV, which weren't present prior to implantation (Figure 4-6). The presence of the new matrix proteins, along with the maintenance of tissue mechanical properties (Figure 4-1d,e, Table 4-1), and the increase in total collagen in the root suggest that the invaded cells conferred true growth, not passive stretching of the engineered tube over time.

We have demonstrated the *in vivo* function and remodeling of our decellularized TEHV in a growing lamb model after previously reporting its *in vitro* tissue and hemodynamic properties [93]. In this study, we observed fusion of the two engineered tubes along the degradable suture line, by design. The valves functioned well for the first 8 weeks, but pulmonary insufficiency increased over time due to the enlargement of the valve root and/or shortening of the leaflets. Extensive host cell invasion was observed following implantation in the engineered root, while the leaflets were partially recellularized. Importantly, host cell invasion and matrix remodeling occurred without large-scale calcification, although isolated regions were observed near the anastomoses.

Future studies will be needed to address the pulmonary insufficiency, the results demonstrate the feasibility of this approach to heart valve tissue engineering. One area that will be further explored relates to the most appropriate animal model to use since it grows much faster than in humans. The pulmonary artery grows at a rate of approximately 0.7 mm per year in humans [103] during childhood compared to approximately 8.5 mm per year in lambs [101]. Identifying a more suitable growth model will allow the recellularization process to occur on the time scale needed for the cells to respond to physiologic growth cues and allow for leaflet growth.

4.6 Acknowledgements

The authors acknowledge technical assistance from Sandy Johnson, Naomi Ferguson, Susan Saunders, the UMN Medical Devices Center, and the staff of the UMN Experimental Surgical Services and funding from NIH R01 HL107572 to R.T.T. Annals of Biomedical Engineering, Implantation of a Tissue-Engineered Tubular Heart Valve in Growing Lambs, 2016, pages 1-13. J. Reimer, Z. Syedain, B. Haynie, M. Lahti, J. Berry, and R. Tranquillo. With permission of Springer".

4.7 Chapter 4 Figures and Tables

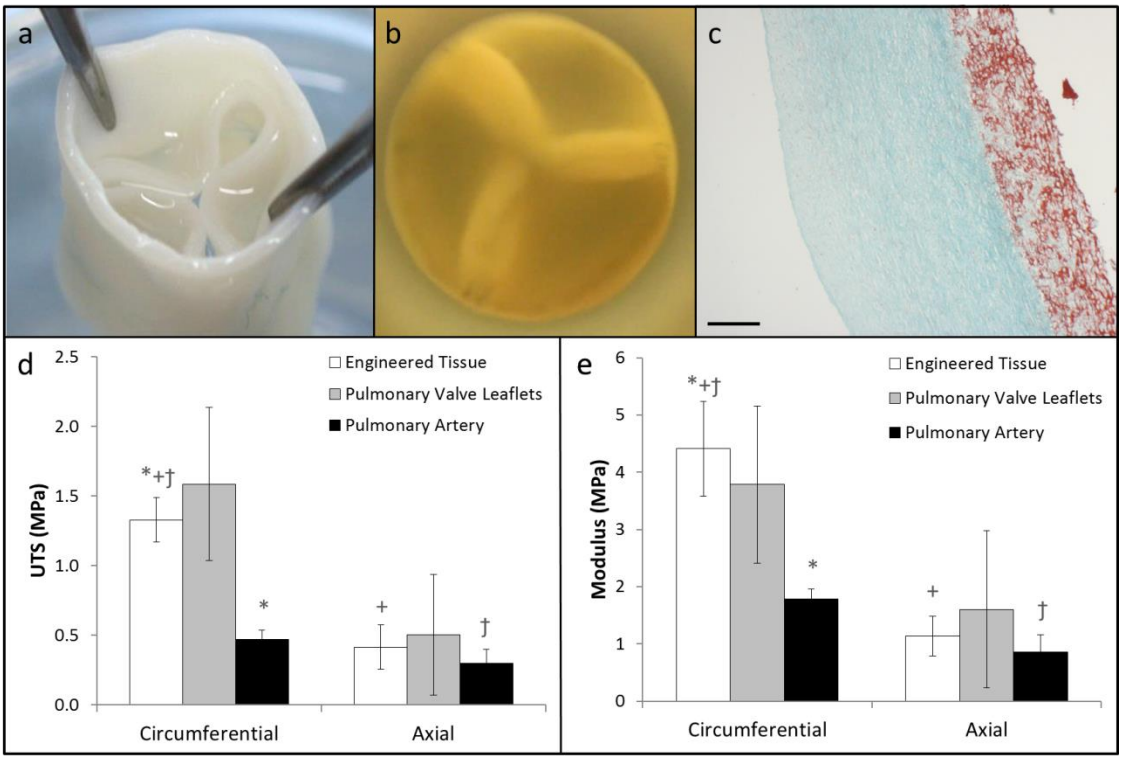

Figure 4-1. Preimplant valve pictures and tissue characterization

Images of the tubular tissue-engineered valve (a) showing the leaflets, root, and (b) short axis view of the valve showing leaflet coaptation under physiologic backpressure. (c) Trichrome stained cross-section of the engineered tissue showing collagen (green) and non-collagen proteins (red); the scale bar is 250 μm. (d) Ultimate tensile stress and (e) tangent modulus of the engineered issue (n=4 for circumferential and axial), pulmonary valve leaflets (circumferential: n=3, axial: n=2), and the pulmonary artery (circumferential: n=4, axial: n=3) in the circumferential and axial directions at the time of implant. Paired symbols indicate a p-value < 0.05 between the two groups.

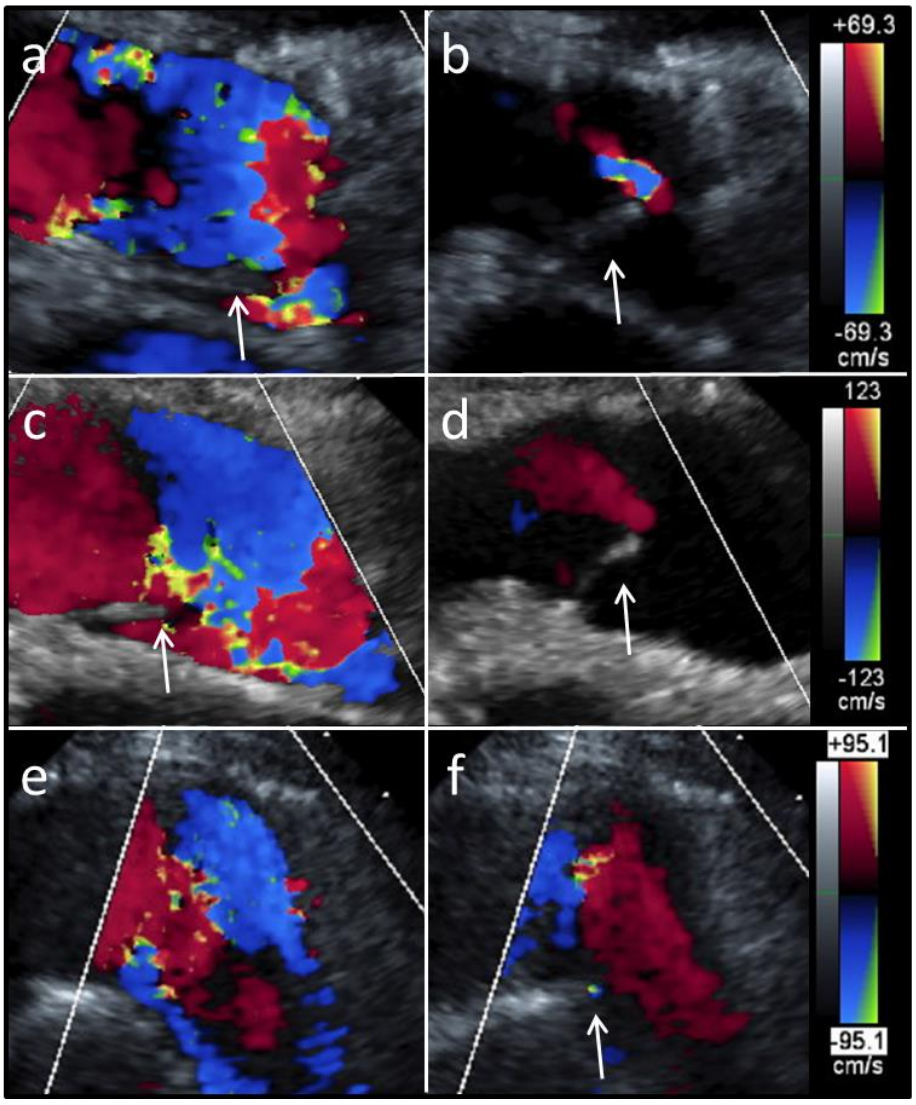

Figure 4-2. Long axis ultrasounds at periodic time points

Long axis ultrasound images of the valve (a,b) 1 week, (c,d) 8 weeks, and (e,f) 20 weeks after implantation. Representative images during (a, c, e) systole and (b, d, f) diastole show valve opening and closing, respectively. For all images, the right ventricle is on the left-hand side and the arrows point to the visible leaflets. Doppler scale bars for each time point are shown on the right.

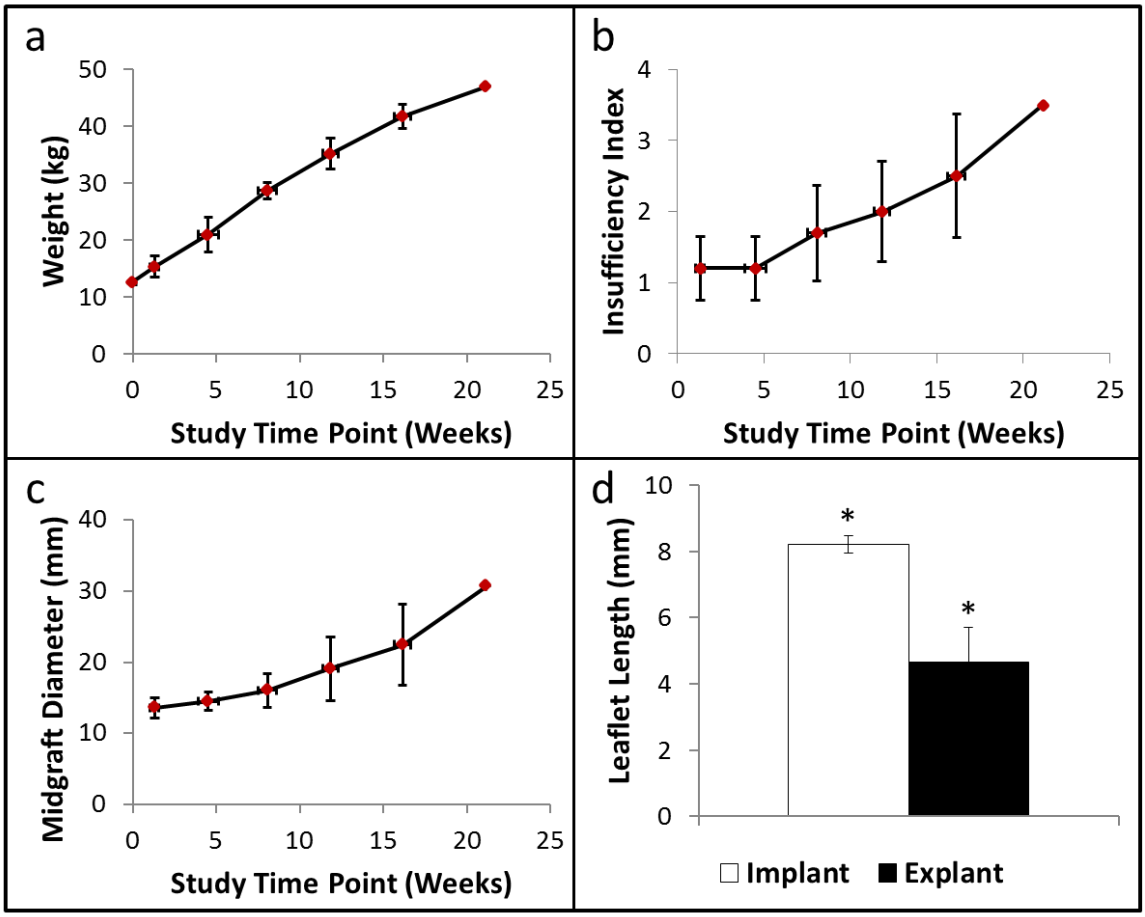

Figure 4-3. Animal and valve metrics over time

(a) Animal weight, (b) valve insufficiency index, and (c) valve diameter midgraft as a function of study time point. (d) Leaflet length before and after implantation. N=5 for all panels. Paired symbols indicate a p-value < 0.05. Error bars in the x- and y-directions represent the standard deviation in the study time point and the measured values, respectively.

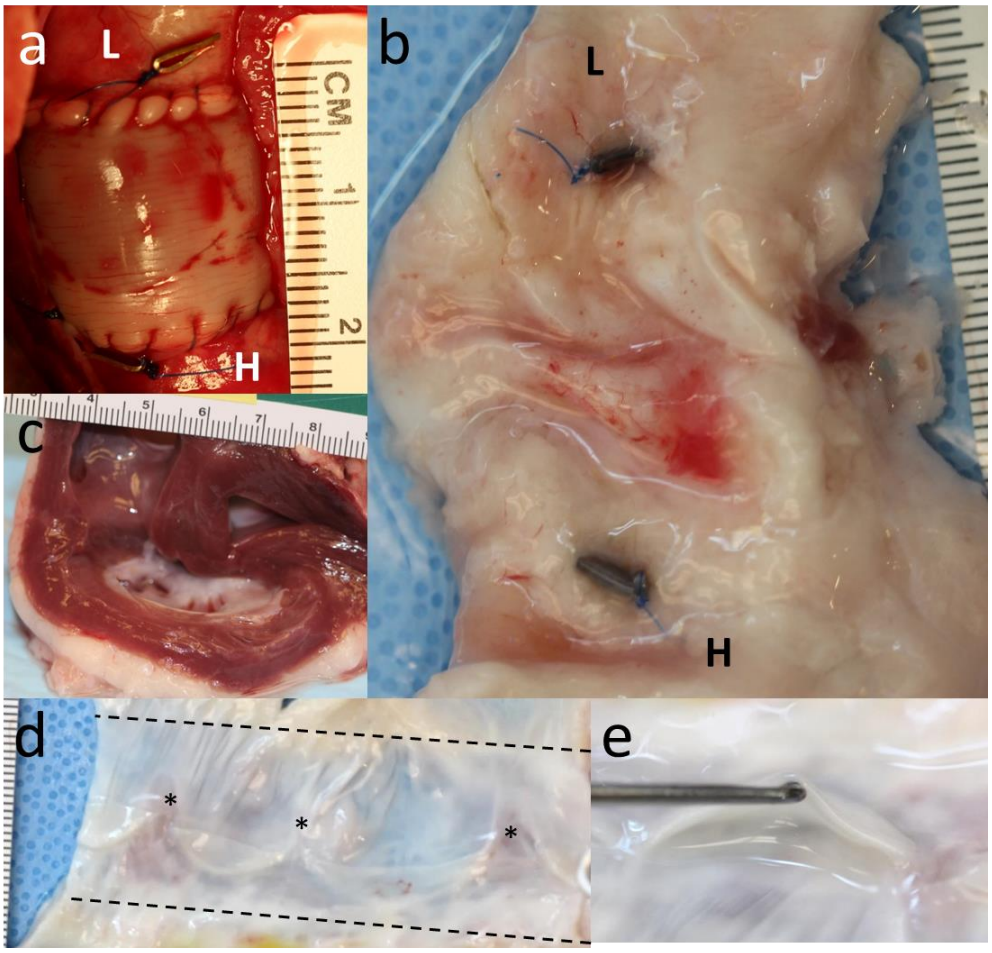

Figure 4-4. Macroscopic valve appearance following implantation

Images of the valve (a) immediately after implantation and (b) explantation after 21.9 weeks at the same scale and in the same orientation. The "L" and "H" refer to the lung and heart end of the valve, respectively. In both images, the clips are visible on the ablumenal surface of the native pulmonary artery. (c) Cross-section of the heart showing normal right ventricle thickness after 21.9 weeks. (d) An explanted valve cut open to show its lumenal surface and leaflets. Stars indicate the original position of the commissures. (e) End-on view of a leaflet.

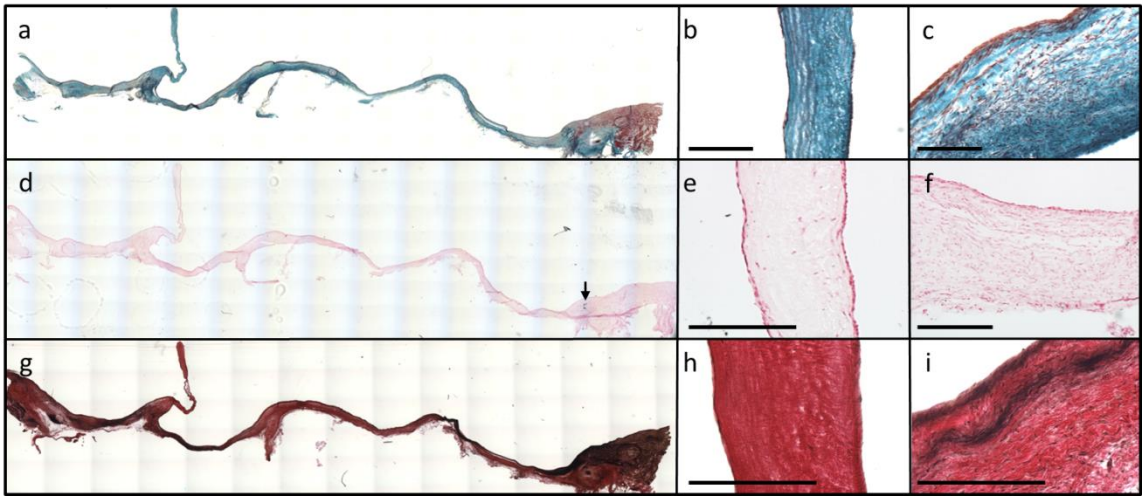

Figure 4-5. Histological characterization of valve matrix following implantation

Reconstructed cross-sectional images of the explanted valves (a, d, g), with the proximal side on the left and the distal side on the right. (a) Trichrome staining revealed collagen (green) throughout the entire valve (b) leaflet and (c) root. (d) Von Kossa staining revealed no apparent calcification in the valve (e) leaflet and (f) root, except near some of the degradable sutures where calcific nodules formed in three animals. Arrow points to calcification present near anastomosis in the pulmonary artery (g) Verhoeff-Van Gieson staining to detect mature elastin (black) in the valve (h) leaflets and (i) root. Scale bars for all images are 250 μm.

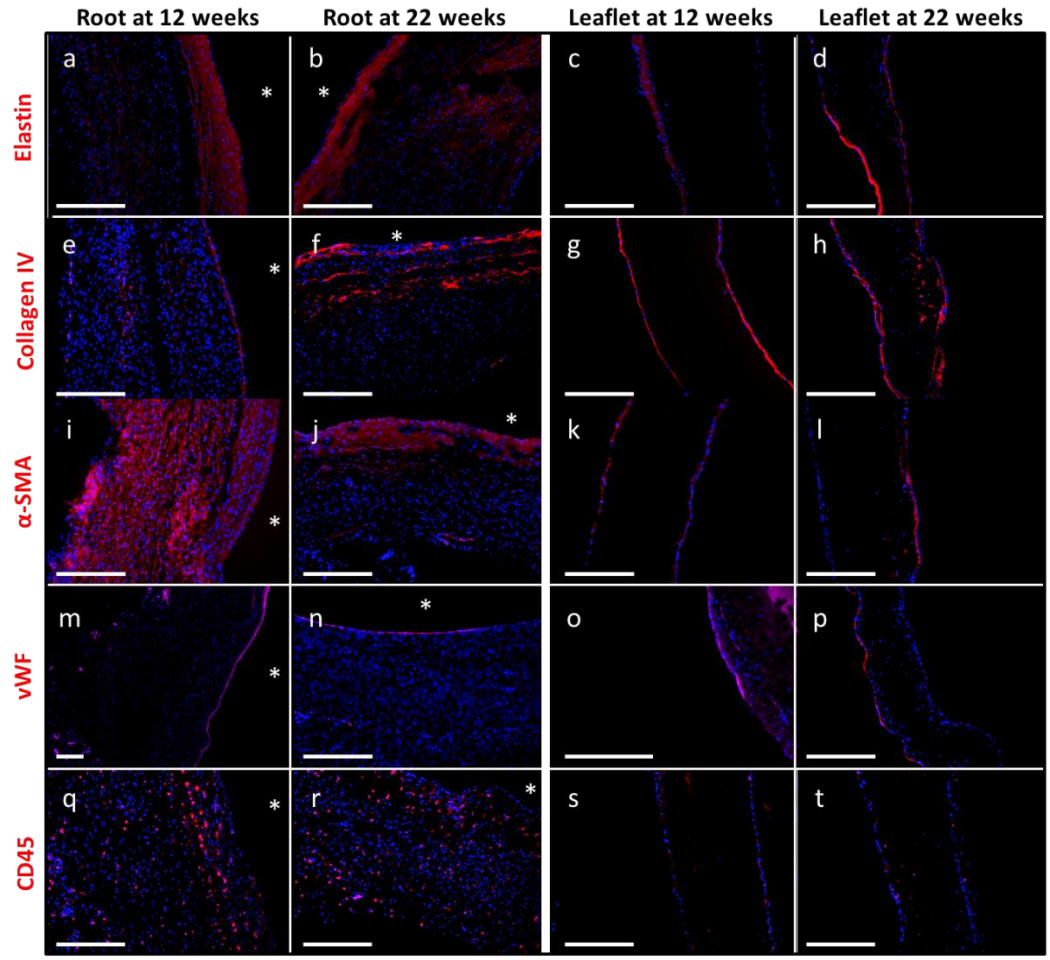

Figure 4-6. Extracellular matrix and cell marker staining following implantation

Comparison of cell markers and matrix proteins in the valve root and leaflet after implantation for 12 or 22 weeks. Immunostaining for matrix proteins revealed the presence of (a-d) elastin and (e-h) collagen IV in the valve root and leaflets. Cell markers included (i-l) α-SMA, (m-p) vWF, and (q-t) CD45. All primary antibodies are pseudo-colored in red and counterstained with Hoechst to visualize cell nuclei. Asterisks indicate the lumenal surface of the valve root.

Table 4-1. Tensile mechanical properties of the explanted engineered root, leaflets, native pulmonary artery, and anastomoses

Sample Description	Sample Orientation	Thickness (mm)	UTS (MPA)	Modulus (MPA)
Explant Root	**Circumferential**	0.93 ± 0.12	1.27 ± 0.20	4.11 ± 1.76
	Axial		0.68 ± 0.27	2.32 ± 1.06
Explant Leaflet	**Circumferential**	0.58 ± 0.12	2.54 ± 0.77	7.93 ± 2.71
	Axial		0.87 ± 0.28	1.94 ± 0.92
Anastomosis	**Axial**	1.59 ± 0.14	0.48 ± 0.29	1.43 ± 0.90
Native Pulmonary Artery	**Circumferential**	1.30 ± 0.23	0.28 ± 0.03	0.93 ± 0.34
	Axial		0.24 ± 0.12	0.64 ± 0.30

Table 4-2. Biochemical properties and DNA concentration of the explanted engineered root, leaflets, and native pulmonary artery

Property	Explanted Root	Explanted Leaflet	Pulmonary Artery
Total Collagen (mg/mL)	63.0 ± 23.7	56.8 ± 15.2	20.5 ± 8.6
Elastin (mg/mL)	9.9 ± 5.0	1.6 ± 0.8	19.6 ± 12.1
Cellularity (Million cells/mL)	170.2 ± 37.0	31.9 ± 25.2	297.9 ± 109.6

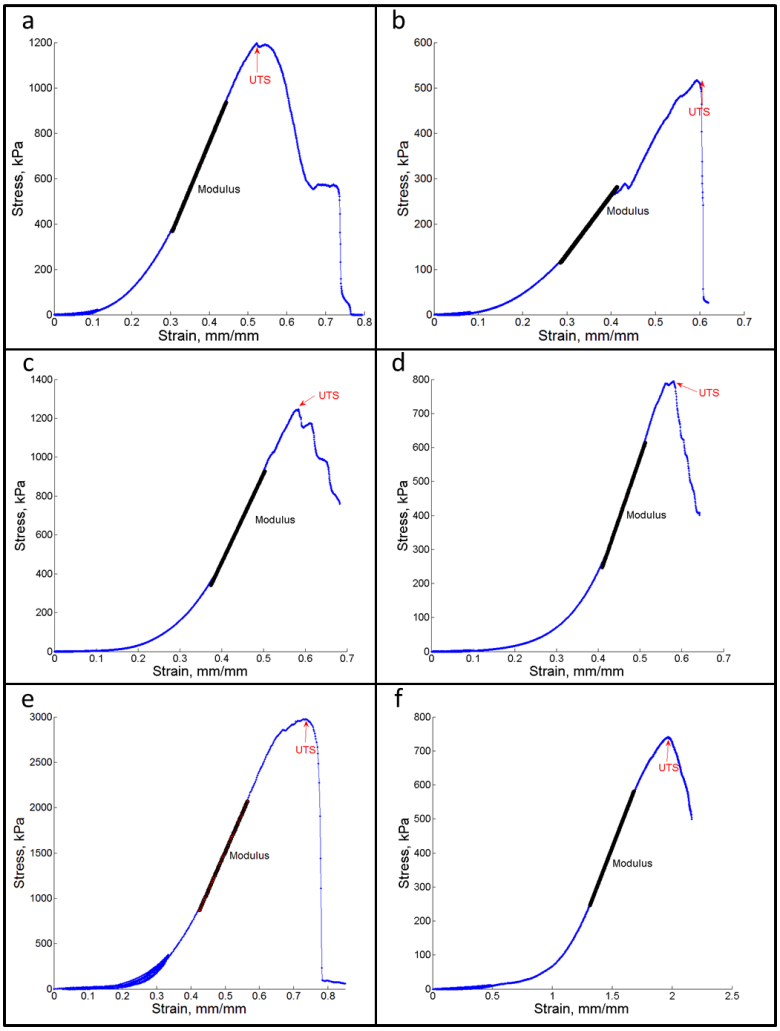

Supplemental Figure 4-1. Stress-strain curves for the engineered tissue

Representative stress-strain curves for the engineered tissue (a,b) before and (c-f) after implantation in the (a,c,e) circumferential and (b,d,f) axial directions. Explant samples include those taken from the valve (c,d) root and (e,f) leaflet. The regions where the modulus (black line) and UTS (arrow) were taken from are also identified.

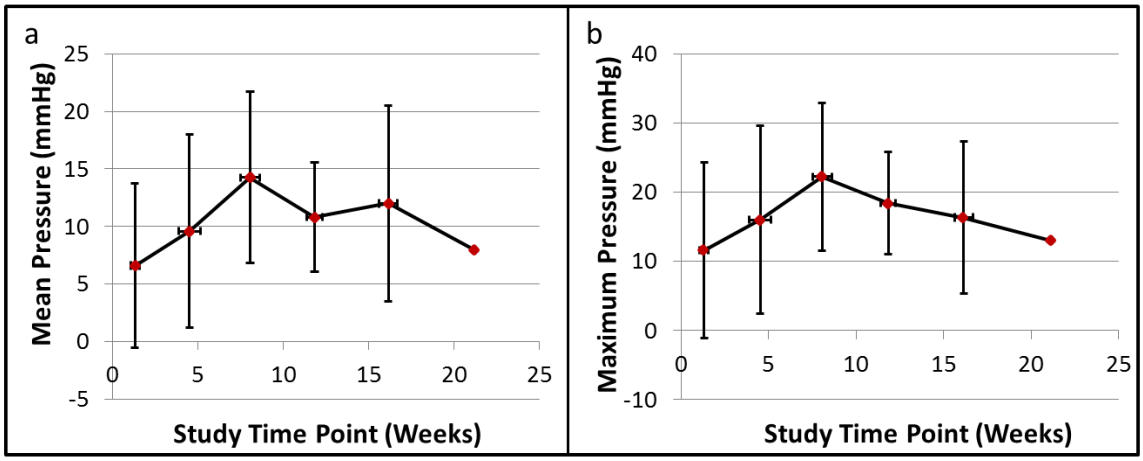

Supplemental Figure 4-2. Valve systolic pressure gradients over time

(a) Mean and (b) maximum valve pressures were measured from the PV VTI. Error bars in the x- and y-directions represent the standard deviation in the study time point and the measured values, respectively. No error bars are provided for the ~21 week time point since n=1.

Chapter 5. Ongoing Work and Future Directions

5.1 Ongoing and Future Studies

Although we achieved many positive outcomes from our *in vivo* pediatric TEHV valve study, we observed diminished valve function at later time points. The functional deterioration that we observed was due, in part, to the absence of leaflet growth. Interestingly, we observed structural leaflet shortening compared to their initial length. Historically this process has been was cell-mediated and spawned a generation of decellularized TEHVs (Chapter 1). In this case, however, we believe that shortening resulted in large part from inadequate fusion at the commissures prior to suture degradation.

Stabilizing the commissure regions with a modified sewing pattern might remedy leaflet shortening. However, valve function would have deteriorated even if the leaflet length was preserved since a rapidly growing animal model was used. The initial leaflet length was not sufficient to accommodate the change in expected range of diameter increase. As we demonstrated in Chapters 3 and 4, this growth is dependent on host cell invasion and their subsequent response to physiological growth cues. Previously in our lab, we demonstrated that host cell invasion proceeded predominantly from the adjacent tissue rather than from blood-born cells [111]. However, the mechanism of recellularization was unclear in this pediatric valve study. While the root was fully recellularized, there was no clear progression of host cell invasion from the leaflet belly towards the free edge. Instead the cellularization in the leaflets was spatially uniform with invasion progressing from the leaflet surfaces.

5.1.1 Human versus Animal Growth

Regardless of the recellularization mechanism, it is clear that additional time is required for the leaflets to more extensively recellularize and thus grow. In the sheep model, time before the leaflets no longer coapt is limited due to how quickly the lambs reach adulthood (within 1 year). Thus, a more suitable animal model is needed in order to study leaflet growth. Ideally, the new animal model would have a growth rate of the main pulmonary artery (MPA) similar to that of humans, while enlarge over the same diameter

range. However, human growth occurs on the time scale of years, whereas sheep fully mature in a matter of months (Figure 5-1a). Growth data for humans and sheep were obtained from published reports and compared to empirical sheep data from the studies described in Chapters 3 and 4 [101,102,163]. The data adapted from Gottlieb et al. [101] is particularly useful because the authors used healthy sheep (no intervention) in order to characterize normal growth.

While Figure 5-1a clearly shows that sheep physically grow much faster compared to humans, it does not directly address differences in organ-level growth. The main pulmonary artery diameter increases on the time scale of years in humans (Figure 5-1b, [103]). The diameter of the MPA in sheep (Figure 5-1c) was adapted from MPA volume and length data reported by Gottlieb et al. [101]. Not surprisingly, the MPA growth is directly related to the physical growth for both sheep and humans. That is, full growth of the sheep MPA occurs in months in sheep, but over the course of years in humans. The MPA growth rate can be reduced in sheep (Figure 5-1d) by utilizing an older animal. However, it will still be faster than in humans even if a 50-60 kg sheep were used. Furthermore, these animals are near adulthood and growth of the pulmonary artery is reduced. Reliably measuring these smaller changes (~1 mm) in diameter can be challenging given the imaging modalities. Thus, our approach to increase the length of time for leaflet recellularization and growth does not rely on drastically reducing the MPA growth rate.

5.1.2 Modified Animal Model

We utilized a valve design that will remain functional following growth of the TEHV root. This design is predicated on eliminating structural leaflet shortening and having a leaflet coaptation length that approaches zero when the maximum MPA diameter is reached. In order to achieve this, we reduced the expected increase in MPA diameter range from ~16-23 mm to ~20-23 mm while keeping the initial leaflet coaptation length the same. Based on the MPA diameter data in Figure 5-1, the native sheep pulmonary artery is 20 mm when it weighs ~30 kg. Although leaflet

recellularization is not expected to occur faster, it will be afforded a longer period of time to occur without the valve becoming insufficient. Furthermore, the invading cells will also be exposed to physiological growth cues for a longer period of time without compromised valve function.

Alternatively, one could utilize the same animal model (12-15 kg), but significantly increase the initial leaflet coaptation length. While leaflet coaptation would be maintained despite root growth, large coaptation lengths can deleteriously affect the valve's hemodynamic performance. This includes abnormal leaflet motion and elevated systolic pressure gradients based on pulse duplicator testing in our lab.

5.1.3 Pulse Duplicator Testing of 20 mm Diameter TEHV

TEHVs were fabricated using 20 mm (Figure 5-2a,b) diameter tubes instead of 16 mm, as described in Chapter 2. In order to validate adequate hemodynamic performance, two TEHVs were tested under pulmonary conditions in the pulse duplicator system. Test conditions (pressure and flowrates) were similar to the testing performed for the 16 mm diameter TEHVs (Table 5-1). A representative flow and pressure waveform is shown in Figure 5-2e.

Leaflet motion, regurgitation, effective orifice area, and systolic pressure gradient were among the metrics recorded for the TEHVs. Three symmetric leaflets were visible when the TEHV was closed (Figure 5-2c) . The leaflets opened rapidly during systole, as evidenced by a minimal systolic pressure gradient (1.5 ± 0.5 mmHg). When fully opened (Figure 5-2d), the TEHVs had a geometric orifice area (GOA) of 75.2% ± 0.9% (Table 5-1). These results were comparable to the 16 mm diameter TEHVs and better than the Contegra valve discussed in Chapter 2.

5.1.4 *In Vivo* Study with 20 mm Diameter TEHVs

A future preclinical study is planned in order to assess TEHV function and growth potential, as discussed above. Since the range of growth is reduced in the older animal model, it is imperative that the TEHV dimensions can be accurately measured prior to,

during, and after implantation. The graft dimensions will be utilized to determine whether the TEHV root and leaflets grew during implantation.

Two different methods or comparisons will be made. First, TEHV dimensions will be measured using macroscopic images prior to and after explanation. TEHV dimensions will also be determined via ultrasound in order to confirm the dimensional changes. While it is possible to track some dimensions (diameter, leaflet length) using transthoracic echocardiograms, image quality often deteriorates as the animal ages and if other organs obscure the view. In order to more reliably compare TEHV dimensions, epicardial echocardiograms will be performed immediately after TEHV implantation and prior to euthanization.

Characterization of the engineered tissue will also be necessary to confirm somatic growth as opposed to stretching. Our approach will rely on characterization methods described in Chapters 3 and 4. The total collagen content in the TEHV root and leaflets will be particularly useful to discern between growth and stretching. Ultimately, these methods aim to confirm and phenotype host cell invasion as well as characterize new extracellular matrix proteins production to support the hypothesis that the invaded cells confer our TEHV with the ability to grow and remodel *in vivo*.

5.2 Chapter 5 Figures and Tables

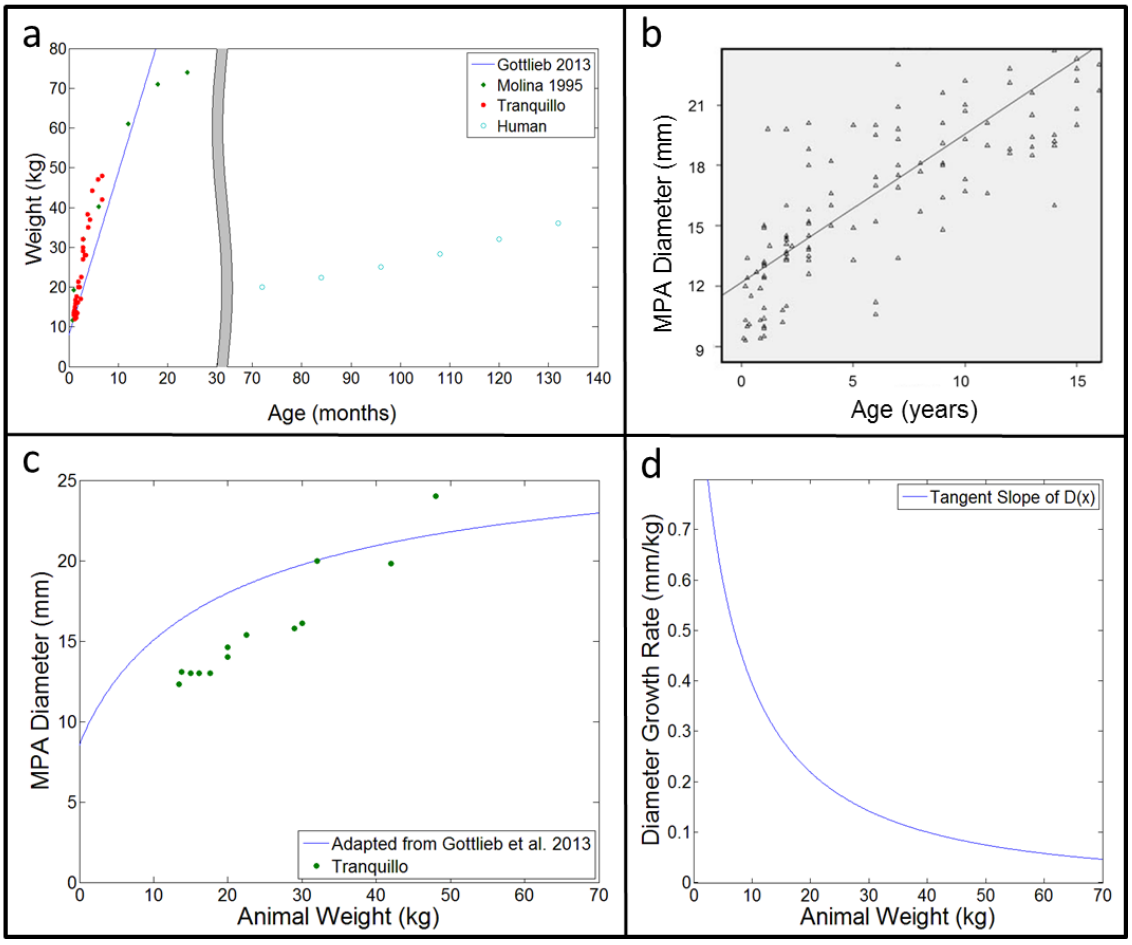

Figure 5-1. Animal versus human growth trends

(a) Weight versus age for humans and sheep using data from the Tranquillo lab and published reports [101,102,163]. Diameter of the main pulmonary artery (MPA) versus (b) age in humans and (c) weight in sheep (adapted from Gottlieb et al. [101]). Comparative data from the Tranquillo lab is also shown (green dots). (d) Diameter growth rate (tangent slope of the curve in panel c) of the MPA versus weight in sheep.

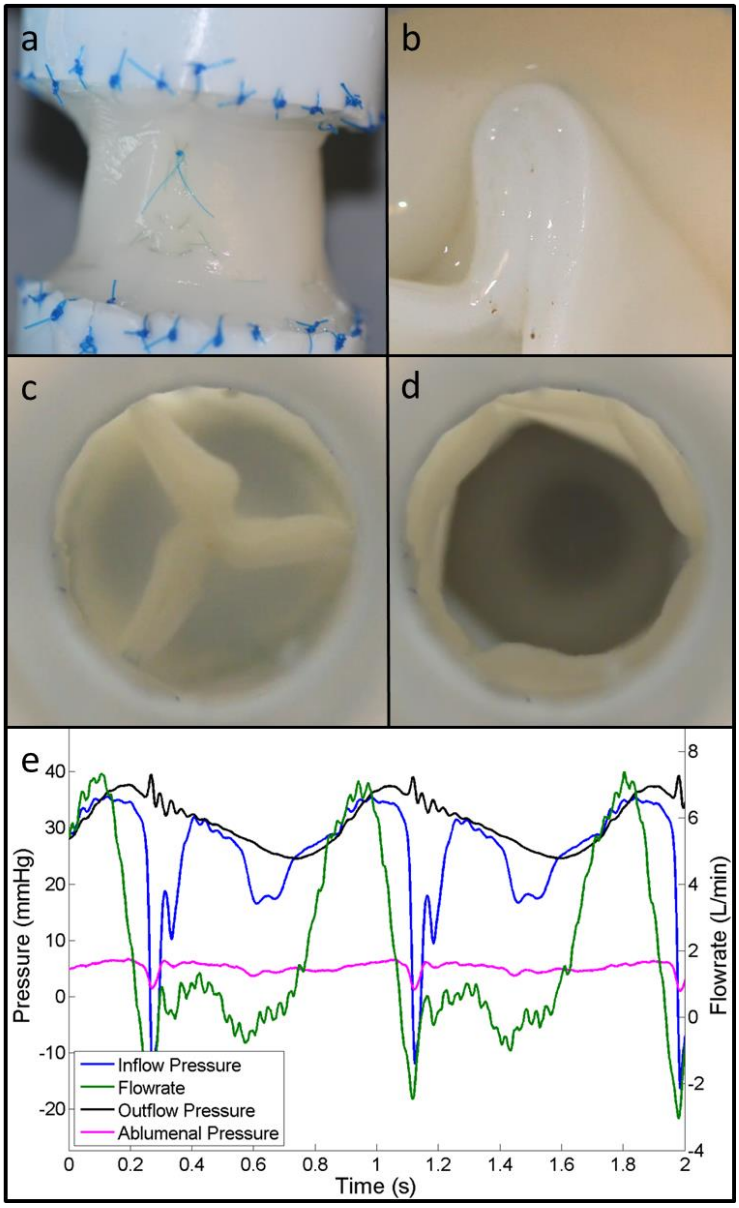

Figure 5-2. Pulse duplicator testing of 20 mm diameter TEHVs

20 mm diameter TEHVs were (a) sewn and hemodynamically characterized in the pulse duplicator system. The (b) leaflet and root tubes were firmly attached when viewed from the lumen after sewing. The TEHV (c) fully closed and (d) open in response to pulmonary pressure and flow conditions as shown in the (e) representative waveform.

Table 5-1. Pulse duplicator testing of 20 mm diameter TEHVs

Property	TEHVs (n=2)
Mean Diastolic ΔP (mmHg)	12.8 ± 4.4
Mean Systolic ΔP (mmHg)	1.5 ± 0.5
Mean Ablumenal Pressure (mmHg)	4.7 ± 0.4
Mean Forward Flow Rate (L/min)	3.6 ± 0.4
Regurgitant Fraction (%)	8.2 ± 0.3
Geometric Orifice Area (%)	75.2 ± 0.9

Chapter 6. References

[1] Mozaffarian D, Benjamin EJ, Go AS, Arnett DK, Blaha MJ, Cushman M, de Ferranti S, Despres JP, Fullerton HJ, Howard VJ, Huffman MD, Judd SE, Kissela BM, Lackland DT, Lichtman JH, Lisabeth LD, Liu S, Mackey RH, Matchar DB, McGuire DK, Mohler ER, 3rd, Moy CS, Muntner P, Mussolino ME, Nasir K, Neumar RW, Nichol G, Palaniappan L, Pandey DK, Reeves MJ, Rodriguez CJ, Sorlie PD, Stein J, Towfighi A, Turan TN, Virani SS, Willey JZ, Woo D, Yeh RW, Turner MB. Heart disease and stroke statistics--2015 update: A report from the american heart association. Circulation 2015;131(4):e29-322.
[2] Moller J. Prevalence and incidence of cardiac malformations. In: Moller J, editor. Surgery of congenital heart disease: Pediatric care consortium 1984-1995. Armonk, New York: Futura Publishing Company Inc; 1998. p. 19-26.
[3] Health MDo. Diseases and conditions identified in children. 2015. 8/24/2015. http://www.health.state.mn.us/divs/cfh/topic/diseasesconds/
[4] Prevention CfDCa. Data & statistics for congenital defects in the us. 2015. 8/24/2015. http://www.cdc.gov/ncbddd/birthdefects/data.html
[5] Liao K, John R. Handbook of cardiac anatomy, physiology, and devices. 2 ed. Minneapolis, MN: Spring Science & Business Media; 2009.
[6] Waterbolk TW, Hoendermis ES, den Hamer IJ, Ebels T. Pulmonary valve replacement with a mechanical prosthesis. Promising results of 28 procedures in patients with congenital heart disease. European journal of cardio-thoracic surgery : official journal of the European Association for Cardio-thoracic Surgery 2006;30(1):28-32.
[7] Bouzas B, Kilner PJ, Gatzoulis MA. Pulmonary regurgitation: Not a benign lesion. Eur Heart J 2005;26(5):433-9.
[8] Yemets IM, Williams WG, Webb GD, Harrison DA, McLaughlin PR, Trusler GA, Coles JG, Rebeyka IM, Freedom RM. Pulmonary valve replacement late after repair of tetralogy of fallot. Ann Thorac Surg 1997;64(2):526-30.
[9] Tweddell JS, Simpson P, Li SH, Dunham-Ingle J, Bartz PJ, Earing MG, Pelech AN. Timing and technique of pulmonary valve replacement in the patient with tetralogy of fallot. Semin Thorac Cardiovasc Surg Pediatr Card Surg Annu 2012;15(1):27-33.
[10] Kheradvar A, Groves EM, Goergen CJ, Alavi SH, Tranquillo R, Simmons CA, Dasi LP, Grande-Allen KJ, Mofrad MR, Falahatpisheh A, Griffith B, Baaijens F, Little SH, Canic S. Emerging trends in heart valve engineering: Part ii. Novel and standard technologies for aortic valve replacement. Ann Biomed Eng 2015;43(4):844-57.
[11] Kheradvar A, Groves EM, Simmons CA, Griffith B, Alavi SH, Tranquillo R, Dasi LP, Falahatpisheh A, Grande-Allen KJ, Goergen CJ, Mofrad MR, Baaijens F, Canic S, Little SH. Emerging trends in heart valve engineering: Part iii. Novel technologies for mitral valve repair and replacement. Ann Biomed Eng 2015;43(4):858-70.
[12] Rahimtoola SH. Choice of prosthetic heart valve for adult patients. J Am Coll Cardiol 2003;41(6):893-904.
[13] Rahimtoola SH. Choice of prosthetic heart valve in adults an update. J Am Coll Cardiol 2010;55(22):2413-26.

[14] Birkmeyer NJ, Birkmeyer JD, Tosteson aN, Grunkemeier GL, Marrin Ca, O'Connor GT. Prosthetic valve type for patients undergoing aortic valve replacement: A decision analysis. Ann Thorac Surg 2000;70(6):1946-52.
[15] El Oakley R, Kleine P, Bach DS. Choice of prosthetic heart valve in today's practice. Circulation 2008;117(2):253-6.
[16] Kaneko T, Cohn LH, Aranki SF. Tissue valve is the preferred option for patients aged 60 and older. Circulation 2013;128:1365-71.
[17] van Geldorp MWa, Eric Jamieson WR, Kappetein aP, Ye J, Fradet GJ, Eijkemans MJC, Grunkemeier GL, Bogers AJJC, Takkenberg JJM. Patient outcome after aortic valve replacement with a mechanical or biological prosthesis: Weighing lifetime anticoagulant-related event risk against reoperation risk. J Thorac Cardiovasc Surg 2009;137(4):881-6, 6e1-e5.
[18] Mankad S. Management of prosthetic heart valve complications. Current treatment options in cardiovascular medicine 2012;14(6):608-21.
[19] Tillquist MN, Maddox TM. Cardiac crossroads: Deciding between mechanical or bioprosthetic heart valve replacement. Patient preference and adherence 2011;5:91-9.
[20] Oterhals K, Fridlund B, Nordrehaug JE, Haaverstad R, Norekvål TM. Adapting to living with a mechanical aortic heart valve: A phenomenographic study. Journal of advanced nursing 2013;69(9):2088-98.
[21] Hammermeister K, Sethi GK, Henderson WG, Grover FL, Oprian C, Rahimtoola SH. Outcomes 15 years after valve replacement with a mechanical versus a bioprosthetic valve: Final report of the veterans affairs randomized trial. J Am Coll Cardiol2000. p. 1152-8.
[22] Delmo Walter EM, de By TMMH, Meyer R, Hetzer R. The future of heart valve banking and of homografts: Perspective from the deutsches herzzentrum berlin. HSR Proc Intensive Care Cardiovasc Anesth 2012;4(2):97-108.
[23] Elkins RC, Goldstein S, Hewitt CW, Walsh SP, Dawson PE, Ollerenshaw JD, Black KS, Clarke DR, O'Brien M F. Recellularization of heart valve grafts by a process of adaptive remodeling. Semin Thorac Cardiovasc Surg 2001;13(4 Suppl 1):87-92.
[24] Neumann A, Cebotari S, Tudorache I, Haverich A, Sarikouch S. Heart valve engineering: Decellularized allograft matrices in clinical practice. Biomedizinische Technik Biomedical engineering 2013;58(5):453-6.
[25] Elkins R, Dawson P, Goldstein S, Walsh S, Black K. Decellularized human valve allografts. Ann Thorac Surg 2001;71(5):S428-S32.
[26] Jones JM, O'kane H, Gladstone DJ, Sarsam Ma, Campalani G, MacGowan SW, Cleland J, Cran GW. Repeat heart valve surgery: Risk factors for operative mortality. J Thorac Cardiovasc Surg 2001;122(5):913-8.
[27] Gurvitch R, Cheung A, Ye J, Wood Da, Willson AB, Toggweiler S, Binder R, Webb JG. Transcatheter valve-in-valve implantation for failed surgical bioprosthetic valves. J Am Coll Cardiol 2011;58(21):2196-209.

[28] Gurvitch R, Cheung A, Bedogni F, Webb JG. Coronary obstruction following transcatheter aortic valve-in-valve implantation for failed surgical bioprostheses. Catheter Cardiovasc Interv 2011;77(3):439-44.
[29] Dvir D, Webb J, Brecker S, Bleiziffer S, Hildick-Smith D, Colombo A, Descoutures F, Hengstenberg C, Moat NE, Bekeredjian R, Napodano M, Testa L, Lefevre T, Guetta V, Nissen H, Hernandez JM, Roy D, Teles RC, Segev A, Dumonteil N, Fiorina C, Gotzmann M, Tchetche D, Abdel-Wahab M, De Marco F, Baumbach A, Laborde JC, Kornowski R. Transcatheter aortic valve replacement for degenerative bioprosthetic surgical valves: Results from the global valve-in-valve registry. Circulation 2012;126(19):2335-44.
[30] Cebotari S, Tudorache I, Ciubotaru A, Boethig D, Sarikouch S, Goerler A, Lichtenberg A, Cheptanaru E, Barnaciuc S, Cazacu A, Maliga O, Repin O, Maniuc L, Breymann T, Haverich A. Use of fresh decellularized allografts for pulmonary valve replacement may reduce the reoperation rate in children and young adults early report. Circulation 2011;124(11):S115-S23.
[31] Erdbrügger W, Konertz W, Dohmen PM, Posner S, Ellerbrok H, Brodde O-EE, Robenek H, Modersohn D, Pruss A, Holinski S, Stein-Konertz M, Pauli G, Erdbrugger W. Decellularized xenogenic heart valves reveal remodeling and growth potential in vivo. Tissue Eng 2006;12(8):2059-68.
[32] Dohmen PM, Lembcke A, Holinski S, Pruss A, Konertz W. Ten years of clinical results with a tissue-engineered pulmonary valve. Ann Thorac Surg 2011;92(4):1308-14.
[33] Konertz W, Angeli E, Tarusinov G, Christ T, Kroll J, Dohmen PM, Krogmann O, Franzbach B, Pace Napoleone C, Gargiulo G. Right ventricular outflow tract reconstruction with decellularized porcine xenografts in patients with congenital heart disease. J Heart Valve Dis 2011;20(3):341-7.
[34] Ruzmetov M, Shah JJ, Geiss DM, Fortuna RS. Decellularized versus standard cryopreserved valve allografts for right ventricular outflow tract reconstruction: A single-institution comparison. J Thorac Cardiovasc Surg 2012;143(3):543-9.
[35] Brown JW, Elkins RC, Clarke DR, Tweddell JS, Huddleston CB, Doty JR, Fehrenbacher JW, Takkenberg JJM. Performance of the cryovalve sg human decellularized pulmonary valve in 342 patients relative to the conventional cryovalve at a mean follow-up of four years. J Thorac Cardiovasc Surg 2010;139:339-48.
[36] Tudorache I, Theodoridis K, Baraki H, Sarikouch S, Bara C, Meyer T, Hoffler K, Hartung D, Hilfiker A, Haverich A, Cebotari S. Decellularized aortic allografts versus pulmonary autografts for aortic valve replacement in the growing sheep model: Haemodynamic and morphological results at 20 months after implantation. European journal of cardio-thoracic surgery : official journal of the European Association for Cardio-thoracic Surgery 2015.
[37] Baraki H, Tudorache I, Braun M, Hoffler K, Gorler A, Lichtenberg A, Bara C, Calistru A, Brandes G, Hewicker-Trautwein M, Hilfiker A, Haverich A, Cebotari S. Orthotopic replacement of the aortic valve with decellularized allograft in a sheep model. Biomaterials 2009;30(31):6240-6.

[38] Bibevski S, Wilkinson D, Ruzmetov M, Fortuna R, Turrentine M, Brown JW, Ohye RG. Performance of synergraft decellularized pulmonary allografts compared with standard cryopreserved allografts: Results from multi-institutional data. Circulation2012. p. a9142.
[39] Tudorache I, Calistru A, Baraki H, Meyer T, Hoffler K, Sarikouch S, Bara C, Gorler A, Hartung D, Hilfiker A, Haverich A, Cebotari S. Orthotopic replacement of aortic heart valves with tissue-engineered grafts. Tissue Eng Part A 2013;19(15-16):1686-94.
[40] Perri G, Polito A, Esposito C, Albanese SB, Francalanci P, Pongiglione G, Carotti A. Early and late failure of tissue-engineered pulmonary valve conduits used for right ventricular outflow tract reconstruction in patients with congenital heart disease. Eur J Cardiothorac Surg 2012;41(6):1320-5.
[41] Kheradvar A, Groves EM, Dasi LP, Alavi SH, Tranquillo R, Grande-Allen KJ, Simmons CA, Griffith B, Falahatpisheh A, Goergen CJ, Mofrad MR, Baaijens F, Little SH, Canic S. Emerging trends in heart valve engineering: Part i. Solutions for future. Ann Biomed Eng 2015;43(4):833-43.
[42] Chester A, Yacoub MH, Taylor PM. Heart valve tissue engineering. In: Boccaccini AR, Harding SE, editors. Myocardial tissue engineering2011. p. 243-66.
[43] Schmidt JB, Tranquillo RT. Tissue-engineered heart valves. In: Iaizzo PA, Bianco R, Hill AJ, St. Louis JD, editors. Heart valves: From design to clinical implantation2013. p. 261-80.
[44] van Loon SLM, Smits AIPM, Driessen-Mol A, Baaijens F, Bouten CV. The immune response in in situ tissue engineering of aortic heart valves. In: Aikawa E, editor. Calcific aortic valve disease2013. p. 207-45.
[45] Bouten CV, Driessen-Mol A, Baaijens FP. In situ heart valve tissue engineering: Simple devices, smart materials, complex knowledge. Expert Rev Med Devices 2012;9(5):453-5.
[46] Hayashida K, Kanda K, Yaku H, Ando J, Nakayama Y. Development of an in vivo tissue-engineered, autologous heart valve (the biovalve): Preparation of a prototype model. J Thorac Cardiovasc Surg 2007;134(1):152-9.
[47] Bouten CV, Smits AI, Talacua H, Muylaert DE, Janssen HM, Bosman A, Verhaar MC, Dankers PY, Driessen A, Kluin J, Baaijens FP. Biomaterial-based in situ tissue engineering of heart valves. 2015 4th TERMIS World Congress. 2015/09/01 ed. Boston, MA: Tissue Engineering Part A; 2015. p. S1-S413.
[48] Ott HC, Matthiesen TS, Goh SK, Black LD, Kren SM, Netoff TI, Taylor DA. Perfusion-decellularized matrix: Using nature's platform to engineer a bioartificial heart. Nature Medicine 2008;14(2):213-21.
[49] Gilbert TW, Sellaro TL, Badylak SF. Decellularization of tissues and organs. Biomaterials 2006;27(19):3675-83.
[50] Taylor PM. Biological matrices and bionanotechnology. Philosophical transactions of the Royal Society of London Series B, Biological sciences 2007;362(1484):1313-20.
[51] Sung HJ, Meredith C, Johnson C, Galis ZS. The effect of scaffold degradation rate on three-dimensional cell growth and angiogenesis. Biomaterials 2004;25(26):5735-42.

[52] Zund G, Breuer CK, Shinoka T, Ma PX, Langer R, Mayer JE, Vacanti JP. The in vitro construction of a tissue engineered bioprosthetic heart valve. European journal of cardio-thoracic surgery : official journal of the European Association for Cardio-thoracic Surgery 1997;11(3):493-7.
[53] Stock UA, Nagashima M, Khalil PN, Nollert GD, Herden T, Sperling JS, Moran A, Lien J, Martin DP, Schoen FJ, Vacanti JP, Mayer JE, Jr. Tissue-engineered valved conduits in the pulmonary circulation. J Thorac Cardiovasc Surg 2000;119(4 Pt 1):732-40.
[54] Knight R, Wilcox HE, Korossis SA, Ingham E. The use of acellular matrices for tissue engineering of cardiac valves. Proc Inst Mech Eng H 2008;222(1):129-43.
[55] Hoerstrup SP, Sodian R, Daebritz S, Wang J, Bacha EA, Martin DP, Moran AM, Guleserian KJ, Sperling JS, Kaushal S, Vacanti JP, Schoen FJ, Mayer JE, Jr. Functional living trileaflet heart valves grown in vitro. Circulation 2000;102(19 Suppl 3):III44-II9.
[56] Knight RL, Booth C, Wilcox HE, Fisher J, Ingham E. Tissue engineering of cardiac valves: Re-seeding of acellular porcine aortic valve matrices with human mesenchymal progenitor cells. J Heart Valve Dis 2005;14(6):806-13.
[57] Rippel RA, Ghanbari H, Seifalian AM. Tissue-engineered heart valve: Future of cardiac surgery. World J Surg 2012;36(7):1581-91.
[58] Glowacki J, Mizuno S. Collagen scaffolds for tissue engineering. Biopolymers 2008;89(5):338-44.
[59] Chevallay B, Herbage D. Collagen-based biomaterials as 3d scaffold for cell cultures: Applications for tissue engineering and gene therapy. Med Biol Eng Comput 2000;38(2):211-8.
[60] Thie M, Schlumberger W, Semich R, Rauterberg J, Robenek H. Aortic smooth muscle cells in collagen lattice culture: Effects on ultrastructure, proliferation and collagen synthesis. European journal of cell biology 1991;55(2):295-304.
[61] Clark RA, Nielsen LD, Welch MP, McPherson JM. Collagen matrices attenuate the collagen-synthetic response of cultured fibroblasts to tgf-beta. J Cell Sci 1995;108(Pt 3):1251-61.
[62] Ma P. Biomaterials and regenerative medicine: Cambridge University Press; 2012.
[63] Coustry F, Gillery P, Maquart FX, Borel JP. Effect of transforming growth factor beta on fibroblasts in three-dimensional lattice cultures. FEBS Lett 1990;262(2):339-41.
[64] Grassl ED, Oegema TR, Tranquillo RT. Fibrin as an alternative biopolymer to type-i collagen for the fabrication of a media equivalent. J Biomed Mater Res 2002;60(4):607-12.
[65] Alavi SH, Kheradvar A. Metal mesh scaffold for tissue engineering of membranes. Tissue Eng Part C Methods 2012;18(4):293-301.
[66] Loger K, Engel A, Haupt J, Li Q, Lima de Miranda R, Quandt E, Lutter G, Selhuber-Unkel C. Cell adhesion on niti thin film sputter-deposited meshes. Materials Science and Engineering: C 2016;59:611-6.

[67] Loger K, de Miranda RL, Engel A, Marczynski-Bühlow M, Lutter G, Quandt E. Fabrication and evaluation of nitinol thin film heart valves. Cardiovasc Eng Technol 2014;5(4):308-16.
[68] Stepan LL, Levi DS, Carman GP. A thin film nitinol heart valve. Journal of biomechanical engineering 2005;127(6):915-8.
[69] Alavi SH, Kheradvar A. A hybrid tissue-engineered heart valve. Ann Thorac Surg 2015;99(6):2183-7.
[70] Alavi SH, Liu WF, Kheradvar A. Inflammatory response assessment of a hybrid tissue-engineered heart valve leaflet. Ann Biomed Eng 2013;41(2):316-26.
[71] Neidert MR, Lee ES, Oegema TR, Tranquillo RT. Enhanced fibrin remodeling in vitro with tgf-beta1, insulin and plasmin for improved tissue-equivalents. Biomaterials 2002;23(17):3717-31.
[72] Ramaswamy S, Gottlieb D, Engelmayr GC, Aikawa E, Schmidt DE, Gaitan-Leon DM, Sales VL, Mayer JE, Sacks MS. The role of organ level conditioning on the promotion of engineered heart valve tissue development in-vitro using mesenchymal stem cells. Biomaterials 2010;31(6):1114-25.
[73] Robinson P, Johnson S, Evans M, Barocas V, Tranquillo R. Functional tissue-engineered valves from cell-remodeled fibrin with commissural alignment of cell-produced collagen. Tissue Eng Part A 2008;14(1):83-95.
[74] Alenghat FJ, Ingber DE. Mechanotransduction: All signals point to cytoskeleton, matrix, and integrins. Sci STKE 2002;2002(119):pe6.
[75] Chiquet M, Renedo AS, Huber F, Fluck M. How do fibroblasts translate mechanical signals into changes in extracellular matrix production? Matrix biology : journal of the International Society for Matrix Biology 2003;22(1):73-80.
[76] Syedain ZH, Weinberg JS, Tranquillo RT. Cyclic distension of fibrin-based tissue constructs: Evidence of adaptation during growth of engineered connective tissue. Proceedings of the National Academy of Sciences of the United States of America 2008;105(18):6537-42.
[77] Syedain ZH, Tranquillo RT. Controlled cyclic stretch bioreactor for tissue-engineered heart valves. Biomaterials 2009;30(25):4078-84.
[78] Schmidt JB, Tranquillo RT. Cyclic stretch and perfusion bioreactor for conditioning large diameter engineered tissue tubes. Ann Biomed Eng 2015.
[79] Dumont K, Yperman J, Verbeken E, Segers P, Meuris B, Vandenberghe S, Flameng W, Verdonck PR. Design of a new pulsatile bioreactor for tissue engineered aortic heart valve formation. Artif Organs 2002;26(8):710-4.
[80] Hildebrand DK, Wu ZJ, Mayer JE, Jr., Sacks MS. Design and hydrodynamic evaluation of a novel pulsatile bioreactor for biologically active heart valves. Ann Biomed Eng 2004;32(8):1039-49.
[81] Mol A, Driessen NJ, Rutten MC, Hoerstrup SP, Bouten CV, Baaijens FP. Tissue engineering of human heart valve leaflets: A novel bioreactor for a strain-based conditioning approach. Ann Biomed Eng 2005;33(12):1778-88.

[82] Ruel J, Lachance G. A new bioreactor for the development of tissue-engineered heart valves. Ann Biomed Eng 2009;37(4):674-81.
[83] Flanagan T, Cornelissen C, Koch S, Tschoeke B, Sachweh J, Schmitz-Rode T, Jockenhoevel S. The in vitro development of autologous fibrin-based tissue-engineered heart valves through optimized dynamic conditioning. Biomaterials 2007;28(23):3388-97.
[84] Hoerstrup SP, Sodian R, Sperling JS, Vacanti JP, Mayer JE, Jr. New pulsatile bioreactor for in vitro formation of tissue engineered heart valves. Tissue Eng 2000;6(1):75-9.
[85] Berry JL, Steen JA, Koudy Williams J, Jordan JE, Atala A, Yoo JJ. Bioreactors for development of tissue engineered heart valves. Ann Biomed Eng 2010;38(11):3272-9.
[86] Engelmayr GC, Jr., Soletti L, Vigmostad SC, Budilarto SG, Federspiel WJ, Chandran KB, Vorp DA, Sacks MS. A novel flex-stretch-flow bioreactor for the study of engineered heart valve tissue mechanobiology. Ann Biomed Eng 2008;36(5):700-12.
[87] Ramaswamy S, Boronyak SM, Le T, Holmes A, Sotiropoulos F, Sacks MS. A novel bioreactor for mechanobiological studies of engineered heart valve tissue formation under pulmonary arterial physiological flow conditions. Journal of biomechanical engineering 2014;136(12):1210091-12100914.
[88] Weber M, Heta E, Moreira R, Gesche VN, Schermer T, Frese J, Jockenhoevel S, Mela P. Tissue-engineered fibrin-based heart valve with a tubular leaflet design. Tissue Eng Part C Methods 2014;20(4):265-75.
[89] Cox JL, Ad N, Myers K, Gharib M, Quijano RC. Tubular heart valves: A new tissue prosthesis design--preclinical evaluation of the 3f aortic bioprosthesis. J Thorac Cardiovasc Surg 2005;130(2):520-7.
[90] Syedain ZH, Meier LA, Reimer JM, Tranquillo RT. Tubular heart valves from decellularized engineered tissue. Ann Biomed Eng 2013;41(12):2645-54.
[91] Driessen-Mol A, Emmert MY, Dijkman PE, Frese L, Sanders B, Weber B, Cesarovic N, Sidler M, Leenders J, Jenni R, Grunenfelder J, Falk V, Baaijens FP, Hoerstrup SP. Transcatheter implantation of homologous "off-the-shelf" tissue-engineered heart valves with self-repair capacity: Long-term functionality and rapid in vivo remodeling in sheep. J Am Coll Cardiol 2014;63(13):1320-9.
[92] Moreira R, Velz T, Alves N, Gesche VN, Malischewski A, Schmitz-Rode T, Frese J, Jockenhoevel S, Mela P. Tissue-engineered heart valve with a tubular leaflet design for minimally invasive transcatheter implantation. Tissue Eng Part C Methods 2015;21(6):530-40.
[93] Reimer JM, Syedain ZH, Haynie BH, Tranquillo RT. Pediatric tubular pulmonary heart valve from decellularized engineered tissue tubes. Biomaterials 2015;62:88-94.
[94] Dijkman PE, Driessen-Mol A, Frese L, Hoerstrup SP, Baaijens FP. Decellularized homologous tissue-engineered heart valves as off-the-shelf alternatives to xeno- and homografts. Biomaterials 2012;33(18):4545-54.

[95] Sodian R, Lueders C, Kraemer L, Kuebler W, Shakibaei M, Reichart B, Daebritz S, Hetzer R. Tissue engineering of autologous human heart valves using cryopreserved vascular umbilical cord cells. Ann Thorac Surg 2006;81(6):2207-16.
[96] Robinson PS, Tranquillo RT. Planar biaxial behavior of fibrin-based tissue-engineered heart valve leaflets. Tissue Eng Part A 2009;15(10):2763-72.
[97] Kelley TA, Marquez S, Popelar CF. In vitro testing of heart valve substitutes. In: Iaizzo PA, Bianco R, Hill AJ, St. Louis JD, editors. Heart valves: From design to clinical implantation2013. p. 283-320.
[98] Ahlberg SE, Bateman MG, Eggen MD, Quill JL, Richardson ES, Iaizzo PA. Animal models for cardiac valve research. In: Iaizzo PA, Bianco R, Hill AJ, St. Louis JD, editors. Heart valves: From design to clinical implantation2013. p. 343-57.
[99] Weber B, Dijkman PE, Scherman J, Sanders B, Emmert MY, Grunenfelder J, Verbeek R, Bracher M, Black M, Franz T, Kortsmit J, Modregger P, Peter S, Stampanoni M, Robert J, Kehl D, van Doeselaar M, Schweiger M, Brokopp CE, Walchli T, Falk V, Zilla P, Driessen-Mol A, Baaijens FP, Hoerstrup SP. Off-the-shelf human decellularized tissue-engineered heart valves in a non-human primate model. Biomaterials 2013;34(30):7269-80.
[100] Roosens B, Bala G, Droogmans S, Van Camp G, Breyne J, Cosyns B. Animal models of organic heart valve disease. Int J Cardiol 2013;165(3):398-409.
[101] Gottlieb D, Fata B, Powell AJ, Cois CA, Annese D, Tandon K, Stetten G, Mayer JE, Jr., Sacks MS. Pulmonary artery conduit in vivo dimensional requirements in a growing ovine model: Comparisons with the ascending aorta. J Heart Valve Dis 2013;22(2):195-203.
[102] Molina JE, Edwards JE, Bianco RW, Clack RW, Lang G, Molina JR. Composite and plain tubular synthetic graft conduits in right ventricle-pulmonary artery position: Fate in growing lambs. J Thorac Cardiovasc Surg 1995;110(2):427-35.
[103] Akay HO, Ozmen CA, Bayrak AH, Senturk S, Katar S, Nazaroglu H, Taskesen M. Diameters of normal thoracic vascular structures in pediatric patients. Surg Radiol Anat 2009;31(10):801-7.
[104] Shinoka T, Breuer CK, Tanel RE, Zund G, Miura T, Ma PX, Langer R, Vacanti JP, Mayer JE, Jr. Tissue engineering heart valves: Valve leaflet replacement study in a lamb model. Ann Thorac Surg 1995;60(6 Suppl):S513-6.
[105] Schmidt D, Dijkman PE, Driessen-Mol A, Stenger R, Mariani C, Puolakka A, Rissanen M, Deichmann T, Odermatt B, Weber B, Emmert MY, Zund G, Baaijens FPT, Hoerstrup SP. Minimally-invasive implantation of living tissue engineered heart valves. J Am Coll Cardiol 2010;56(6):510-20.
[106] Weber B, Scherman J, Emmert MY, Gruenenfelder J, Verbeek R, Bracher M, Black M, Kortsmit J, Franz T, Schoenauer R, Baumgartner L, Brokopp C, Agarkova I, Wolint P, Zund G, Falk V, Zilla P, Hoerstrup SP. Injectable living marrow stromal cell-based autologous tissue engineered heart valves: First experiences with a one-step intervention in primates. Eur Heart J 2011;32(22):2830-40.

[107] Nakayama Y, Takewa Y, Sumikura H, Yamanami M, Matsui Y, Oie T, Kishimoto Y, Arakawa M, Ohmuma K, Tajikawa T, Kanda K, Tatsumi E. In-body tissue-engineered aortic valve (biovalve type vii) architecture based on 3d printer molding. Journal of biomedical materials research Part B, Applied biomaterials 2015;103(1):1-11.
[108] Yamanami M, Yahata Y, Uechi M, Fujiwara M, Ishibashi-Ueda H, Kanda K, Watanabe T, Tajikawa T, Ohba K, Yaku H, Nakayama Y. Development of a completely autologous valved conduit with the sinus of valsalva using in-body tissue architecture technology: A pilot study in pulmonary valve replacement in a beagle model. Circulation 2010;122(11 Suppl):S100-6.
[109] Flanagan TC, Sachweh JS, Frese J, Schnoring H, Gronloh N, Koch S, Tolba RH, Schmitz-Rode T, Jockenhoevel S. In vivo remodeling and structural characterization of fibrin-based tissue-engineered heart valves in the adult sheep model. Tissue Eng Part A 2009;15(10):2965-76.
[110] Syedain ZH, Lahti MT, Johnson SL, Robinson PS, Ruth GR, Bianco RW, Tranquillo RT. Implantation of a tissue-engineered heart valve from human fibroblasts exhibiting short term function in the sheep pulmonary artery. Cardiovasc Eng Technol 2011;2(2):101-12.
[111] Syedain Z, Reimer J, Schmidt J, Lahti M, Berry J, Bianco R, Tranquillo RT. 6-month aortic valve implantation of an off-the-shelf tissue-engineered valve in sheep. Biomaterials 2015;73:175-84.
[112] Emmert MY, Weber B, Behr L, Sammut S, Frauenfelder T, Wolint P, Scherman J, Bettex D, Grunenfelder J, Falk V, Hoerstrup SP. Transcatheter aortic valve implantation using anatomically oriented, marrow stromal cell-based, stented, tissue-engineered heart valves: Technical considerations and implications for translational cell-based heart valve concepts. Eur J Cardiothorac Surg 2014;45(1):61-8.
[113] Schoen FJ. Heart valve tissue engineering: Quo vadis? Current Opinion in Biotechnology 2011;22(5):698-705.
[114] Quality AfHRa. Healthcare cost and utilization project (hcup). 2014. http://hcupnet.ahrq.gov/
[115] Lloyd-Jones D, Adams RJ, Brown TM, Carnethon M, Dai S, De Simone G, Ferguson TB, Ford E, Furie K, Gillespie C, Go A, Greenlund K, Haase N, Hailpern S, Ho PM, Howard V, Kissela B, Kittner S, Lackland D, Lisabeth L, Marelli A, McDermott MM, Meigs J, Mozaffarian D, Mussolino M, Nichol G, Roger VL, Rosamond W, Sacco R, Sorlie P, Thom T, Wasserthiel-Smoller S, Wong ND, Wylie-Rosett J. Heart disease and stroke statistics--2010 update: A report from the american heart association. Circulation 2010;121(7):e46-e215.
[116] Protopapas AD, Athanasiou T. Contegra conduit for reconstruction of the right ventricular outflow tract: A review of published early and mid-time results. J Cardiothorac Surg 2008;3:62.
[117] Gulbins H, Goldemund A, Anderson I, Haas U, Uhlig A, Meiser B, Reichart B. Preseeding with autologous fibroblasts improves endothelialization of glutaraldehyde-fixed porcine aortic valves. J Thorac Cardiovasc Surg 2003;125(3):592-601.

[118] Gottlieb D, Kunal T, Emani S, Aikawa E, Brown DW, Powell AJ, Nedder A, Engelmayr GC, Jr., Melero-Martin JM, Sacks MS, Mayer JE, Jr. In vivo monitoring of function of autologous engineered pulmonary valve. J Thorac Cardiovasc Surg 2010;139(3):723-31.
[119] Syedain ZH, Lahti MT, Johnson SL, Ruth GR, Bianco R, Tranquillo RT. Implantation of a tissue-engineered heart valve from human fibroblasts exhibiting short term function in the sheep pulmonary artery. Cardiovasc Eng Technol 2011;2(2):101-12.
[120] Driessen-Mol A, Dijkman PE, Frese L, Emmert MY, Grunenfelder J, Sidler M, Weber B, Sanders B, Jenni R, Baaijens FPT, Hoerstrup SP. Decellularized in-vitro tissue-engineered heart valves - first in-vivo results. QScience Proceedings 2012;2012(4.
[121] Robinson PS, Johnson SL, Evans MC, Barocas VH, Tranquillo RT. Functional tissue-engineered valves from cell-remodeled fibrin with commissural alignment of cell-produced collagen. Tissue Eng Part A 2008;14(1):83-95.
[122] Jockenhoevel S, Chalabi K, Sachweh JS, Groesdonk HV, Demircan L, Grossmann M, Zund G, Messmer BJ. Tissue engineering: Complete autologous valve conduit--a new moulding technique. Thorac Cardiovasc Surg 2001;49(5):287-90.
[123] Syedain ZH, Bradee AR, Kren S, Taylor DA, Tranquillo RT. Decellularized tissue-engineered heart valve leaflets with recellularization potential. Tissue Eng Part A 2013;19(5-6):759-69.
[124] Syedain ZH, Meier LA, Bjork JW, Lee A, Tranquillo RT. Implantable arterial grafts from human fibroblasts and fibrin using a multi-graft pulsed flow-stretch bioreactor with noninvasive strength monitoring. Biomaterials 2011;32(3):714-22.
[125] Dayan D, Hiss Y, Hirshberg A, Bubis JJ, Wolman M. Are the polarization colors of picrosirius red-stained collagen determined only by the diameter of the fibers? Histochemistry 1989;93(1):27-9.
[126] Syedain ZH, Meier LA, Lahti MT, Johnson SL, Tranquillo RT. Implantation of completely biological engineered grafts following decellularization into the sheep femoral artery. Tissue Eng Part A 2014;20(11-12):1726-34.
[127] Meier LA, Syedain ZH, Lahti MT, Johnson SS, Chen MH, Hebbel RP, Tranquillo RT. Blood outgrowth endothelial cells alter remodeling of completely biological engineered grafts implanted into the sheep femoral artery. J Cardiovasc Transl Res 2014;7(2):242-9.
[128] Hoerstrup SP, Cummings Mrcs I, Lachat M, Schoen FJ, Jenni R, Leschka S, Neuenschwander S, Schmidt D, Mol A, Gunter C, Gossi M, Genoni M, Zund G. Functional growth in tissue-engineered living, vascular grafts: Follow-up at 100 weeks in a large animal model. Circulation 2006;114(1 Suppl):I159-66.
[129] Brennan MP, Dardik A, Hibino N, Roh JD, Nelson GN, Papademitris X, Shinoka T, Breuer CK. Tissue-engineered vascular grafts demonstrate evidence of growth and development when implanted in a juvenile animal model. Ann Surg 2008;248(3):370-7.
[130] Ivy DD, Abman SH, Barst RJ, Berger RM, Bonnet D, Fleming TR, Haworth SG, Raj JU, Rosenzweig EB, Schulze Neick I, Steinhorn RH, Beghetti M. Pediatric pulmonary hypertension. J Am Coll Cardiol 2013;62(25 Suppl):D117-26.

[131] Rubin LJ. Primary pulmonary hypertension. N Engl J Med 1997;336(2):111-7.
[132] Fung YC. Biomechanics: Mechanical properties of living tissues. 2 ed: Springer-Verlag; 1993.
[133] DiBardino DJ, Jacobs JP. Current readings: Long-term management of patients undergoing successful pediatric cardiac surgery. Semin Thorac Cardiovasc Surg 2014;26(2):132-44.
[134] Downing TE, Kim YY. Tetralogy of fallot: General principles of management. Cardiol Clin 2015;33(4):531-41.
[135] Yuan SM, Mishaly D, Shinfeld A, Raanani E. Right ventricular outflow tract reconstruction: Valved conduit of choice and clinical outcomes. J Cardiovasc Med (Hagerstown) 2008;9(4):327-37.
[136] Jacobs JP, Mavroudis C, Quintessenza JA, Chai PJ, Pasquali SK, Hill KD, Vricella LA, Jacobs ML, Dearani JA, Cameron D. Reoperations for pediatric and congenital heart disease: An analysis of the society of thoracic surgeons (sts) congenital heart surgery database. Semin Thorac Cardiovasc Surg Pediatr Card Surg Annu 2014;17(1):2-8.
[137] Mol A, Smits AI, Bouten CV, Baaijens FP. Tissue engineering of heart valves: Advances and current challenges. Expert Rev Med Devices 2009;6(3):259-75.
[138] Funayama M, Takewa Y, Oie T, Matsui Y, Tatsumi E, Nakayama Y. In situ observation and enhancement of leaflet tissue formation in bioprosthetic "biovalve". J Artif Organs 2015;18(1):40-7.
[139] Robinson PS, Tranquillo RT. Planar biaxial behavior of fibrin-based tissue-engineered heart valve leaflets. Tissue Eng Part A 2009;15(10):2763-72.
[140] Shin'oka T, Imai Y, Ikada Y. Transplantation of a tissue-engineered pulmonary artery. N Engl J Med 2001;344(7):532-3.
[141] Shin'oka T, Matsumura G, Hibino N, Naito Y, Watanabe M, Konuma T, Sakamoto T, Nagatsu M, Kurosawa H. Midterm clinical result of tissue-engineered vascular autografts seeded with autologous bone marrow cells. J Thorac Cardiovasc Surg 2005;129(6):1330-8.
[142] Hibino N, McGillicuddy E, Matsumura G, Ichihara Y, Naito Y, Breuer C, Shinoka T. Late-term results of tissue-engineered vascular grafts in humans. J Thorac Cardiovasc Surg 2010;139(2):431-6, 6 e1-2.
[143] Matsumura G, Shinoka T. First report of histological evaluation of human tissue-engineered vasculature. J Biotechnol Biomater 2015;5-3(3.
[144] Hibino N, Mejias D, Pietris N, Dean E, Yi T, Best C, Shinoka T, Breuer C. The innate immune system contributes to tissue-engineered vascular graft performance. Faseb J 2015;29(6):2431-8.
[145] Tara S, Kurobe H, Maxfield MW, Rocco KA, Yi T, Naito Y, Breuer CK, Shinoka T. Evaluation of remodeling process in small-diameter cell-free tissue-engineered arterial graft. J Vasc Surg 2015;62(3):734-43.
[146] James IA, Yi T, Tara S, Best CA, Stuber AJ, Shah KV, Austin BF, Sugiura T, Lee YU, Lincoln J, Trask AJ, Shinoka T, Breuer CK. Hemodynamic characterization of a mouse model for investigating the cellular and molecular mechanisms of neotissue

formation in tissue-engineered heart valves. Tissue Eng Part C Methods 2015;21(9):987-94.
[147] Roh J, Sawh-Martinez R, Brennan M, Jay S, Devine L, Rao D, Yi T, Mirensky T, Nalbandian A, Udelsman B, Hibino N, Shinoka T, Saltzman W, Snyder E, Kyriakides T, Pober J, Breuer C. Tissue-engineered vascular grafts transform into mature blood vessels via an inflammation-mediated process of vascular remodeling. Proc Natl Acad Sci U S A 2010;107(10):4669-74.
[148] Harrington JK, Chahboune H, Criscione JM, Li AY, Hibino N, Yi T, Villalona GA, Kobsa S, Meijas D, Duncan DR, Devine L, Papademetri X, Shin'oka T, Fahmy TM, Breuer CK. Determining the fate of seeded cells in venous tissue-engineered vascular grafts using serial mri. FASEB J 2011;25(12):4150-61.
[149] Hibino N, Villalona G, Pietris N, Duncan DR, Schoffner A, Roh JD, Yi T, Dobrucki LW, Mejias D, Sawh-Martinez R, Harrington JK, Sinusas A, Krause DS, Kyriakides T, Saltzman WM, Pober JS, Shin'oka T, Breuer CK. Tissue-engineered vascular grafts form neovessels that arise from regeneration of the adjacent blood vessel. FASEB J 2011;25(8):2731-9.
[150] Hibino N, Yi T, Duncan DR, Rathore A, Dean E, Naito Y, Dardik A, Kyriakides T, Madri J, Pober JS, Shinoka T, Breuer CK. A critical role for macrophages in neovessel formation and the development of stenosis in tissue-engineered vascular grafts. FASEB J 2011;25(12):4253-63.
[151] Kelm JM, Emmert MY, Zurcher A, Schmidt D, Begus Nahrmann Y, Rudolph KL, Weber B, Brokopp CE, Frauenfelder T, Leschka S, Odermatt B, Jenni R, Falk V, Zund G, Hoerstrup SP. Functionality, growth and accelerated aging of tissue engineered living autologous vascular grafts. Biomaterials 2012;33(33):8277-85.
[152] Stegemann H, Stalder K. Determination of hydroxyproline. Clin Chim Acta 1967;18(2):267-73.
[153] Starcher BC, Galione MJ. Purification and comparison of elastins from different animal species. Anal Biochem 1976;74(2):441-7.
[154] Kim YJ, Sah RL, Doong JY, Grodzinsky AJ. Fluorometric assay of DNA in cartilage explants using hoechst 33258. Anal Biochem 1988;174(1):168-76.
[155] Hibino N, McGillicuddy E, Matsumura G, Ichihara Y, Naito Y, Breuer C, Shinoka T. Late-term results of tissue-engineered vascular grafts in humans. J Thorac Cardiovasc Surg 2010;139(2):431-6, 6 e1-2.
[156] Molina JE, Edwards JE, Bianco RW, Clack RW, Lang G, Molina JR. Composite and plain tubular synthetic graft conduits in right ventricle-pulmonary artery position: Fate in growing lambs. J Thorac Cardiovasc Surg 1995;110(2):427-35.
[157] Tudorache I, Cebotari S, Sturz G, Kirsch L, Hurschler C, Hilfiker A, Haverich A, Lichtenberg A. Tissue engineering of heart valves: Biomechanical and morphological properties of decellularized heart valves. J Heart Valve Dis 2007;16(5):567-73; discussion 74.

[158] Zubairi R, Malik S, Jaquiss RD, Imamura M, Gossett J, Morrow WR. Risk factors for prosthesis failure in pulmonary valve replacement. Ann Thorac Surg 2011;91(2):561-5.
[159] Maxon monofilament synthetic absorbable suture. 2008. http://www.medtronic.com/content/dam/covidien/library/global/english/product/wound-closure/absorbable-sutures/maxon-monofilament-absorbable-sutures/maxon-absorbable-suture-info-sheet.pdf
[160] Syedain Z, Reimer J, Lahti M, Berry J, Bianco R, Tranquillo R. 50-week implant of a tissue-engineered pulmonary conduit in a growing lamb model. 2015 4th TERMIS World Congress. Boston, MA: Tissue Engineering Part A; 2015. p. s-82.
[161] Stegemann H, Stalder K. Determination of hydroxyproline. Clin Chim Acta 1967;18(2):267-73.
[162] Raymond TE, Khabbaza JE, Yadav R, Tonelli AR. Significance of main pulmonary artery dilation on imaging studies. Ann Am Thorac Soc 2014;11(10):1623-32.
[163] Nudelman L. Age norms: Child and adolescent physical development. 2016. 4/1/2016. http://parentingliteracy.com/component/content/article/56-physical-development/135-age-norms-child-and-adolescent-physical
[164] Standardization IOf. Iso 5840. Cardiovascular implants - Cardiac valve prostheses. 2005. http://www.iso.org/iso/catalogue_detail.htm?csnumber=34164

Appendix A. Pulse Duplicator System and Waveform Analysis Code

A.1 Motivation

Pulse duplicator testing is an integral method to characterize heart valve hemodynamics in the laboratory. The International Organization for Standardization (ISO) 5840 outlines the applicable testing for prosthetic heart valves and their components [1]. Although ISO 5840 was not written specifically for tissue engineered heart valves, its contents are highly relevant. Of particular interest are the descriptions of appropriate *in vitro* testing and relevant metrics for hydrodynamic valve function.

A.2 Pulse Duplicator Test Chamber

The Tranquillo laboratory's custom pulse duplicator system (Appendix Figure A-1.a) utilizes a Vivitro pump, fluid reservoir, valve mounting chamber, and compliance chambers [2]. Prior to the studies described in Chapter 2, hemodynamic valve testing focused only on leaflet motion with a rigid root. Since the pediatric TEHV described in Chapter 2 incorporated an outer tissue tube, it was necessary to consider the effect of root motion on valve performance. This was achieved by modulating the pressure on the ablumenal surface of the valve (i.e. in the fluid-filled valve mounting chamber) using a second flow loop equipped with a downstream needle valve (Appendix Figure A-1.b). Next, an "open" valve holder was fabricated using 3D printing (Appendix Figure A-1.c) so that root motion was uninhibited (Appendix Figure A-1.d). A tubular silicon mold was used to insert the valve within the holder.

A.3 Appendix A Figures and Tables

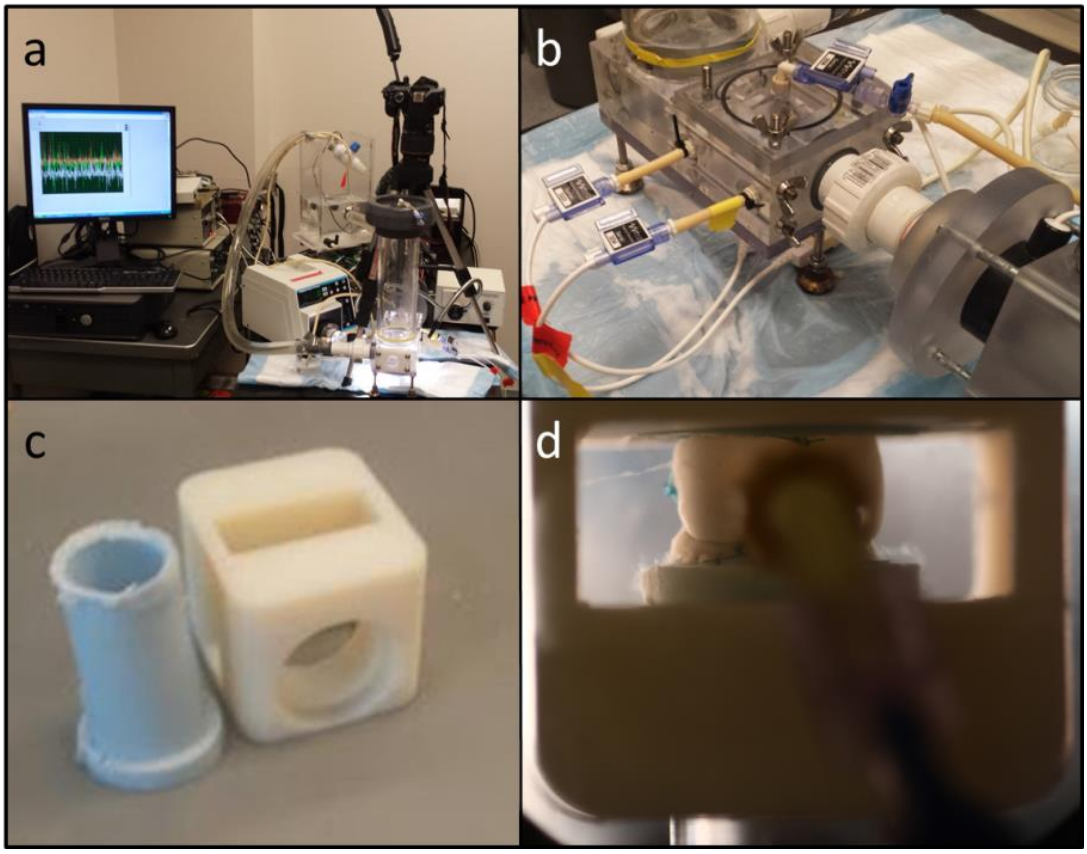

Appendix Figure A-1. Pulse duplicator testing apparatus

Pulse duplicator system showing the (a) primary flow loop, data acquisition system, fluid reservoir, and lumenal compliance chamber. The (b) valve mounting chamber houses the (c) valve holder and (d) does not inhibit TEHV root motion. Silicon tubes are attached to the ends of the TEHV to connect it to the valve holder.

A.4 Pulse Duplicator Analysis Code

TEHV designs were modified based on the outcomes observed in pulse duplicator testing. In order to accelerate the design iteration process, a custom Matlab script was written to analyze pulse duplicator test data. Metrics such as regurgitant fraction, effective orifice area, systolic and diastolic pressure gradients, and mean forward flow rate were tabulated in a spreadsheet. The code for this analysis is included below.

```
%% Pulse Duplicator Analysis Code
% PDWaveformanalysis.m is written to automatically analyze labview
% generated files for constructs tested in a pulse duplicator system.
% Outputs include: flow & pressure traces, regurgitant fraction, mean
% systolic DP, and average forward flowrate

% Written by Jay M. Reimer (June 2014) with components adapted from J.
% Bjork, L. Black, and P. Robinson
% Written with Matlab R2014a

%IMPORTANT NOTES
% 1. This program is written for Labview generated files (.LVM) with a 23 line
% header
% 2. Data in labview files is organized into 5 columns; Col 1 = time, Col
% 2=pressure 1, Col 3 = pressure 2, Col 4 = flowrate, Col 5 = ablumenal
% pressure

%%Initialize Workspace
clear all
close all
clc

Xcelname='dVRE26 - Pulmonary & Aortic PD Testing.xls'; % specify the name of the file
that it will export
%% Obtain File(s)
cd('Z:\Jay Reimer\Tube in Tube Work\dVRE26 - 1-27-16 Sewing\Pulse Duplicator
Testing\Waveforms (aortic_lower flow - 3.7.2016)');

[fname,fpath] = uigetfile('*.LVM','Select data file(s) to analyze.',...
   'MultiSelect','on');       %%%%%USE FOR INSTRON CSV FILESC:\Documents and
Settings\JanR\My Documents\Mechanical Testing\Biaxial Testing\VE Casting 03.13.2012
```

```
[a,b] = size(char(fname));

if fpath == 0
   errordlg('File not specified.');
   return
end
cd(fpath);

fname = cellstr(fname);
headerlines = 23;       % Number of non-data rows for data.

%Pressure Head Offset for Ablumenal Pressure Sensor - IMPORTANT -THIS ASSUMES
THAT IT IS NOT ACCOUNTED FOR by the sensor calibration
head=.05;%in meters - distance the ablumenal pressure gauge is above the lumenal
pressure gauges
h2oDensity=1000;%kg/m^3
g=9.81;%m/s^2
Pa2mmHg=0.00750061683;%1 Pa=0.00750061683 mmHg
AbPhead=(h2oDensity*g*head)*Pa2mmHg; % in mmHg

%%PreAllocating Vectors
regurg=zeros(a,1);reg_std=zeros(a,1);fflowrate=zeros(a,1);fflowrate_std=zeros(a,1);stro
kevolume=zeros(a,1);strokevolume_std=zeros(a,1);closingvolume=zeros(a,1);closingvolu
me_std=zeros(a,1);leakagevolume=zeros(a,1);leakagevolume_std=zeros(a,1);cycletime=
zeros(a,1);cycletime_std=zeros(a,1);closingtime=zeros(a,1);closingtime_std=zeros(a,1);le
aktime=zeros(a,1);leaktime_std=zeros(a,1);abPressure=zeros(a,1);abPressure_std=zeros
(a,1);peakflow=zeros(a,1);peakflow_std=zeros(a,1);Qv_rms=zeros(a,1);Qv_rms_std=zero
s(a,1);avg_sysDP=zeros(a,1);avg_sysDP_std=zeros(a,1);max_sysDP=zeros(a,1);max_sysD
P_std=zeros(a,1);systime=zeros(a,1);systime_std=zeros(a,1);EOA=zeros(a,1);EOA_std=ze
ros(a,1);avg_diasDP=zeros(a,1);avg_diasDP_std=zeros(a,1);max_diasDP=zeros(a,1);max_
diasDP_std=zeros(a,1);min_diasDP=zeros(a,1);min_diasDP_std=zeros(a,1);diastime=zero
s(a,1);diastime_std=zeros(a,1);abPressure2=zeros(a,1);
for i=1:a;
   fileID = fopen(char(fname(i)));
   C = textscan(fileID,'%f32 %f32 %f32 %f32 %f32', 'HeaderLines', headerlines);
   fclose(fileID);
   time=C{1};
   pressure1=C{2};
   pressure2=C{3};
   flow=C{4};
```

```
   TP=C{5}+AbPhead; %Adds in the pressure that is not accounted for by the sensor due
to the difference in height in relation to the lumenal pressure sensors (above the
lumenal sensors)
   array=[time pressure1 pressure2 flow TP];

   %% Detect and eliminate data associated with negative time (due to LabVIEW code
malfunction)
   if any(time<0)
      index=find(time<0);
      time(1:max(index))=[];
      pressure1(1:max(index))=[];
      pressure2(1:max(index))=[];
      flow(1:max(index))=[];
      TP(1:max(index))=[];
   else
   end

   %% Filtering the data: 7 window moving average filter
   for z=5:length(time)-4;
      time(z)=mean(time(z-4:z+4));
      pressure1(z)=mean(pressure1(z-4:z+4));
      pressure2(z)=mean(pressure2(z-4:z+4));
      flow(z)=mean(flow(z-4:z+4));
   end

   %% Waveform Traces
   figure(i);
   set(gcf,'color','w', 'units','normalized','outerposition',[.1 .1 .6 .8],'PaperPositionMode',
'auto'); % specify location and size of figure ==[left, bottom, width, height]

   % Subplot 1
   %subplot(2,2,1:2);
   [haxes,hline1,hline2] = plotyy(time,pressure1,time, flow,'plot');
   ylabel(haxes(1),'Pressure (mmHg)', 'FontSize', 20, 'Color', 'k') % label left y-axis
   ylabel(haxes(2),'Flowrate (L/min)', 'FontSize', 20, 'Color','k') % label right y-axis
   xlabel(haxes(2),'Time (s)', 'FontSize', 20) % label x-axis
   filename=strrep(char(fname(i)),'.lvm','');
   title(filename,'FontSize', 18)

   % Modifying Axis Values
```

```
   if min(TP)<=min(pressure1);
      if min(TP)<=min(pressure2);
         set(haxes(1),'Ylim', [(min(TP)-10), (max(pressure2)+10)],'Xlim', [0 2],'FontSize', 16,
'ycolor','k') % Set properties for left axis
      else
         set(haxes(1),'Ylim', [(min(pressure2)-10), (max(pressure2)+10)],'Xlim', [0
2],'FontSize', 16, 'ycolor','k') % Set properties for left axis
      end
   elseif min(TP)>min(pressure1);
      if min(pressure1)<=min(pressure2);
         set(haxes(1),'Ylim', [(min(pressure1)-10), (max(pressure2)+10)],'Xlim', [0
2],'FontSize', 16, 'ycolor','k') % Set properties for left axis
      else
         set(haxes(1),'Ylim', [(min(pressure2)-10), (max(pressure2)+10)],'Xlim', [0
2],'FontSize', 16, 'ycolor','k') % Set properties for left axis
      end
   end

   set(haxes(1),'YTick', [-40, -30, -20, -10, 0, 10, 20, 30, 40, 50, 60, 70]); % sets tick marks
for left axis
   box(haxes(1),'off')
   set(haxes(2), 'Ylim',[(round(min(flow)-1)),(round(max(flow)+2))],'Fontsize', 16,'Xlim',
[0 2], 'ycolor','k');
   set(haxes(2),'Ytick',[-6,-4,-2,0,2,4,6,8,10]);
   set(hline1, 'LineWidth', 2); % change thickness of line for pressure1
   set(hline2, 'LineWidth',2); % change thickness of line for flow

   hold on
   hline3=plot(time,pressure2, 'k', 'LineWidth', 2);
   hold on
   hline4=plot(time, TP, 'm', 'LineWidth', 2);
   legend([hline1;hline2;hline3; hline4],'Inflow Pressure', 'Flowrate', 'Outflow
Pressure','Ablumenal Pressure','Location', 'SouthWest');
   hold on
   xlim([0 2]);

   %% Subplot 2
%    subplot(2,2,3)
%    [haxes,hline1,hline2] = plotyy(time,pressure1,time, flow,'plot');
%    title('Lumenal Pressures & Flow Traces','FontSize', 16)
```

```
%    ylabel(haxes(1),'Pressure (mmHg)', 'FontSize', 14,'Color','k') % label left y-axis
%    ylabel(haxes(2),'Flowrate (L/min)', 'FontSize', 14,'Color','k') % label right y-axis
%    xlabel(haxes(2),'Time (s)', 'FontSize', 14) % label x-axis
%
%    if min(pressure1)<min(pressure2);
%        set(haxes(1),'Ylim', [(min(pressure1)-10), (max(pressure2)+10)],'Xlim', [0
2],'FontSize', 12, 'ycolor','k') % Set properties for left axis
%    else
%        set(haxes(1),'Ylim', [(min(pressure2)-10), (max(pressure2)+10)],'Xlim', [0
2],'FontSize', 12, 'ycolor','k') % Set properties for left axis
%    end
%    set(haxes(1),'YTick',[-20,-10, 0, 10, 20, 30, 40, 50, 60, 70], 'FontSize', 12, 'ycolor', 'k');
% set tick marks for left axis
%    set(haxes(2), 'Fontsize', 12,'Xlim', [0 2], 'ycolor', 'k');
%    set(hline1, 'LineWidth', 2); % change thickness of line for pressure1
%    set(hline2, 'LineWidth',2); % change thickness of line for flow
%     xlim([0 2]);
%    box off
%
%    hold on
%    hline3=plot(time,pressure2, 'k', 'LineWidth', 2);
%    legend([hline1;hline2;hline3],'Inflow Pressure', 'Flowrate', 'Outflow
Pressure','Location', 'SouthWest');

%    %% Subplot 3
%    subplot(2,2,4);
%    plot(time, pressure1,time,pressure2,'k',time,TP,'m','LineWidth', 2);
%    ylabel('Pressure (mmHg)', 'FontSize', 14, 'Color','k');
%    xlabel('Time (s)', 'FontSize', 14, 'Color','k');
%    set(gca,'FontSize', 12);
%     xlim([0 2]);
%    legend('Inflow Pressure','Outflow Pressure','Ablumenal Pressure', 'Location',
'SouthWest');
%    title('Pressure Traces', 'FontSize', 16)

   %% Export Figures to file
   filename=strrep(char(fname(i)),'.lvm','');
   saveas(gcf,filename, 'tif')

   %% Select Points to calculate regurgitation & Mean Ablumenal Pressure
```

```
   figure (i+1)
   set(gcf,'color','w', 'units','normalized','outerposition',[0 0 .9 .9],'PaperPositionMode',
'auto' ); % specify location and size of figure ==[left, bottom, width, height]
   plot(time, flow, 'LineWidth', 4);
   title('Click 1: beginning of cycle - Click 2: end of closing volume - Click 3: end of cycle --
-> Repeat 3 times (9 total clicks)')
   ylabel('Flowrate(L/min)', 'FontSize', 14, 'Color','k');
   xlabel('Time (s)', 'FontSize', 14, 'Color','k');
   xlim([0 4]);
   points = 9; %total number of points to select (3 points per cycle) (Point 1: right at
beginning of forward flow; Point 2: end of closing volume; Point 3: end of the cycle)
   [x] = ginput(points);

   % Find indices associated with selected times
   for j=1:points
      for t=1:length(time)
         tol=.001; % gives the tolerance for how much difference there can be for the
index associated with the user-selected time
         if abs(x(j)-time(t))<tol
            index(j)=t;
         else
            'Error - no corresponding point could be found';
         end
      end
      %temp=abs(time-x(j));
      %temp=temp-min(temp);
      %index(j)=find(~temp);
   end

   %Preallocating vectors

cycletime1=zeros(points);peakflow1=zeros(points);abPressure1=zeros(points);fflowrate
1=zeros(points);Qv_rms1=zeros(points);strokevolume1=zeros(points);closingtime1=zero
s(points);closingvolume1=zeros(points);leaktime1=zeros(points);leakvolume1=zeros(poi
nts);regurg1=zeros(points);abpressurestd=zeros(points);

   for k=3:3:points % runs a loop to calculate regurgitant fraction - starts at k=2 and runs
to k=points by skipping 2
      timestep=.001/60;%timestep of data acquisition in minutes
```

```
%Total Cycle Time& Max Flow
flowtemp=flow(index(k-2):index(k)); %populates the vector with flowrates for the entire cycle
cycletime1(k)=length(flowtemp)*timestep*60; %gives the total cycle time - (seconds)

%Peak Flow for given cycle
peakflow1(k)=max(flowtemp);

%Mean Ablumenal Pressure
abPtemp=TP(index(k-2):index(k)); %populates the vector with ablumenal pressures for the entire cycle
abPressure1(k)=mean(abPtemp); % calculates the mean ablumenal pressure for the entire cycle
abpressurestd(k)=std(abPtemp); %calculates the standard deviation associated within each cycle

%Cardiac Output & Stroke Volume
flowtemp1=flow(index(k-2):index(k-1)); %populates vector with flowrates for the beginning of the cycle to the end of the closing volume (stroke volume & closing volume)
positiveflow1=flowtemp1(flowtemp1>=0); % populates a vector with only the positive flow rate points (or zeros)
posflow_time=length(positiveflow1)*timestep;%gives the amount of time for the stroke volume - units in minutes
fflowrate1(k)=mean(positiveflow1); %gives the average forward flowrate (cardiac output) through the valve in one cycle
Qv_rms1(k)=sqrt(sum((positiveflow1.^2)*timestep)/posflow_time)*1000; % units must be in mL per ISO 5840 for the equation to be valid
strokevolume1(k)=sum(positiveflow1*timestep)*1000; %volume of fluid moved through the valve in forward direction in one cycle (ISO 5840)

%Calculate Closing Volume
closing=flowtemp1(flowtemp1<0); % populates vector of negative flowrate values during specified time period
closingtime1(k)=length(closing)*(timestep*60); %Gives the time associated with the closing volume - (units in seconds)
closingvolume1(k)=sum(closing*timestep)*1000; % gives the total amount of negative flow during valve closure - (Units in mL)
```

```
        % Calculate Leakage Volume
        flowtemp2=flow(index(k-1):index(k));   %populates vector with flowrates from the
end of the closing volume through the end of the cycle (leakage)
        leakage=sum(flowtemp2);%(flowtemp2<0); % populates vector of negative flowrate
values during specified time period
        leaktime1(k)=length(flowtemp2)*timestep*60; %gives time after closing until the
end of the cycle - (units in seconds)
        leakvolume1(k)=sum(leakage*timestep)*1000; %gives the total volume of negative
flow after valve closure - (units in mL)

        %Calculating Regurgitation (Closing volume + leakage volume)
        regurg1(k)=abs((closingvolume1(k)+leakvolume1(k))/strokevolume1(k));

    end

    %populate vectors with regurgitation and standard deviations
    regurg(i)=mean(regurg1(regurg1~=0)); %gives the average regurgitation for the 3
cycles
    reg_std(i)=std(regurg1(regurg1~=0)); % gives the standard deviation for the 3 cycles of
the given plot
    fflowrate(i)=mean(fflowrate1(fflowrate1~=0)); % '>' symbol is there because the
vector is populated with zeros because the indices skip by 3
    fflowrate_std(i)=std(fflowrate1(fflowrate1~=0));
    strokevolume(i)=mean(strokevolume1(strokevolume1~=0)); % gets rid of the data
points that are 0 because the indices increased by 3 for strokevolume1
    strokevolume_std(i)=std(strokevolume1(strokevolume1~=0));
    closingvolume(i)=mean(closingvolume1(closingvolume1~=0));
    closingvolume_std(i)=std(closingvolume1(closingvolume1~=0));%takes the average of
a vector populated only of the data points; gets rid of the zeros that come from the
indexing
    leakagevolume(i)=mean(leakvolume1(leakvolume1~=0));%takes the mean of the
values not equal to zero
    leakagevolume_std(i)=std(leakvolume1(leakvolume1~=0));%(abs(leakvolume1)>0));
    cycletime(i)=mean(cycletime1(cycletime1~=0));
    cycletime_std(i)=std(cycletime1(cycletime1~=0));
    closingtime(i)=mean(closingtime1(closingtime1~=0));
    closingtime_std(i)=std(closingtime1(closingtime1~=0));
    leaktime(i)=mean(leaktime1(leaktime1~=0));
    leaktime_std(i)=std(leaktime1(leaktime1~=0));
    abPressure(i)=mean(abPressure1(abPressure1~=0));
```

```
   %abPressure_std(i)=std(abPressure1(abs(abPressure1)>0));
   abPressure_std(i)=mean(abpressurestd(abpressurestd~=0));

   peakflow(i)=mean(peakflow1(peakflow1~=0));
   peakflow_std(i)=std(peakflow1(peakflow1~=0));
   Qv_rms(i)=mean(Qv_rms1(Qv_rms1~=0));
   Qv_rms_std(i)=std(Qv_rms1(Qv_rms1~=0));

   close(figure(i+1)); %closes the regurgitation calculation figure

   %% Select Points to Calculate Average Systolic DP
   figure (i+2)
   set(gcf,'color','w', 'units','normalized','outerposition',[0 0 .9 .9],'PaperPositionMode',
'auto' ); % specify location and size of figure ==[left, bottom, width, height]
   plot(time, pressure1, time, pressure2, 'k', 'LineWidth', 3);
   title('Calculate Average Systolic Pressure Drop (Pventricle>Paorta) - click at beginning,
then end of desired zone ---> Repeat 3 times (6 total clicks)')
   ylabel('Pressure (mmHg)', 'FontSize', 14, 'Color','k');
   xlabel('Time (s)', 'FontSize', 14, 'Color','k');
   xlim([0 4]);
   Ppoints = 6; %total number of points to select (2 points per cycle)
   [a] = ginput(Ppoints);

 Pindex=zeros(Ppoints);
   % Find indices associated with selected times
   for l=1:Ppoints
      for t2=1:length(time)
         tol=.001; % gives the tolerance for how much difference there can be for the
index associated with the user-selected time
         if abs(a(l)-time(t2))<tol
            Pindex(l)=t2;
         else
            'Error - no corresponding point could be found';
         end
      end
      %Ptemp=abs(time-a(l));
      %Ptemp=Ptemp-min(Ptemp);
      %Pindex(l)=find(~Ptemp);
   end
```

```
avg_sysDP_temp=zeros(Ppoints);max_sysDP_temp=zeros(Ppoints);systime1=zeros(Ppoi
nts);
   for m=2:2:Ppoints % runs a loop to calculate average systolic DP - starts at k=2 and
runs to k=points by skipping 2
      Ptimestep=.001;%timestep of data acquisition - in seconds
      p1temp=pressure1(Pindex(m-1):Pindex(m));
      p2temp=pressure2(Pindex(m-1):Pindex(m));
      sysDP=p2temp-p1temp;
      avg_sysDP_temp(m)=abs(mean(sysDP)); % mmHg
      max_sysDP_temp(m)=max(abs(sysDP));  % mmHg
      systime1(m)=length(p1temp)*Ptimestep; % gives time for 2 pressures to equilibrate
- in seconds
   end
   %populate vectors with regurgitation and standard deviations
   avg_sysDP(i)=mean(avg_sysDP_temp(avg_sysDP_temp>0)); %gives the average
systolic DP for the 3 cycles  - in mmHg
   avg_sysDP_std(i)=std(avg_sysDP_temp(avg_sysDP_temp>0)); % gives the standard
deviation for the average systolic DP for the 3 cycles of the given plot
   max_sysDP(i)=mean(max_sysDP_temp(max_sysDP_temp>0));
   max_sysDP_std(i)=std(max_sysDP_temp(max_sysDP_temp>0));

   systime(i)=mean(systime1(systime1>0));
   systime_std(i)=std(systime1(systime1>0));

   %%Calculate Effective Orifice Area
   rho=.9982;% grams/mL
   b=Qv_rms1(Qv_rms1>0)/60; % converts the Qv_rms to mL/sec
   c=avg_sysDP_temp(avg_sysDP_temp>0);
   EOA_1=b./(51.6*sqrt(c/rho));
   EOA(i)=mean(EOA_1);
   EOA_std(i)=std(EOA_1);

   close(figure(i+2)); %closes the systolic DP calculation figure

    %% Select Points to Calculate Average Diastolic DP
   figure (i+3)
   set(gcf,'color','w', 'units','normalized','outerposition',[0 0 .9 .9],'PaperPositionMode',
'auto' ); % specify location and size of figure ==[left, bottom, width, height]
```

```
   [haxes,hline1,hline2] = plotyy(time,pressure1,time, flow,'plot');
   ylabel(haxes(1),'Pressure (mmHg)', 'FontSize', 14, 'Color', 'k') % label left y-axis
   ylabel(haxes(2),'Flowrate (L/min)', 'FontSize', 14, 'Color','k') % label right y-axis
   xlabel(haxes(1),'Time (s)', 'FontSize', 14) % label x-axis
   set(haxes(1),'Ylim', [min(pressure1), max(pressure2)],'Xlim', [0 4],'FontSize', 12,
'ycolor','k') % Set properties for left axis
   set(haxes(1),'YTick', [-40, -30, -20, -10, 0, 10, 20, 30, 40, 50, 60, 70]); % sets tick marks
for left axis
   box(haxes(1),'off')
   set(haxes(2), 'Ylim',[(round(min(flow)-1)),(round(max(flow)+2))],'Fontsize', 12,'Xlim',
[0 4], 'ycolor','k');
   set(haxes(2),'Ytick',[-6,-4,-2,0,2,4,6,8,10]);
   set(hline1, 'LineWidth', 3); % change thickness of line for pressure1
   set(hline2, 'LineWidth',3); % change thickness of line for flow
   hold on
   hline3=plot(time,pressure2, 'k', 'LineWidth', 3);
   xlim([0 4]);

   title('Calculate Average Diastolic Pressure Drop - click at beginning, then end of
desired zone ---> Repeat 3 times (6 total clicks)')

   Dpoints = 6; %total number of points to select (2 points per cycle)
   [d] = ginput(Dpoints);

 Dindex=zeros(Dpoints);
   % Find indices associated with selected times
   for l=1:Dpoints
      for t3=1:length(time)
         tol=.001; % gives the tolerance for how much difference there can be for the
index associated with the user-selected time
         if abs(d(l)-time(t3))<tol
            Dindex(l)=t3;
         else
            'Error - no corresponding point could be found';
         end
      end
   end
```

```
avg_diasDP_temp=zeros(Dpoints);max_diasDP_temp=zeros(Dpoints);min_diasDP_temp
=zeros(Dpoints);diastime1=zeros(Dpoints);
   for n=2:2:Dpoints % runs a loop to calculate average systolic DP - starts at k=2 and
runs to k=points by skipping 2
      Dtimestep=.001;%timestep of data acquisition - in seconds
      dp1temp=pressure1(Dindex(n-1):Dindex(n));
      dp2temp=pressure2(Dindex(n-1):Dindex(n));
      diasDP=dp2temp-dp1temp;
      avg_diasDP_temp(n)=abs(mean(diasDP)); % mmHg - Gives mean
      max_diasDP_temp(n)=max(abs(diasDP));  % mmHg
      min_diasDP_temp(n)=min(abs(diasDP)); % mmHg
      diastime1(n)=length(dp1temp)*Dtimestep; % gives time for 2 pressures to
equilibrate - in seconds
   end
   %populate vectors with regurgitation and standard deviations
   avg_diasDP(i)=mean(avg_diasDP_temp(avg_diasDP_temp>0)); %gives the average
systolic DP for the 3 cycles  - in mmHg
   avg_diasDP_std(i)=std(avg_diasDP_temp(avg_diasDP_temp>0)); % gives the standard
deviation for the average systolic DP for the 3 cycles of the given plot
   max_diasDP(i)=mean(max_diasDP_temp(max_diasDP_temp>0));
   max_diasDP_std(i)=std(max_diasDP_temp(max_diasDP_temp>0));
   min_diasDP(i)=mean(min_diasDP_temp(min_diasDP_temp>0));
   min_diasDP_std(i)=std(min_diasDP_temp(min_diasDP_temp>0));
   diastime(i)=mean(diastime1(diastime1>0));
   diastime_std(i)=std(diastime1(diastime1>0));

   close(figure(i+3)); %closes the diastolic DP calculation figure
end

%% Writing data to an excel file
%name=strrep(char(fname),'.lvm','');
%name=cellstr(name);
summary_data=[regurg,EOA,fflowrate,Qv_rms,peakflow,strokevolume,closingvolume,le
akagevolume,cycletime,closingtime,leaktime,avg_sysDP,max_sysDP,abPressure,systime,
diastime,avg_diasDP,max_diasDP,min_diasDP];
st_deviations=[reg_std,EOA_std,fflowrate_std,Qv_rms_std,peakflow_std,strokevolume_
std,closingvolume_std,leakagevolume_std,cycletime_std,closingtime_std,leaktime_std,
avg_sysDP_std,max_sysDP_std,abPressure_std,systime_std,diastime_std,avg_diasDP_st
d,max_diasDP_std,min_diasDP_std];
```

```
header1a= {'Filename', 'Regurg.','EOA','[Forward','Qv_rms','Peak','Stroke',
'Closing','Leakage','Cycle', 'Closing', 'Leak','[Systolic','Max Sys','Mean
Ab.','Systolic','Diastolic', '[Dia. DP]','Max','Min Dia.'};
header1b={'','','','Flowrate]','','Flow','Volume', 'Volume','Volume','Time','Time', 'Time',
'DP]','DP', 'Pressure', 'time','time','', 'Dia. DP','DP'};
header2={'','','cm^2','L/min','mL/min','L/min','mL','mL','mL','sec','sec','sec','mmHg','mm
Hg','mmHg','sec','sec','mmHg','mmHg','mmHg'};
header3={'Standard Deviations','','','','','','','','};
xlswrite(Xcelname, header1a, 1);
xlswrite(Xcelname,header1b,1,'A2')
xlswrite(Xcelname,header2,1,'A3')
xlswrite(Xcelname,transpose(fname),1,'A4');
xlswrite(Xcelname, (summary_data),1, 'B4');
xlswrite(Xcelname,header3,1,'A12');
xlswrite(Xcelname,transpose(fname),1,'A13');
xlswrite(Xcelname, (st_deviations),1,'B13');
```

Appendix B. TEHV Implant Procedure Modifications

B.1 Motivation

The method to surgically implant TEHVs on the right side of the heart is fairly well defined. The pulmonary artery was accessed via a lateral thoracotomy with dissection through the intercostal space. The TEHVs were implanted interpositionally with resection of a length-matched segment of the native pulmonary artery. Over the course of the study, several specific aspects of the implant procedure were modified and are discussed in more detail below.

B.2 Hydration of the TEHV Leaflets

It is also important to ensure that the TEHV remains hydrated during implantation and especially prior to closing the anastomoses. If the engineered tissue becomes dry, the root and leaflet tubes can adhere to one another and compromise valve function. This was implicated in two different instances for the animal study discussed in Chapter 4. In one animal, epicardial echocardiography revealed minimal leaflet motion immediately following TEHV implantation. In order to remedy this situation, a catheter was introduced distal to the TEHV and was used to physically adjust the leaflet.

Leaflet immobility was observed in another animal approximately 1 week after implantation. It was not detected at implantation since an epicardial echocardiogram was not performed (due to the limited resolution provided by the available machine). Following animal euthanization, leaflet adhesion was clearly visible as seen in Appendix Figure B-1.a. After the leaflet was detached, full leaflet opening and closing (Appendix Figure B-1.b,c) was observed under simulated pulmonary pressure and flow conditions in the pulse duplicator system.

B.3 Order of Anastomosis Sewing

Resection of the native pulmonary artery imparts an axial stress on the TEHV since it interpositionally implanted. This situation is particularly relevant when the second anastomosis is being sewn since the axial stress is distributed through the sutures. Thus, the first suture throw will bear all of stress. While this stress is typically well-

tolerated by the engineered and native tissue, it can result in tissue tearing if the stress is too high. This risk was initially mitigated by sewing the proximal anastomosis last, which is twice as thick as the distal anastomosis (2 tubes at the proximal anastomosis versus 1 at the distal anastomosis). While the stress can be distributed better when sewing the distal anastomosis first, it is challenging to adequately hydrate the TEHV. Thus, the distal anastomosis was sewn last so that the access to the area between the leaflets and the root could be accessed.

B.4 Appendix B Figures and Tables

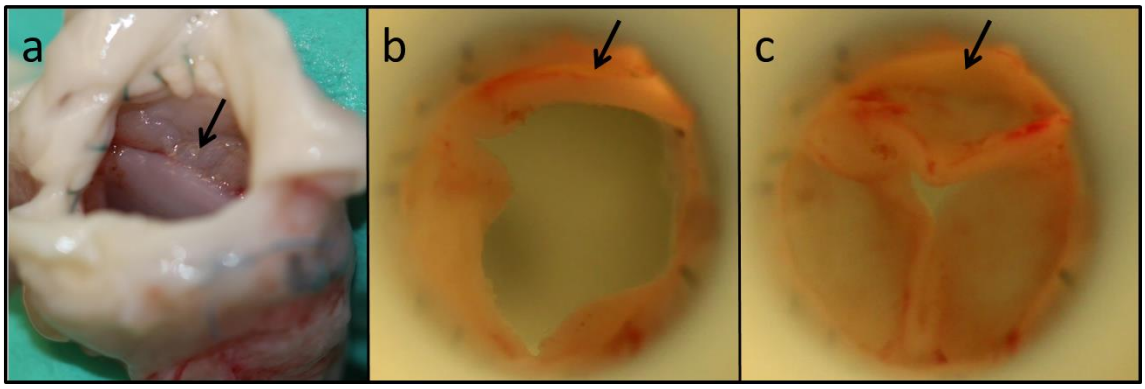

Appendix Figure B-1. Pulse duplicator testing of TEHV with an adhered leaflet

The (a) leaflet was clearly adhered to the root wall upon valve explantation. After detaching it, valve (b) opening and (c) closing was observed under pulmonary conditions. The black arrows indicate the adhered leaflet in all panels.

Appendix C. Protocols

C.1 Engineered Tube Fabrication Procedure

1. Autoclave (or otherwise sterilize) mold components and necessary tools
    a. Glass rods (with the desired diameter), polycarbonate outer shell, Dacron cuffs (2 per construct), culture jars, Teflon tape
    b. 20 mm diameter final = start with ~22 mm diameter rods
    c. 16 mm diameter final = start with ~18 mm diameter rods
2. Soak all components (except culture jars) in sterile 5% Pluronic F-127 for 0.5 – 3 hours
3. Dry mold components on a sterile drape for ~1 hour in a biosafety cabinet
4. Assemble molds sterilely, utilizing Teflon tape to eliminate fluid leaks
5. Prepare intermediate gel (fibrinogen, thrombin, and cell) solutions
    a. Fibrinogen = 6 mg/mL diluted in 20 mM HEPES buffer
    b. Thrombin = 2.27 units/mL & 30 mM $CaCl_2$ diluted in DMEM + HEPES
    c. Cells (passage 7) = 6 million ovine dermal fibroblasts (ODFs)/mL diluted in DMEM + HEPES
6. Mix intermediate gel solutions in a 4:1:1 ratio (Fibrinogen:cells:thrombin)
    a. First add cells to fibrinogen and mix well,then add thrombin and mix again
    b. Prepare enough solution to fill one VRE mold at a time
    c. Final fibrinogen concentration = 4 mg/mL
    d. Final thrombin concentration = 0.38 units/mL
    e. Final cell concentration = 1 million cells/mL
7. Inject the solutions using a syringe and needle, being careful to avoid bubbles
8. Let mold/solution sit for 8 minutes to ensure adequate gelation
9. Place in incubator for 24 additional minutes of gelation (using a sterile 1 L beaker covered with sterile aluminum foil

10. Add culture medium (DMEM + 10% FBS + 1% antibiotic/antimycotic + 2 μg/mL insulin + 50 μg/mL ascorbic acid)
11. Eject the glass rods and gels from the outer casing and place into the culture jars
12. Culture in incubator (37°C, 5% CO_2, 95% humidity)
    a. Jars sit statically until the first feeding (3-4) days and then sit on a rocker until they are mounted in the bioreactor
13. Engineered tubes are manually shortened and returned to their original length using sterile gloves to ensure that the gel does not adhere to the glass
    a. This process should be repeated as needed until the desired length is reached

NOTE: the desired length is dependent on the its application; common dimensions of use for the TEHV project are listed below

14. Constructs are fed 3x/week; 30% of medium is sterile filtered and placed back in the container
    a. Fresh medium consists the rest of it

1. Leaflet tube
    a. 20 mm diameter = >15 mm
    b. 16 mm diameter = >13 mm
2. Root tube
    a. 20 mm diameter = >19 mm
    b. 16 mm diameter = >15 mm

C.2 Mounting Tubular Constructs in Bioreactors

1. Wash polymer sleeves by sonicating in Branson diluted in distilled water, then 1 hour in distilled water
    a. 20 mm diameter final = 20 mm diameter silicone tube
    b. 16 mm diameter final = 16 mm diameter latex tube
2. Sterilize components
    a. Autoclave Ultem end pieces, 3 way valves, scissors, tweezers, Teflon tape, cable ties, silk sutures, nylon sutures, male luer lock caps, and bioreactor lids and jars
    b. Latex tubes are soaked in 70% isopropanol for at least 4 days
    c. Silicone tubes can be autoclaved
3. Lay down a sterile drape and empty sterilized components onto it
    a. If using latex tubes, be sure to let the isopropanol to evaporate
4. Using sterile gloves place latex/silicone tube on one Ultem manifold, secure it with a zip tie, and hydrate it with culture medium
5. Remove VRE from its mandrel carefully and place it over the latex/silicone tube
6. Fasten it with a silk and/or nylon suture to the Ultem manifold
7. Cut the latex/silicone tube to the appropriate length, insert the other Ultem manifold, and secure it with a zip tie
8. Secure the engineered tube with sutures
9. Use a syringe to fill the lines and lumen of the latex/silicone tube (try to remove air bubble)
10. Fill bioreactor jar with culture medium (as described above) and screw on the lid
11. Cap the 3 way valve, place a sterile syringe filter to the port on the lid, and place the bioreactor jar in the incubator
12. Fill bioreactor lines using a large syringe and cap one end; place an appropriate sized syringe

13. Insert bioreactor line into the incubator side port and connect it to the 3 way valve on the bioreactor lid
14. Secure syringe in a reciprocating syringe pump and start the pump, watching for leaks

NOTE: Set the syringe pump stroke volume based on the desired strain for the engineered tubes (get calibration curve using laser micrometer)

Appendix Table C-1. Reagents and equipment for bioreactors

Name	Company	Product Number
PharMed Tubing	US Plastics	57318
Bioreactor jar (Tall 250 mL)	US Plastics	71301
ULTEM rods	McMaster Carr (machined)	8686K76
Cable ties	McMaster Carr	70215K62
3 way valves	Nordson Medical	DCV125-001
Sterile syringe filter	Millex	SLGP033RS
Luer lock caps	Value Plastics	Female: FTLLP-1 Male: LP4-1
Syringe pump	Various, modified	

C.3 Decellularization Protocol

1. Aspirate medium off of VRE
2. 3 x 10 minute rinses in 1X PBS on shaker at room temperature (RT)
3. 1% SDS (in ddH_2O) washes – all steps done at RT on shaker
    a. 1 hour with VRE still on the mandrel
    b. 1 x 5 minute rinse in PBS
    c. 2 hours (still on mandrel) in fresh SDS
    d. 1 x 5 minute rinse in PBS
    e. Remove VRE from the mandrel and **place it back in the original container; NOT A 50 CC CONICAL**
    f. 2 hours in fresh SDS
    g. 1 x 5 minute rinse in PBS
    h. 1 hour SDS wash
4. 3 x 10 minute rinses in 1X PBS on shaker at RT OR overnight at 4 degrees Celsius
5. 3 x 10 minute wash in 1% Triton X-100 (in ddH_2O) at RT
6. 3 x 1 hour rinse in PBS or overnight
7. DNase in DMEM + 10% FBS overnight at 37 degrees Celsius
    a. *DNAse was dissolved in sterile filtered 100 mM Tris pH 7.5 @ 2000 U/ml. It was added at 1:1000 in DMEM C (10% FBS) low Fz, and sterile filtered.*
8. 3 x 1 hour wash in PBS
9. Move to a smaller container or 50 cc conical and store at 4 degrees C in 1X PBS

Appendix Table C-2. Reagents for decellularization

Name	Company	Product Number
Phosphate Buffered Saline (PBS)	Corning	21-031-CM
Sodium dodecyl sulfate (SDS)	ThermoFisher Scientific	15525017
Triton X-100	Sigma Aldrich	T9-284-1L
Deoxyribonuclease I, recombinant (DNAse)	Worthington Biochemical	LS006361

C.4 Mechanical Testing Protocol

1. Cut tissue strips using a razor blade to the desired dimensions
    a. Uniaxial strain to failure: ~12 mm long x ~2 mm wide)
    b. Suture retention testing: ~10 mm wide x ~ 5 long
        i. Tie suture knot 2 mm from the tissue free edge orthogonal to the direction it will be pulled (per ISO 7198)
2. Measure and record sample dimensions using a digital calipers prior to testing
3. Set up Instron testing machine, calibrate load cells and arm position, and storage location
4. Attach custom grips to opposing arms and immerse in a 1X PBS bath
5. Place tissue in the grips, straighten it with a 0.005 N load, and commence testing
    a. Uniaxial strain to failure
        i. 6 preconditioning cycles at 0-10% strain
        ii. Displace arms at a rate of 3 mm/min until strip failure
    b. Suture retention
        i. Displace arms at a rate of 50 mm/min until failure

C.5 Freezing and Fixing Tissue

Modified from Katie Ahmann

Procedure

1. Rinse the sample 3 x 10 min in PBS at room temperature on orbital shaker if possible or mix occasionally by hand.
2. Fix the sample for 3 hours at 4^{o}C in 4% para-formaldehyde on orbital shaker.
3. Rinse the sample 3 x 10 min in PBS at RT, orbital shaker if possible.
4. Place samples in infiltration solution 1 overnight at 4^{o}C on a shaker.
5. Place samples in infiltration solution 2 for 4 hours at room temperature on a shaker.
6. Place samples in dry sample block cup and carefully side/transfer sample. Top off with OCT. Freeze in pre-chilled isopentane in liquid N_2. Freeze until opaque. Store samples at -20^{o}C.

Infiltration Solution 1

30% w/v sucrose + 5% w/v DMSO in 1X PBS

e.g. for 100 ml: 30 g sucrose + 5 ml DMSO + 10 ml 10X PBS

Dilute to 100 ml with ddH_2O

Infiltration Solution 2

50% v/v infiltration solution 1 and 50% v/v OCT

e.g. for 40 ml: Place 20 ml of Infiltration Solution 1 in a 50 cc conical

Dilute to 40 ml with OCT

Mix well, avoid bubbles. If you get bubbles, centrifuge briefly to remove.

C.6 Lillie's Trichrome Staining Protocol

Solutions

1. **Weigert's Iron Hematoxylin**

   Solution A

   Hematoxlyin: 5.0 g

   95% alcohol: 500 ml

   Mix well, label with initial and date. Stable for 1 year. *Caution: Flammable, avoid contact and inhalation.*

   Solution B

   ferric chloride (iron III chloride): 5.8 g

   dd H_20: 495 ml

   conc. HCl (12 N, 37%): 5.0 ml

   Mix well, label with initial and date.

   Stable for 1 year. *Caution: Corrosive, avoid contact and inhalation.*

2. **Weigert's Hematoxylin Working Solution**

   Combine equal parts Solution A and Solution B and mix well. Stable for 3-4 days.

   For staining dish: 160 ml total = 80 ml of each

   For Coplin jar: 50-60 ml total, depending on number of slides = 25-30 ml of each

3. **Beibrich Scarlet**

   Biebrich scarlet (a.k.a. Ponceau BS): 2.5 g

   Acetic Acid, glacial: 5.0 ml

   Dilute to 500 ml with ddH_2O. Stir 20 minutes

   Store in dark bottle. Solution stable for 6 months.

4. **PMA-PTA:**

   Phosphomolybdic Acid Solution (PMA), Sigma HT153

   Phosphotungstic Acid Solution (PTA), Sigma HT152

1 part PMA: 1 part PTA : 2 parts ddH_2O

For 1 full staining dish: 40 ml PMA + 40 ml PTA + 80 ml ddH_2O

Can use 2x in 1 day. Prepare fresh each day (i.e. do not store used solution).

5. **Fast Green:**

   Fast Green FCF: 12.5 g

   Acetic Acid, glacial: 10.0 ml

   Dilute to 500 ml with ddH_2O. Stir 20 minutes. Filter through Whatman #1. Store in dark bottle. Solution stable for 6 months.

   Use 2x. Can store as used solution in staining dish.

6. **1% Acetic Acid:**

   Acetic Acid, glacial: 5.0 ml

   ddH_2O

Procedure

1. Warm Bouin's fixative to 56 C in water bath while slides warm to RT and are formalin fixed (see below).
2. Remove OCT slides from freezer. Let warm to room temperature (about 10 min).
3. Place in neutral buffered formalin 20 min to further fix cells. Can use formalin 2x. Dispose of spent formalin in hazardous waste.
4. Rinse slides with running tap distilled water for 5 min.
5. Bouin's should now be at 56 C. Transfer Bouin's to fume hood and add slides. Seal with parafilm and place in 56 C bath. Incubate 1 hr.
6. Transfer slides and Bouin's to fume hood and remove slides to clean staining dish or Coplin jar.
7. Rinse slides with tap water until no color remains on sections, about 5 min. Discard used Bouin's (hazardous waste).
8. Weigert's Hematoxylin Working Solution: 5 min.

9. Rinse with running tap water for 5 min. (need tap to get proper bluing of stained nuclei).
10. Rinse in ddH_2O (good distilled water from lab purifier).
11. Beibrich Scarlet: 5 min.
12. Rinse with tap distilled H_2O until rinse water is colorless.
13. Rinse once with ddH_2O.14. PMA/PTA solution: 5 min.
14. Fast Green (no rinse in between PMA/PTA and Fast Green): 5 min
15. 1% Acetic Acid: 1 min. (start timer and walk slides to hood with dehydration pots, when timer goes off immediately place slides into first alcohol)
16. Dehydrate and coverslip with Permount:
    a. 95% EtOH 2 x 3 min
    b. 100% EtOH 2 x 3 min
    c. Xylene 3 x 3 min
    d. Permount hardens within about 20 minutes or so and then slides can be viewed. No need to keep slides as protected from light as for fluorescence, but avoid excess light. Store slides at RT.

C.7 Von Kossa Staining Protocol for Calcium

From IHCWorld: http://www.ihcworld.com/_protocols/special_stains/von_kossa.htm

Description: This technique is for demonstrating deposits of calcium or calcium salt so it is not specific for the calcium ion itself. In this method, tissue sections are treated with a silver nitrate solution and the silver is deposited by replacing the calcium reduced by the strong light, and thereby visualized as metallic silver.

Fixation: formaldehyde, formalin fixed, paraffin embedded tissue sections or alcohol fixed, frozen sections.

Solutions and Reagents:

1. 1% Aqueous Silver Nitrate Solution:
    a. Silver nitrate ---------- 1 g
    b. Distilled water ---------- 100 ml
2. 5% Sodium Thiosulfate:
    a. Sodium thiosulfate ---------- 5 g
    b. Distilled water ---------- 100 ml
3. 0.1% Nuclear Fast Red Solution:
    a. Nuclear fast red ---------- 0.1 g
    b. Aluminum sulfate---------- 5 g
    c. Distilled water ----------100 ml
    d. Dissolve aluminum sulfate in water. Add nuclear fast red and slowly heat to boil and cool. Filter and add a grain of thymol as a preservative.

Procedure:

1. Deparaffinize paraffin sections and hydrate to water.
2. Rinse in several changes of distilled water.
3. Incubate sections with 1% silver nitrate solution in a clear glass coplin jar placed under ultraviolet light for 20 minutes (or in front of a 60-100 watt light bulb for 1 hour or longer). Note: If stain was weak or rinsed off in washing steps, it

indicated the UV light was not strong enough. Longer staining is required for up to several hours.

4. Rinse in several changes of distilled water
5. Remove un-reacted silver with 5% sodium thiosulfate for 5 minutes.
6. Rinse in distilled water.
7. Counterstain with nuclear fast red for 5 minutes.
8. Rinse in distilled water.
9. Dehydrate through graded alcohol and clear in xylene.
10. Coverslip using permanent mounting medium.

Results:

Calcium salts ---------- black or brown-black

Nuclei ---------- red

Cytoplasm ---------- pink

Positive Controls

16-18 days mouse embryo, calcium containing tissues or undecalcified bone.

Notes:

UV light usually gives stronger reaction so the calcium salts are often stained black. The regular 60-100 watt light bulb usually gives weaker reaction so the calcium salts are often stained brown-black.

Oxalate salts are usually believed to give a negative von Kossa staining.

A negative control may be needed when there is any doubt that the resulting black deposits are calcium. This is done by treating a test slide in 10% formic acid for 10 minutes prior to step 3. The test slide should show negative reaction.

References

Sheehan D, Hrapchak B, Theory and Practice of Histotechnology, 2nd Ed, 1980, pp 226-227, Battelle Press, Ohil.

C.8 Verhoeff-Van Gieson (VVG) Staining for Elastic Fibers

From IHCWorld: http://www.ihcworld.com/_protocols/special_stains/vvg.htm

Description: This method is used for identifying elastic fibers in tissues such as skin, aorta, etc. on formalin-fixed, paraffin-embedded sections, and may be used for frozen sections as well. The elastic fibers will be stained blue-black and background will be stained yellow.

Fixation: 10% formalin or 4% PFA

Section: paraffin sections at 5 um or OCT at 9 um.

Solutions and Reagents:

1. 5% alcoholic hematoxylin
    a. Hematoxylin ---------- 5 g
    b. 100% alcohol ---------- 100 ml
    c. Mix to dissolve with the aid of gentle heat. Filter.
2. 10% aqueous ferric chloride (prepare fresh, not necessary)
    a. Ferric chloride ---------- 10 g
    b. Distilled water ---------- 100 ml
3. Weigert's iodine solution
    a. Potassium iodide ---------- 2 g
    b. Iodine ---------- 1 g
    c. Distilled water ---------- 100 ml
    d. Use 4 ml of distilled water to dissolve potassium iodide. And then add iodine. Once iodine is dissolved, dilute this solution by adding 96 ml of distilled water. This solution may be prepared fresh as needed or made in larger quantities and stored in brown bottle in the dark at room temperature.
4. Verhoeff's Working Solution

a. The working staining solution should be made up fresh for best results. It will not stain satisfactorily if it is kept more than one working day. Prepare the working solution by adding in order the following reagents:
b. 5% alcoholic hematoxylin ---------- 20 ml
c. 10% ferric chloride ---------- 8 ml
d. Weigert's iodine solution ---------- 8 ml
e. Mix the above amounts (or needed proportions thereof) well. Solution should be jet black. Use immediately and discard after use.

5. 2% aqueous ferric chloride (prepare fresh, not necessary)
    a. 10% ferric chloride from above ---------- 10 ml
    b. Distilled water ---------- 50 ml
6. 5% aqueous sodium thiosulfate
7. Van Gieson's counterstain
    a. 1% aqueous acid fuchsin ---------- 5 ml
    b. Saturated aqueous picric acid ---------- 100 ml

For nervous tissues may be prepared as follows:

1% aqueous acid fuchsin ---------- 15 ml

Saturated aqueous picric acid ---------- 50 ml

Distilled water ---------- 50 ml

Procedure:

1. Deparaffinize and hydrate slides to distilled water.
2. Stain in Verhoeff's solution for 1 hour. Tissue should be completely black.
3. Rinse in tap water with 2-3 changes.
4. Differentiate in 2% ferric chloride for 1-2 minutes
5. Stop differentiation with several changes of tap water and check microscopically for black elastic fiber staining and gray background. It is better to slightly under differentiate the tissue, since the subsequent Van Gieson's counterstain can extract the elastic stain somewhat.

6. Wash slides in tap water.
7. Treat with 5% sodium thiosulfate for 1 minute. Discard solution.
8. Wash in running tap water for 5 minutes.
9. Counterstain in Van Gieson's solution for 3-5 minutes.
10. Dehydrate quickly through 95% alcohol, 2 changes of 100% alcohol.
11. Clear in 2 changes of xylene for 3 minutes each.
12. Coverslip with resinous mounting medium.

Results:

Elastic fibers ---------- blue-black to black

Nuclei ---------- blue to black

Collagen ---------- red

Other tissue elements ---------- yellow

Positive Controls:

Aorta, Kidney, Myometrium.

C.9 Immunostaining Protocol & Antibody Information

Modified from Sandy Johnson and Katie Ahmann

1. Warm slides to room temperature and rinses in 1X PBS 2 x 2’
2. Permeabilize using .1% Triton in PBS for 5’ at room temperature
3. *For elastin staining*: *Hyaluronidase unmasking for 30’ at 37 C*
    a. *Sigma H3884*
4. Wash 3 x 3’ in 1X PBS
5. Block in 5% normal donkey serum (to match secondary antibody host) for 30 minutes – 2 hours at room temperature
6. Incubate in 1° antibody for 1 hour at room temperature or overnight at 4°C

Appendix Table C-3. Immunostaining suppliers, product numbers, and dilutions

Name	Supplier	Product Number	Dilution
CD45	US Biological	214696	1:200
SMA	Sigma	5228	1:200
Ki67	Abcam	15580	1:400
VwF (endothelial)	Abcam	6994	1:200
Vimentin	Abcam	80667	1:1000
Elastin	Sigma	E4013	1:2000
Collagen IV	Abcam	6586	1:200
Collagen I	Novus	NB600-408	1:1000

7. Rinse 3 x 3’ in PBS
8. Incubate in 2° antibody in PBS for 1 hour at room temperature
    a. Stock solutions of secondary antibodies are stored at 4C for short durations (recommended <6 weeks) in PBS; stock solutions can be diluted 1:2 in glycerol and stored at -20 C (1 year or greater)
    b. Jackson DyLight at 1:200
9. Rinse 3 x 3’ in PBS
10. Hoescht at 1:10,000 for 10 minutes at room temperature
    a. Hoescht 33342 (H3570)
11. Rinse 3 x 3’ in PBS
12. Remove last PBS rinse with vacuum to dry surface
13. Place drop of Dako Mounting medium on slide and place coverslip